Modulation of Tau Dysfunction In Vitro

By

Kellen Ranero Voss

B.S. University of Iowa 2005

Submitted to the graduate degree program in the Department of Molecular Biosciences and the Graduate Faculty of the University of Kansas in partial fulfillment of the requirements for the degree of Doctor of Philosophy.

_____

Chairperson: Dr. Paul Kelly

_____

Advisor: Dr. Truman Christopher Gamblin

_____

Dr. Erik A. Lundquist

_____

Dr. Yoshiaki Azuma

_____

Dr. David Davido

_____

Outside Member: Dr. John Kelly

Date Defended: April 13th, 2011

The Dissertation Committee for Kellen Ranero Voss

certifies that this is the approved version of the following dissertation:

Modulation of Tau Dysfunction In Vitro

_____

Chairperson: Dr. Paul Kelly

_____

Advisor: Dr. Truman Christopher Gamblin

Date approved: April 25th, 2011

Abstract

The microtubule associated protein tau is a causative factor in a class of neurodegenerative diseases termed tauopathies. Alzheimer's disease (AD) is the most prevalent tauopathy. In AD, natively unfolded, tau becomes hyperphosphorylated, and undergoes a conformational change allowing hexapeptide regions near microtubule binding repeat region 2 to aggregate into fibers. Tau exists in neurons as six alternatively spliced isoforms. The expression levels of tau are not changed in many tauopathies; however, various levels of each isoform can be included in aggregation depending on the disease. This indicates post-translational modifications or interactions with other proteins causes certain tau isoforms to be included in or excluded from these insoluble inclusions. Tau functions by assembling and stabilizing microtubules and is regulated by phosphorylation. In AD, the phosphorylation state of tau is altered so the affinity for microtubules is reduced; however, how changes in tau phosphorylation affect polymerization of tau isoforms is not fully understood. Abnormal aggregation of protein in a cell is mediated by molecular chaperones. A class of molecular chaperones, heat shock proteins, is upregulated in response to cellular stress. The most widely involved is heat shock protein 70 (Hsp70), which has upregulated and inversely proportional protein levels to tau aggregation in hippocampal neurons. Hsp70 can increase tau solubility in cells; however, it is unknown if Hsp70 can act directly on tau to prevent its dysfunction. This dissertation explores how phosphorylation with GSK-3β, the major kinase believed to be involved in tau hyperphosphorylation, and interactions with Hsp70,

affect tau dysfunction (polymerization) and function (microtubule binding and assembly). Tau isoforms were found to be differentially affected by phosphorylation, as indicated by differences in their overall polymerization and various morphologies. Likewise, tau phosphorylation differentially affected their affinity for stabilized microtubules. Tau isoform polymerization was inhibited by Hsp70, with various concentrations of Hsp70 needed for complete inhibition. Finally, while Hsp70 altered the microtubule assembly properties of tau isoforms, each individual isoform was able to assemble microtubules robustly. Taken together, this dissertation shows tau isoforms respond differently to modifications and interaction with Hsp70, indicating each isoform could play a specific role in the progression of tauopathies.

Acknowledgements

Throughout life, a select few individuals can provide the needed guidance to tackle the current challenges of the day. For the past five years, Dr. Chris "Professor Chaos" Gamblin has provided me with this guidance. He has always wanted a nickname, and what better place to give him one than an official publication. Dr. Gamblin was generous enough to give me the opportunity to do a summer rotation during 2006, and accept me into his lab. While I am sure I have tried his patience more than once a week, he has stuck with me and continues to provide advice on how to be a better scientist and writer. I would definitely like to thank him for kicking me in the hand "accidentally" during indoor soccer in February 2011, while I was writing my dissertation and making it extremely difficult to type using only one good hand.

Next, I would like to thank all the lab members that have come and gone through the years. Shaun Carlson, an undergrad who was here during the beginning of my graduate career and the first author on the paper I contributed to during my rotation. Dr. Carolyn Rankin, whose insight and expertise was much appreciated during my beginning years. On a personal note, she was a great help when I got my dog and her expertise in dog training aided in my becoming an owner. I would like to thank the excellent lab technician, Michael Branden, who taught me about protein purification and helped with learning techniques early on. Dr. Qian Sun, who was the first graduate student in the lab, and who gave me a lot of advice dealing with graduate school. Benjamin Combs, a current graduate student in the lab, who loves to discuss

why the University of Iowa will always trump Iowa State University. I would also like to acknowledge the numerous undergrads that have helped with the background preparation work for experiments.

I am most appreciative to my committee members Drs. Kelly, Lundquist, Azuma, Davido, and Michaelis who gave me the opportunity to continue and recommended me for doctoral candidacy. Their guidance through grant writing and in completing my degree has been insightful.

I would like to thank most of all, my parents, who I owe my life. Without them, I would never have had this opportunity. They have provided encouragement and advice throughout my life, and I appreciate their support every day.

Finally, I would like to thank my dog, Monty, who has put up with the long hours, and sometimes the lack of attention as I have been writing my grant and dissertation, and completing my research. He will not understand how much I wish I could hang out with him more, but dad has to pay the bills. I am grateful to him for not retaliating by pooping on the carpet.

Figures

Chapter 1 Introduction

1.1 Tau

1.1.1 Overview

The microtubule associated protein tau was discovered in 1975, as a protein that could assemble neuronal tubulin into microtubules (*1*). Tau association with microtubules is regulated primarily by phosphorylation of tau. Excessive phosphorylation severely reduces the affinity of tau for microtubules and can induce a conformational change that allows tau to aggregate with itself. This aggregation is seen in many diseases associated with dementia, of which Alzheimer's disease (AD) is the most prevalent. Modeling the mechanism by which tau polymerizes has proven difficult, as many factors such as other post-translational modifications and other cellular proteins such as chaperones can influence the process. We propose that our in vitro system can be used to study how phosphorylation of tau and interactions of tau with other proteins influences the function of tau, such as microtubule assembly and binding, and tau dysfunction such as polymerization into filaments. This chapter provides background information on the current knowledge of tau biology germane to the studies performed.

1.1.2 Tau is alternatively spliced

The gene for tau, MAPT, is located on chromosome 17 at position 17q21 (*2*) and contains 16 exons (*3*, *4*). Tau mRNA contains up to 13 exons, as exon 4A, 6, and 8 are never transcribed in human neurons (*5*, *6*). Exons -1 (part of the promoter) and 14

are transcribed, but never translated (*5, 7, 8*). Exons 2, 3 and 10 of tau mRNA can be alternatively spliced to form 6 different isoforms in human neurons (*3*). Exons 2 and 3 in the N-terminal region can take the pattern of +2+3, +2-3, or -2-3 resulting in the naming of 2N, 1N or 0N, respectively. Exon 3 is only included in the presence of exon 2 (*4*). Exon 10 encodes for the second of four functional microtubule binding repeat (MTBR) regions. The absence of exon 10 results in three MTBR (3R) while the presence of exon 10 results in four MTBR (4R). The alternative splicing of tau results in the 6 isoforms that vary in size from 352 to 441 amino acids (Figure 1.1) (*7*).

1.1.3 Tau is expressed mainly in neurons

The fetal form of tau, 0N3R is the only isoform expressed in neurons during development and up to 8 days postnatal in rats (*9*). After this time all six isoforms are expressed (*10*), however not at equivalent levels. Tau protein levels of normal human adult cortex indicate equal levels of 3R and 4R tau. The differences arise when examining the number of N-terminal exons. 1N isoforms compose about 50%, 0N isoforms compose about 40% and 2N isoforms compose about 10% of cellular tau (*11*). It is presently unknown what regional and neuron to neuron specific differences in tau isoform expression levels are. Due to these differences in expression, tau isoforms may have specific functions as defined by their primary sequence. This dissertation examines whether differences in primary sequences can lead to changes in function and dysfunction.

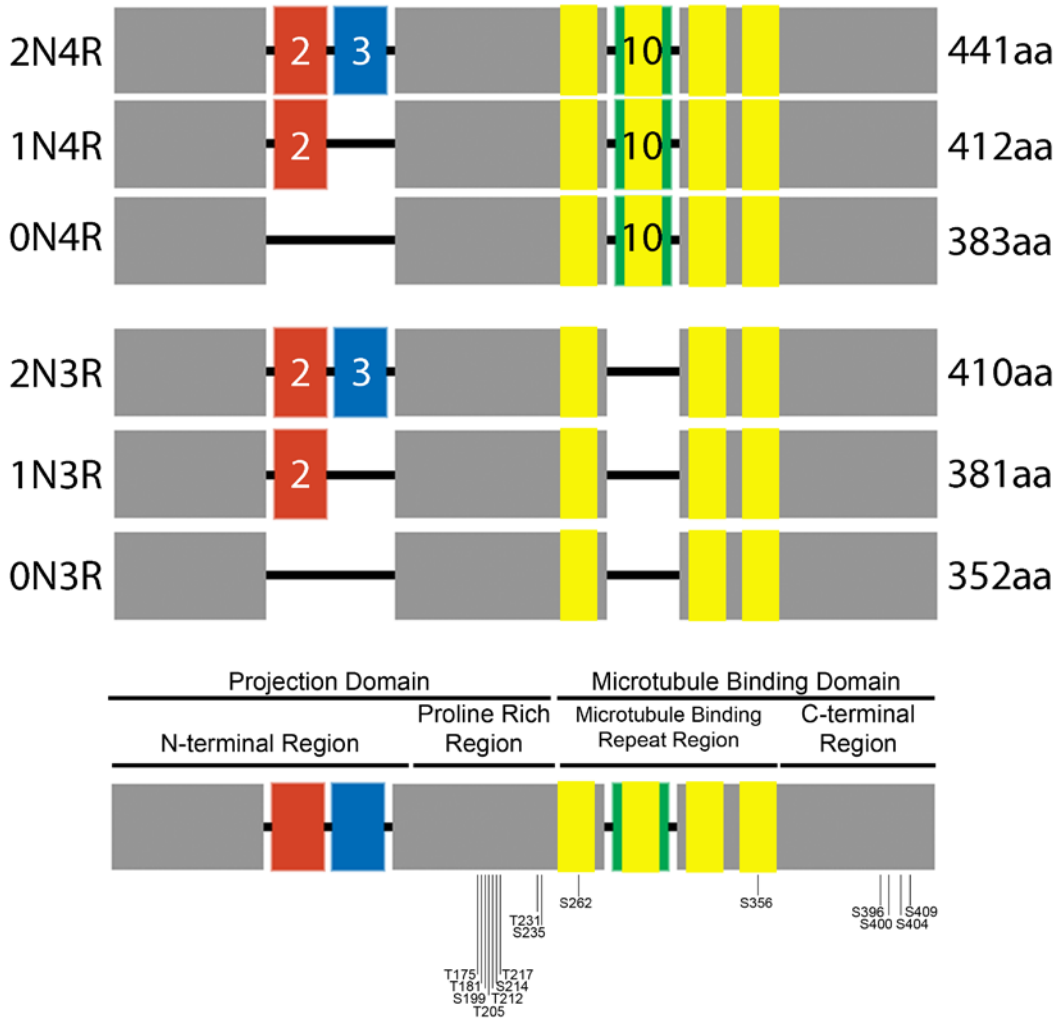

Figure 1.1 Tau isoforms are alternatively spliced at exons 2, 3 and 10 and known GSK-3β sites. Tau exists as six alternatively spliced isoforms that differ by the inclusion of exons 2 (red box), 3 (blue box) in the N-terminal region and exon 10 (green box) in the microtubule binding repeat region (repeats are colored yellow). Inclusion of exons 2 and 3 results in the naming 2N, inclusion of exon 2 results in the naming 1N, and inclusion of neither exon results in the naming 0N. Exon 10 encodes for microtubule binding repeat 2, and in the absence of exon 10, only 3 microtubule binding repeats are present resulting in 3R, or 4R if exon 10 is included. The number of amino acids in each isoform is indicated on the right side of the figure. The various domains and regions are labeled in the bottom figure. Also labeled are GSK-3β phosphorylation sites. Numbering is patterned on the 2N4R isoform.

1.1.4 Primary sequence

The primary sequence of tau can be divided into two domains as defined based upon their proposed functions (Figure 1.1). The projection domain is composed of two regions, the acidic N-terminal region of the protein, which includes exons 2 and 3, and a proline rich region, that is basic. The projection domain is so named because it projects away from the microtubule and can interact with cytoskeletal elements, the plasma membrane (*12, 13*), or tau on other microtubules (*14*). The second domain is the microtubule binding domain that includes the 3 or 4 microtubule binding repeats and the C-terminus of tau. The microtubule binding repeats are highly conserved 18 amino acid (aa) repeats that begin with the amino acid sequence VXSK, separated by less conserved 13 or 14 amino acid inter-repeat regions (*5, 8, 15, 16*). One 18aa repeat is sufficient for tau to promote microtubule assembly in vitro (*17*). These repeats bind microtubules through a number of weak amino acid groupings and the repeats have flexible linker regions to allow tau to bind tubulin in multiple conformations (*18*). ^{274}KVQIINKK^{281} in inter-repeat region between microtubule binding repeat 1 and microtubule binding repeat 2 is present only in 4R isoforms and contributes to the higher binding affinity of tau for tubulin than 3R isoforms that lack this sequence (*19, 20*).

1.1.5 Tau interacts with tubulin

The main function of tau is to bind to tubulin and promote assembly into microtubules as well as stabilize assembled microtubules. Tau interacts with tubulin

at approximately 1 tau per 4-5 tubulin dimers, implying one microtubule binding repeat of tau per tubulin dimer (*21*). Tau binds to the C-terminal region of tubulin as determined by subtilisin digestion (*22*). Digestion of both α and β tubulin with subtilisin resulted in two fragments per tubulin monomer, the smaller of which corresponds with the C-terminal domain of α- or β- tubulin (*23*). When tau was incubated with the two tubulin fragments, tau was able to bind only to the smaller C-terminal fragment as determined by column chromatography of tau and [^{3}H] tyrosinated tubulin (*22*). Additionally, tau failed to assemble tubulin that lacks this C-terminal region, but assembles full length tubulin indicating this region is required for tau and tubulin to interact (*22*). Mutations of charged lysines 274, 280, 281, located in the microtubule binding repeat region of tau, can reduce binding of tau to the C-terminus of tubulin, which indicates electrostatic interactions play an important role in binding (*24*). In addition, hydrophobic regions in the MTBR of tau seem to play a role in mediating binding (*25*, *26*). By deleting or mutating these hydrophobic regions, tau has a reduced affinity for microtubules (*26*). This indicates the mechanism by which tau and tubulin interact is very complex and the multiple interactions involved could have compensatory effects to prevent a loss of interaction between tau and tubulin.

Overall, tau is transported along the axon, primarily anterogradally, at a rate similar to tubulin (~0.003 μm/s) (*27*). Over short-intermediate distances tau rapidly diffuses in a cell at a rate of ~3 μm^2/s (*28*). The long range transport of tau is thought to proceed

by association with microtubule fragments (*29*). The exact mechanism of tau transport along the axon is unclear, however, due to the exchange rate of tau on microtubules, which blurs visualization of fluorescently labeled tau. Phosphorylated tau, which has a reduced affinity for microtubules, is found to be less concentrated along the microtubules, and is able to diffuse at a higher rate (~11 $\mu m^2/s$) than non-phosphorylated tau (*28*). Aggregated tau, similar to that of AD tau, can move bidirectionally at a fast-axonal transport rate (~0.3 μm/s) (*29*). In AD, aggregated tau is found in somatodendritic compartments, although the mechanism of how aggregated tau is transported to these compartments has not been elucidated (*30*). This observation could occur when aggregated tau, which moves faster (*28*), and inhibits kinesin more than dynein (*31*), results in a net retrograde transport. Determination of influences on tau/microtubule interactions could lead to the elucidation of how tau affects transport of itself and other protein along an axon.

Tau binding to tubulin is regulated by phosphorylation of tau. To date, 71 of a potential 85 serine, threonine and tyrosine sites on tau have been shown to be phosphorylated in vivo under either normal or diseased conditions. This large proportion of sites can be phosphorylated by over 30 kinases (discussed later; see section 1.5). Alternatively, there are three known phosphatases that work to regulate the phosphorylation state of tau (see 1.5). Tau is normally phosphorylated to regulate its affinity for microtubules (*32-38*). Phosphorylation at residue S262, in the microtubule binding domain, drastically reduces the affinity of tau for microtubules

(*39*), albeit not completely (*40*). Tau phosphorylation is dramatically different between early development and adult states. The dynamic nature of phosphorylation of tau isoforms plays a major role in the structure and differentiation of neurons in neurite outgrowth, axonal extension, and polarity by regulation of microtubule properties such as stability, spacing, and length. During fetal development, 0N3R is phosphorylated at a higher level than what is found on normal post-natal tau isoforms (*41, 42*). It makes sense then that 0N3R tau is highly phosphorylated to allow these processes to occur, and once a neuron has fully differentiated, to lower the phosphorylation state of tau to be less dynamic. In AD, abnormal phosphorylation occurs and plays a role in the progression of the disease; however, it is unknown the exact mechanisms by which this occurs (Figure 1.2). If a neuron has too much phosphorylated tau, it may occur because the cell wants to change its organization, which it cannot achieve and results in a diseased state. The role phosphorylation on tau function and dysfunction is one of the foci of this dissertation.

1.2 Amyloid

1.2.1 Overview

Most proteins, when synthesized from the ribosome, adopt a folded structure. Protein folding is achieved by attaining the most thermodynamically stable state. This includes the internalization of hydrophobic regions and externalization of hydrophilic regions to the solvent. To reach this state, the protein usually passes through a series of partially folded intermediates. These intermediates can be stabilized with help

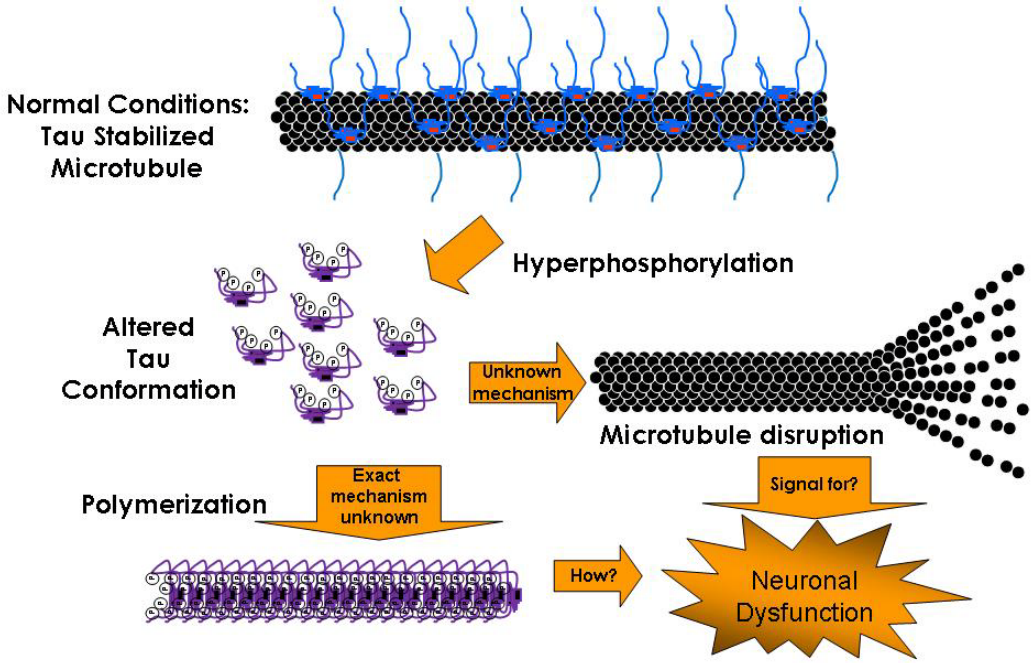

Figure 1.2 Overview of tau phosphorylation leading to dysfunction. (adapted from Dr. Lester Binder). Tau normally binds to and stabilizes microtubules in the axon of a neuron. Upon hyperphosphorylation, tau undergoes a conformational change that increases its propensity to polymerize into filaments. The exact mechanism for how phosphorylation causes conformational changes and increased polymerization is unknown. Reducing the concentration of bound tau to microtubules can lead to destabilization of the microtubule, however, the mechanism is unknown in a neuron and could be compensated for by other microtubule associated proteins. The mechanism by which polymerized tau and/or microtubule disruption lead a neuron to become dysfunctional is still unknown.

from molecular chaperones that bind to exposed hydrophobic regions (see section 1.6). If these hydrophobic regions are left exposed, there is a possibility of interaction with exposed hydrophobic regions on other proteins resulting in protein aggregation.

A class of diseases, termed amyloidoses, results from the deposition of misfolded proteins into organs and tissues. These proteins that have misfolded and escaped degradation result in self aggregation into insoluble fibrous structures termed amyloid. Nearly every protein has the ability to form amyloid (*43*). However, to date about 26 amyloid diseases exist, such as AD, type II diabetes and mad cow disease (reviewed in (*44*)). The proteins involved in these diseases vary in their normal folding and function. However, in their amyloid states, they all share characteristics, such as structural similarities, that make them indistinguishable from each other.

1.2.2 Formation

Amyloidogenic proteins characteristically form cross β-sheet secondary structure that aggregate into fibers as determined by Congo red staining (*45*) and X-ray diffraction (*46*). Cross β–sheet structure is defined as β-sheets aligned parallel to each other and perpendicular to the axis of the fibril (Figure 1.3). The β-sheets can either adopt a parallel or antiparallel orientation and the fiber is unbranched and helical in nature. The fiber is stabilized by axial hydrogen bonds that occur between the peptide backbone (*47*, *48*) and lateral interactions between side chains (Figure 1.3) (*49*).

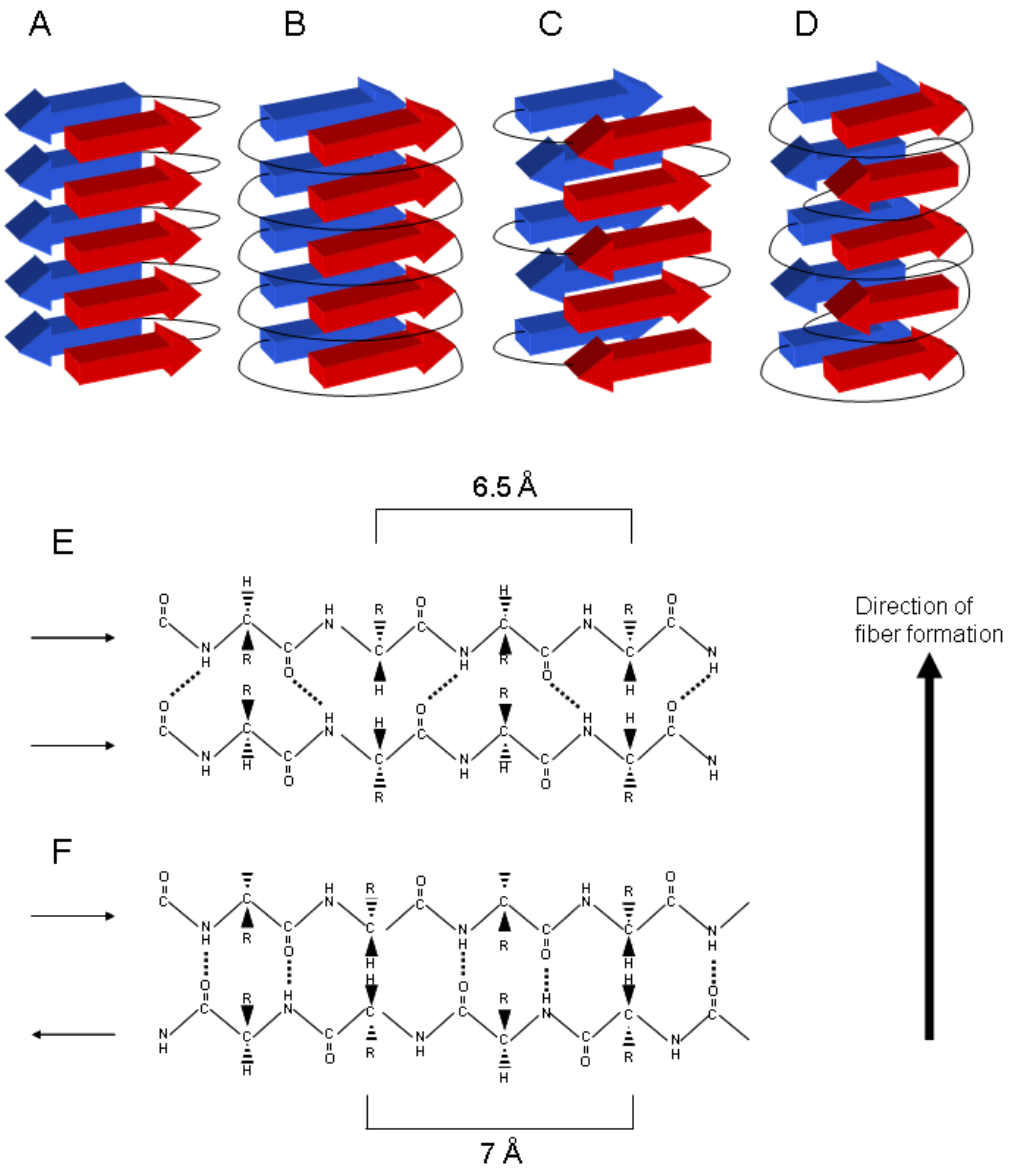

Figure 1.3 General Amyloid structure. (A-D) Four ways β sheets could stack in an amyloid fibril. (A, B) parallel β sheets, (C, D) antiparallel β sheets. Each red and blue sheet is part of the same monomer, indicated by the joining lines, and different monomers interact in the direction of fiber formation, as denoted by the arrow. Hydrogen bonding of (E) parallel β sheets or (F) anti-parallel β sheets. Based upon X-ray diffractions, the distance between R-groups for tau fibers is 6.9 Å, corresponding with an anti-parallel conformation. Alternatively, each red and blue sheet could be part of different monomers (known as domain swapping).

Despite the overall structure, the mechanism of fiber formation is unknown. This is the overall question we are trying to answer, and the work done here is a good primary step in the direction of determining the mechanism of amyloid fiber formation.

Aggregation of protein to form amyloid fibrils is thought to follow a nucleation-elongation mechanism. This means monomer aggregates to form a nucleus and upon reaching a certain nucleus size. Addition of subsequent monomers will be added to elongate into fibrils. It is unknown whether addition of monomer in the elongation phase is unidirectional or bidirectional. The concentration of monomer required to form a nucleus is defined as the critical concentration for polymerization. At protein concentrations below the critical concentration, nucleation does not occur, but once the critical concentration is reached, polymerization proceeds at a constant rate until the monomer pool reaches the critical concentration and steady state is achieved, meaning no further polymerization occurs. This nucleation mechanism has been shown to occur for a variety of proteins such as prion protein (PrP), amyloid β (Aβ), tau and α-synuclein (*50, 51*). The formation of the nucleus occurs very slowly in vivo and in vitro in the absence of any external influences. However, reduction of the critical concentration for nucleation, for use in studying polymerization in a relative short time period, can be achieved by addition of oligomer seeds (*52*) or inducer molecules (*51*). The critical concentration of monomer in the presence of these factors is reduced to smaller than detectable levels, resulting in nearly spontaneous

filament formation. The elongation phase can also be affected by a number of factors. Mutations (*53-55*), protein concentration (*51*), pH changes (*56-58*), post-translational modifications (*59, 60*), and interaction with other molecules (*61-63*) or proteins (*64*) can alter the rate of elongation. Because of these factors, we would predict that local variations to the environment, such as changes in protein concentration, buffer or interactions with other factors in a cell and in vitro would have consequences on the formation of tau filaments. Therefore, one of our overall goals is to elucidate the impact of the molecular environment on tau filament formation in vitro, as we can more precisely control the environment.

1.3 Tau Dysfunction

Most proteins have a distinct natively folded state and in order to form amyloid fibers, need to undergo unfolding and misfolding into a conformation that allows β-sheet structures to interact. A second type of protein that can form amyloid undergoes a different transition. Instead of being folded in a distinct natively folded state, natively unfolded or intrinsically disordered proteins, such as tau, α-synuclein and Aβ, exist without discernable structure and only need to adopt a partially misfolded state in order to form amyloid fibers (*65*). Assembly of tau into amyloid fibers can result in paired helical filaments (PHFs) or straight filaments (SFs). However, it is unknown if PHFs are the result of SF combination or through a distinct mechanism. Studies examining recombinant tau protein in the form of PHFs or SFs in vitro have shown that they look similar to PHFs and SFs isolated from AD brains. This indicates in

vitro studies can model the diseased state and have a direct impact on AD research. PHFs have two distinct traits, a fuzzy coat (*66*) and a pronase resistant core. The PHF core, as analyzed by mass spectroscopy, is composed of two main regions of tau, encoded by exons 10 and 11 (*67*). This implies the coat is composed of the remainder of tau (N- and C-terminal regions), projecting away from the filament. The minimal sequence needed to generate filaments has been mapped to ^{275}VQIINK^{280}, located in exon 10 between MTBR1 and MTBR2 and ^{306}VQIVYK^{311}, located in exon 11 between MTBR2 and MTBR3. The ^{275}VQIINK^{280} is absent in 3-repeat tau isoforms, which is thought to contribute to why 3R isoforms polymerize less well than 4R. The ~10 residues following these two regions can form helical structure and associate with phospholipid micelles. These negatively charged, phosphate covered micelles are thought to mimic the microtubule surface and could be used as a nucleation source for tau polymerization (*68*). While most tauopathies are associated with non-mutated tau, certain mutations, such as ΔK280 and P301L (naming based upon 2N4R tau), increase the propensity of beta sheet formation in these hexapeptides (*69*). Conversely, proline substitutions in the 275-280 and 306-311 regions can inhibit β-sheet formation and aggregation (*69*). Being able to correlate results of in vitro tau polymerization with in vivo studies allows us to more precisely alter tau, through post-translational modifications, and conditions for polymerization. These controlled experimental manipulations will allow us to make more accurate conclusions about how tau polymerization occurs. This dissertation will examine the role of specific interactions on tau polymerization.

1.4 Tauopathies

1.4.1 Overview

Tauopathies are a class of brain disorders that are characterized by abnormal tau aggregates. These aggregates manifest themselves in various forms in various diseases talked about briefly in this section. However, there are some common traits these tau aggregates share. Normal tau phosphorylation is beneficial for regulation of its affinity for microtubules. Under certain conditions, tau can become abnormally "hyperphosphorylated" and lose the ability to bind to microtubules. This creates a pool of tau that, if not degraded by the cell, can aggregate to form amyloid fibrils. Hyperphosphorylation refers to increased phosphorylation of tau such that it can induce a SDS-resistant conformational change when visualized by SDS-PAGE. Tau isolated from tauopathies is mainly hyperphosphorylated and insoluble. This is interesting because phosphorylation decreases hydrophobicity, which is thought to be a contributing factor to tau aggregation. The question of how hyperphosphorylation promotes tau aggregation is a major focus of the field. One large and interesting difference between tauopathies is despite similar soluble tau levels to normal aged brains, the various tauopathies have different amounts of the tau isoforms in the insoluble form associated with the tauopathy (Table 1.1). This indicates that something in the cell promotes or prevents the inclusion of certain tau isoforms into the insoluble fractions. These events could include post-translational modifications and/or interactions with other proteins. In this section, general similarities and differences in tau inclusions from various tauopathies are discussed as a reason for

why examining tau isoforms and post-translational modifications are important for understanding tau biology. By determining how the various tau isoforms polymerize, we can start to understand the etiology of various tauopathies.

1.4.2 Alzheimer's disease (AD)

The most common form of dementia is Alzheimer's disease accounting for 60-80% of cases (*70*). First described in 1907 by Alois Alzheimer (*71*), the disease now affects 5.4 million Americans and is the 6th leading cause of death in the United States (*70*). The most common symptoms in patients are a decline in the ability to remember names and events, eventually leading to a decline in the ability to perform daily functions and loss of motor skills. Compared to normal aged brains, there is a quantifiable increase of neuronal loss of hippocampal neurons in AD brains, a region high in tau pathology (*72*). Likewise rapid atrophy of the brain is elevated in AD as compared to normal aged brains (*73*) Pathologically, there are two hallmarks that define the AD brain. Extracellular senile plaques are composed of Aβ protein, which is processed from amyloid precursor protein and are found located near synapses. There are multiple types of plaques, but neuritic plaques are considered the most pathologically relevant (*74*). Neuritic plaques stain with Congo red, an amyloid stain, and have a dense core and a halo of Aβ amyloid. Plaques composed of Aβ do not seem to originate in a particular region of the brain and can be found all over the cerebral cortex, but are also seen in normal aged patients (*75*). The second pathological hallmark of AD are intracellular neurofibrillary tangles (NFTs),

composed of hyperphosphorylated tau protein. Tau from NFTs is known to be hyperphosphorylated because NFTs stained with both antibodies to anti-PHF tau, and antibodies to normal tau. However, upon tau dephosphorylation, a greater amount of normal tau staining is observed (*76-79*). Tau isolated from NFTs in AD brains can be found as both paired helical filaments (PHFs) (*80*) and straight filaments (*81*). PHFs, are composed of entwined tau filaments, and are insoluble inclusions that can be isolated from affected neurons in various tauopathies. Insoluble means after addition of detergents, such as sarkosyl, where normal proteins would denature, the filaments stay together. This is a useful property, as isolation of insoluble aggregates can be achieved through detergent treatment and ultracentrifugation, resulting in insoluble tau in the pellet and soluble tau in the supernatant (see Table 1.1). In 1986, PHFs isolated from AD brains contained mainly hyperphosphorylated tau, as determined by staining with antibodies specific to phosphorylated tau (P-tau) (*82, 83*). When AD brain tubulin was assembled into microtubules, only tau from aged-matched controls and DEAE-dextran, a polycation that mimics tau in stimulating microtubule assembly, was able to accomplish assembly, not PHF tau. This indicates hyperphosphorylated tau from AD brain tissue has a lowered affinity for microtubules compared to aged matched control tau (*84*).

Tau is normally found in the axon, but in AD, is aggregated and missorted to somatodendritic compartments (*30*). While many neurons that contain NFTs are still functional, they show signs of stress by having upregulated levels of ubiquitin, a

stress response protein (*85*). Neurons containing NFTs that die and disintegrate leave proteolytically degraded "ghost" tangles that lack the C- and N-terminus, indicating that processing of filamentous tau could result in increased tau insolubility.

The type and severity of AD is closely associated with NFT load (*86-88*). There are two types of AD, familial (early onset) and sporadic (late onset). Familial AD (FAD) accounts for less than 5% of AD cases and occurs in patients younger than 65. FAD is usually associated with mutations in the amyloid precursor protein (APP), presenilin 1, and/or presenilin 2 genes that are all involved with generating Aβ pathology. Sporadic AD (SAD) accounts for almost all cases of AD. The largest risk factor for developing SAD is age. However, apolipoprotein E isoform 4 (ApoE4) has been found to be associated with increased risk of AD development (*89*). Having one ApoE4 allele increases the risk of SAD, while having two alleles increases the risk even further, but does not guarantee AD development. AD is not associated with any mutations in the tau gene or upregulated expression of any isoform. This indicates that all tau pathologies are a result of post-translational modifications and interactions with other molecules or proteins. We propose that these post-translational modifications and interactions with other molecules will have diverse effects on tau isoform polymerization and function.

1.4.3 Pick's Disease (PiD)

Pick's disease is characterized by changes in personality and social behavior (*90*). The pathological hallmark characteristic of PiD are intracellular Pick bodies composed primarily of 3R hyperphosphorylated tau, although 4R tau is also present in smaller amounts (*91*). This is different from AD where all six isoforms are incorporated into the pathology, despite both AD and PiD having similar levels of soluble tau isoform expression (*30*). Pick bodies are found in the frontal and temporal cortex and hippocampus as spherical cytoplasmic inclusions mainly in neurons. PiD is considered a sporadic tauopathy, even though tau mutations are associated with the disease. However, the pathology between non-mutated and mutated forms are indistinguishable (*92*). Mechanisms for 3R tau polymerization in vitro could lead to the elucidation of how PiD progresses, and will be examined in this dissertation.

1.4.4 Progressive supranuclear palsy (PSP) and corticobasal degeneration (CBD)

Progressive supranuclear palsy (PSP) and corticobasal degeneration (CBD) can be grouped together, because unlike in AD, where tau is found almost exclusively in neurons, PSP/CBD tau is also found in glial cells. Unlike AD which has mixed incorporation of 3R and 4R isoforms in insoluble aggregates, PSP/CBD brains have a higher amount of 4R tau than 3R tau in these aggregates. This is interesting because both AD and PSP/CBD have similar expression of all six isoforms in their soluble

extracts, indicating different mechanisms by which tau isoforms can aggregate (*30*). In PSP, glial cells containing tau are called tufted astrocytes (astrocytes) or coiled bodies (oligodendrocytes) (*93-95*). NFTs found in PSP are composed of straight filaments and long-period twisted filaments of predominately 4R tau (*96-98, 99*). In CBD, neuropil threads composed of tau are found located more in the cortex as compared to PSP where tau pathology is found in the brainstem (*100-103*). CBD tau is found aggregated in the form of PHFs and SFs (*94*, *104*).

1.4.5 Frontotemporal dementia with parkinsonism associated with chromosome 17 (FTDP-17)

It was not until mutations in tau associated with neurodegenerative disease were discovered that tau gained wide acceptance as causing dementia and neurodegeneration. Most mutations in tau result in similar phenotypes to those of the sporadic tauopathies (*30*). FTDP-17 is a class of familial neurodegenerative tauopathies in which mutations in tau are associated with disease. A variety of symptoms can be associated with FTDP-17 such as changes in behavior, cognition and motor function. These diverse symptoms are due to the many types of mutations in tau associated with FTDP-17. 32 different mutations have been observed in over 100 families (*105*). Mutations either change the way tau is spliced and alters the ratio of 3R and 4R tau (*106-115*), the way tau interacts with microtubules (*11* , *116*) and how tau polymerizes (*69, 117-123*). While this dissertation does not address mutated

	AD FTDP-17 (G272V, V337M, R406W)	CBD/PSP FTDP-17 (N279K, P301L/S, S305N)	PiD FTDP-17 (K257T, G389R)	Other single site FTDP-17 mutations and intronic mutations
isoforms expressed in soluble fractions	all six	all six	all six	all six
percentage of isoforms expressed in soluble fractions (N-terminal exons)	~50% 0N, ~40% 1N, ~10% 2N	~50% 0N, ~40% 1N, ~10% 2N	~50% 0N, ~40% 1N, ~10% 2N	~50% 0N, ~40% 1N, ~10% 2N
percentage of isoforms expressed in soluble fractions (repeats)	~50% 3R, ~50% 4R	~50% 3R, ~50% 4R	~50% 3R, ~50% 4R	~33% 3R, ~66% 4R
isoforms expressed in insoluble fractions	all six	all six	all six	all six
percentage of isoforms expressed in insoluble fractions	1:1 4R:3R (no change from soluble)	2:1 4R:3R	1:3 4R:3R	2:1 4R:3R
phosphorylation state	Hyperphosphorylated (~4x normal)	Hyperphosphorylated (~4x normal)	Hyperphosphorylated (~4x normal)	Hyperphosphorylated (~4x normal)

Table 1.1 Summary of differences between tauopathies. A large difference between tauopathies is the inclusion of various levels of tau isoforms in insoluble inclusions (see definition in section 1.4.2).

tau associated with FTDP-17, the research presented can be applied to future studies examining how mutations on tau can affect the wild-type properties.

1.5 Tau phosphorylation

Tau is known to be post-translationally modified by phosphorylation, glycosylation, ubiquitination, oxidation, nitration, glycation and truncation (reviewed in (*124*)). The interplay of the various modifications is still unknown, meaning does phosphorylation cause changes in glycation, or do changes in glycation cause subsequent changes in phosphorylation. However, the most studied single post-translational modification of tau is phosphorylation at serine and threonine residues. Tau has 85 potential phosphorylation sites, with 71 being described under pathological or physiological conditions and being controlled by over 30 kinases that can be divided into three groups (reviewed in (*60, 125*)). The first group includes kinases that are proline directed to serine and threonine residues (S/T-P) and include CDK2/5 (*126*), MAPK (*127*) and GSK-3β (*128*). The second group includes non-proline directed kinases such as tau-tubulin kinase, casein kinase, MARK, PKA and PKC that phosphorylate serines and threonines (*128-135*). The third group is tyrosine protein kinases which include Src (*136*) and C-Abl (*137*). Phosphatases that dephosphorylate tau include PP1, PP2A, and PP2B (*138-143*). It is thought PP2A is the major phosphatase involved in modifying tau as inhibition of PP2A, but not PP1 and PP2B, results in increased tau hyperphosphorylation and accumulation in rat brains (*144, 145*). Additionally, PP2A binds tau in the MTBR and mutations in the MTBR found in

FTDP-17 patients can decrease PP2A binding, leading to increased phosphorylation and aggregation when examined in vitro (*146*). Hyperphosphorylated tau can undergo conformational changes that alter phosphatase binding by preventing or making accessible the sites of phosphorylation. This is supported by evidence showing chaperones can alter tau conformation and promote phosphatase activity (reviewed (*147*)). This is important because having too many phosphorylation changes could create an irreversible conversion of tau to its misfolded state. By determining how phosphorylation changes affect tau, we can potentially determine a way to stop the conversion of tau into an altered conformation earlier.

Phosphorylation of tau is known to regulate microtubule binding (*37, 148*) and GSK-3β has been shown to accomplish this regulation in vitro and in cell assays (*149, 150*). Induced over expression of GSK-3β in mice has shown free tau accumulates in hippocampal neurons indicating GSK-3β as a major kinase involved in tau phosphorylation and aggregation (*151, 152*). Investigation into the role of GSK-3β on tau function and dysfunction will be addressed in Chapter 3.

Tau is normally phosphorylated at 2-3 moles of phosphate per mole of tau, but in AD is hyperphosphorylated to 5-9 moles of phosphate per mole of tau (*32*). As mentioned previously, hyperphosphorylated tau is found in NFTs. The majority of tau phosphorylation occurs at sites outside MTBRs and can decrease tau-microtubule interactions 2-3 fold (*153, 154*). Phosphorylation in the MTBRs, such as at Ser262

causes more drastic changes to the microtubule binding of tau (~10 fold decrease in microtubule affinity as compared to non-phosphorylated tau) (*40, 155*). However, complete inhibition of microtubule binding has not been observed with phosphorylated tau. Alternatively, phosphorylation of tau can inhibit microtubule assembly while not changing microtubule binding affinities (*153, 154, 156*). This indicates specific roles for phosphorylation at various sites by the various kinases. Understanding the precise role each kinase plays in regulating tau/tubulin interactions is key to understanding the progression of tauopathies. While we cannot address all the kinases involved in the scope of this dissertation, we will focus on GSK-3β, as it is most widely believed to play the largest role in disease progression (see Chapter 3).

Hyperphosphorylated tau is found in different states in different tauopathies, indicating different mechanisms of phosphorylation. Missense mutations in tau present in FTDP-17 can cause a decrease in microtubule affinity resulting in accumulated phospho-tau. PP2A has a decreased affinity for these mutated tau forms, resulting in increased phospho-tau (*146*). Aβ protein, the other major pathological protein in AD has been shown to downregulate PP2A, resulting in increases in hyperphosphorylated tau (*157, 158*). Since tau aggregation correlates better with the severity of dementia, it is possible that small amounts of Aβ, which have not accumulated into plaques and therefore are unable to be correlated to severity, could downregulate PP2A, increasing tau phosphorylation and aggregation. The results published thus far indicate the regulation of tau phosphorylation plays a large role not

only in the normal function of tau in regulating microtubule dynamics, but also as a regulator of tau aggregation. We have investigated the role of GSK-3β on tau function and dysfunction in order to determine if GSK-3β alone is sufficient to cause significant changes to tau functions.

1.6 Chaperones

1.6.1 Overview

In order to function properly, a protein needs to be folded into a conformation that confers activity. A class of cellular proteins, termed molecular chaperones, facilitates proper folding of nascent proteins and refolding of proteins that have undergone partial or total denaturation to prevent these proteins from aggregating. In the case a misfolded protein cannot refold into its native conformation, chaperones can aid in their degradation. Chaperones are also involved in protein translocation across membranes, vesicular transport regulation and multimeric complex formation and protein destruction (*159-161*). While some molecular chaperones are constitutively expressed and active, groups of chaperones are elevated in response to cellular stress. In 1962, a paper described "puffs" on DNA in *Drosophila busckii* after heat stressing the flies (*162*). These puffs were determined to be proteins that were only expressed in response the heat stress and thus were termed heat shock proteins. It was later discovered other cellular stresses also produced a small number of these new stress-dependent proteins (*163-166*).

1.6.2 Heat shock protein 70 (Hsp70)

The most evolutionarily conserved heat shock protein is Hsp70 (*167-169*). DnaK, the *E. coli* homologue, is ~60% identical in sequence to mammalian Hsp70. The Hsp70 family in mammals contains 8 different genes that differ in primary sequence by up to 48%, and also differ by expression levels and localization (*170*). Most Hsp70 family members are localized in the cytosol/nucleus, except for Hsp70-5 which is found in the lumen of the ER and Hsp70-9 which is found in the mitochondrial matrix (reviewed in (*171*)). What makes the different gene products part of the same protein family is the common structure domains. Hsp70 family members consist of an ATPase domain, a protease sensitive site, a substrate binding domain (SBD), a variable region and an EEVD motif where co-chaperones can bind (*161, 170, 172*). The major Hsp70 genes are HSPA1A (encoding Hsp70-1a) and HSPA1B (encoding Hsp70-1b) which differ by only two amino acids (*173*). Hsp70-1a/b proteins are upregulated in response to stress, but are present at low levels that vary with cell type and cell cycle (*174, 175*). HSPA1A/B knockout mice are viable, but have increased susceptibility to many stress related disorders such as UV light stress and cerebral ischemia (*176-178*). This dissertation will focus on HSP70-1a protein because it is implicated to play a large role in AD (see 1.6.4).

1.6.3 Hsp70 Mechanism of action

Hsp70 generally acts by hydrolyzing ATP in the ATPase domain to increase binding to its substrate. The ATPase domain has two subdomains that create a pocket in

which ATP binds. These subdomains are flexible and can alter conformation between ATP, ADP or nucleotide-free states (*179*). The substrate binding domain also has two subdomains, the bottom subdomain has a hydrophobic groove where the substrate binds and the top subdomain is an α–helical lid that can come in closer proximity to the groove portion (*180*). The hydrophobic groove is where binding of exposed hydrophobic patches of unfolded or misfolded proteins occurs (*180*). The linker region between the two domains seems to confer signals between the two domains. In the ATP bound state, the SBD enters a more open conformation, and upon substrate binding, ATP is hydrolyzed to "close" the lid of the SBD (*159*).

1.6.4 Hsp70 in AD

The initial indication the heat shock response could act as a control mechanism in AD was implicated in 1988 when analyzing the promoter of APP, the protein from which Aβ protein is cleaved, and discovering a consensus binding site for heat shock control element binding proteins (*181*). Since then, numerous heat shock proteins have been found to be elevated in AD hippocampal brain tissue compared to age matched controls (*182*). In particular, Hsp70/90 are found upregulated in specific hippocampal neurons devoid of tau aggregation (*183*). Other chaperones such as Hsp27, Hsp70 and carboxy terminus of Hsc70 interacting protein (CHIP) can indirectly dephosphorylate and degrade abnormal tau in cell models (*183-185*). Upregulation of Hsp70/90 can increase tau interactions with microtubules and decrease insoluble tau aggregates in cell models (*183*). The constitutively expressed

heat shock cognate 70 (Hsc70), is 86% identical to Hsp70 and both have been shown to interact with tau protein (*186*). Finally, addition of Hsp70 and/or Hsp40, a known Hsp70 co-chaperone, to heparin mediated tau polymerization in vitro resulted in decreased tau aggregation (*187*).

Taken together the heat shock response seems to play a major role in preventing tau mediated neuronal damage and degeneration. We have examined the influence of Hsp70 on tau to inhibit its aggregation in vitro. In addition, even though Hsp70 can increase tau localization to microtubules in cells, it may be indirectly accomplishing this. We examined if Hsp70 allows tau to interact with tubulin to promote or inhibit microtubule assembly.

1.7 Overall summary and hypothesis

We have a set of tools to examine tau polymerization and microtubule interactions in vitro, and based upon the current literature, believe this will be applicable to the processes that occur in AD. We know tau can polymerize in vitro in the presence of inducer molecules, but we are uncertain how this occurs. Likewise, most research focuses on how 2N4R tau polymerizes, since 2N4R tau is the longest isoform and includes all residues making comparison of other isoforms easy because differences can then be attributed to loss of exons 2, 3, and/or 10. However, different mechanisms by which the other tau isoforms polymerize may exist. We believe this because there is a significant difference between tau isoforms when comparing their primary sequences. For example, due to alternative splicing of exon 10, the 3R

isoforms are missing a functional microtubule binding domain, which has been shown to play a large role in both microtubule affinity, and polymerization. We also seek to determine how phosphorylation affects the characteristics of tau isoforms, based again on the fact that the isoforms vary in length that could affect folding and whether tau isoforms can adopt conformations that promote or hinder aggregation and microtubule assembly. Finally, since Hsp70 has been implicated as a protein that could aid in preventing tau accumulation, we have investigated whether Hsp70 can directly act on tau isoforms to prevent aggregation and whether this potential interaction will affect the normal functions of tau.

Chapter 2- Methods

2.1 Tau expression and purification

Individual tau isoforms in pT7C vectors were a gift from Dr. Jeff Kuret (Ohio State University), and were described previously (*188*). For each isoform, the pT7C vector was transformed into BL21 (DE3) competent cells and plated on LB-agar with ampicillin. An individual colony was used to seed overnight 80 ml cultures of LB-broth with ampicillin in Erlenmeyer flasks at 25 ^{o}C. Once an OD_{600} close to 0.5 was achieved, three 600 ml wide bottom Fernbach flask containing LB-broth with ampicillin were inoculated with 20 ml of the overnight culture at 37 ^{o}C until an OD_{600} of around 0.7 was reached. Cells were induced to express tau with 500 mM IPTG (Calbiochem) at a final concentration of 1 mM at 37 ^{o}C for 2 hours. Cells were then centrifuged at 5000 RPM at 4 ^{o}C for 10 min in a Sorvall SLA-3000 rotor. The supernatant was discarded and cells were resuspended with 5 ml of ice cold lysis buffer (500 mM NaCl, 10 mM Tris base, 5 mM Imidazole, pH 8) per bottle. All resuspensions were pooled into a 50 ml conical tube and protease inhibitors (aprotinin, pepstatin A, leupeptin, phenylmethanesulfonylfluoride (PMSF)) were added to 1x, along with DTT (0.1 mM final). Cells were lysed three times using a French pressure cell (Thermo). Brij 35 (0.1% final) and more PMSF were then added and the lysate was centrifuged at 11,500 RPM in a Sorvall SS-34 rotor, 30 min at 4 ^{o}C. The supernatant was purified by Nickel affinity chromatography using an ÄKTA FPLC (GE Healthcare). Collected fractions after elution with elution buffer (500 mM NaCl, 10 mM Tris base, 250 mM Imidazole, pH 8) were analyzed by SDS-PAGE on 10%

polyacrylamide gels. Fractions containing tau were pooled and concentrated to 2-4 ml using an ultrafiltration stirred cell (Millipore) with a 30,000 MWCO YM30 cellulose filter. Concentrated samples were purified by size exclusion chromatography over a Superdex 200 column using the same ÄKTA FLPC (GE Healthcare). Fractions were analyzed by SDS-PAGE to determine where tau was the most abundant, and the least contaminated with other proteins. Usually, three fractions are pooled (6 ml total), DTT to 0.1 mM is added and protein is aliquoted into 75 µl, and stored at -80 ^{o}C. Tau protein concentration was determined using a commercially available BCA assay (Pierce), using BSA as the standard. Briefly, BSA at 2 mg/ml was used to generate a standard curve, and tau was diluted from 20x-2x and compared to the standard curve. Only absorbance readings for tau that fell within the standard curve were used, and the assay was repeated three times and averaged to determine a protein concentration. This concentration was confirmed by running the new tau prep against old tau preps of known concentration by SDS-PAGE. Tau molecular weights with a histidine tag, reported in (*188*), were used for future experiments and are as follows: 2N4R (48,013 Da), 2N3R (44,766 Da), 1N4R (45,130 Da), 1N3R (41,883 Da), 0N4R (42,170 Da), 0N3R, (38,923 Da).

2.2 Arachidonic acid (ARA) induced tau polymerization (Chapter 3 Part 1)

2N4R tau (0-4 µM) was incubated in polymerization buffer (10 mM Hepes, pH 7.64, 100 mM NaCl, 0.1 mM EDTA and 5 mM DTT) with varying concentrations of ARA

(0-300 µM; the ethanol vehicle concentration was constant at 3.75% for all reactions) at room temperature, overnight (~20 hours).

2.3 Heparin induced tau polymerization (Chapter 3 Part 1)

Low salt (50 mM NaCl) 2N4R tau (0-4 µM), was incubated in low salt polymerization buffer (10 mM Hepes, pH 7.64, 15-40 mM NaCl, 0.1 mM EDTA and 5 mM DTT) with various concentrations of heparin (0-6.25 µM, made in water) at 37 ^{o}C, overnight (~20 hours). The higher temperature was used as heparin induced polymerization proceeds more slowly than ARA induced, but is accelerated at higher temperatures.

2.4 ARA induced tau polymerization (Chapter 3 Part 2)

The final concentration of components in a polymerization reaction of 200 µl using ARA were: 2 µM Tau, 10 mM Hepes pH 7.64, 100 mM NaCl, 0.1 mM EDTA, 5 mM DTT, and 0-150 µM ARA (concentration of ethanol carrier was kept constant at 3.75% for all reactions). Reactions were incubated at 23 ^{o}C for 18 hours in a tabletop incubator. Room temperature in Chapter 3 Part 1 fluxuates, but averages 23 ^{o}C and this temperature was used to maintain consistency throughout experiments.

2.5 Heparin induced tau polymerization (Chapter 3 Part 2)

The final concentrations of components in a heparin polymerization reaction of 200 µl were 2 µM tau, 30 mM Hepes pH 7.64, 20 mM NaCl, 5 mM DTT and heparin (0

mg/ml–0.024 mg/ml). Reactions were incubated at 37°C for 18 hours in a tabletop incubator. Data for one of the three trials for 2N4R with 0.006 and 0.018 mg/ml heparin, 1N4R with 0.024 mg/ml heparin, and 0N4R with 0.018 mg/ml heparin were found to be inconsistent (greater than 33% different) from the other data and were not included in the graphs.

2.6 Right angle laser light scattering (LLS)

After incubation, tau polymerization reactions were assayed by right angle laser light scattering. Reactions were placed into 5 x 5 mm fluorometer cuvettes (Starna) and reactions in Chapter 3 were illuminated with a 5 mW solid state 475 nm laser (B & W Tek), while reactions in Chapter 4 were illuminated with a 5mW solid state 532 nm laser (B&W Tek). The original laser broke and was replaced with a different wavelength. The resulting images of scattered light perpendicular to the incoming light were captured with a digital camera (Sony XC-ST270); imported into Adobe Photoshop and using the histogram function of the program assigned an arbitrary value where increases correspond to more polymerization (*189*).

2.7 Thioflavine S (ThS) Fluorescence

After incubation, tau polymerization reactions were assayed by ThS fluorescence, a planar aromatic dye that binds tau polymer, but not monomer. ThS was added to reactions at a final concentration of 20 μM and fluorescence was measured at λ

excitation of 440 nm and λ emission of 520 nm in 96-well plate format in a Cary Eclipse fluorescence spectrophotometer (Varian) (*189*).

2.8 Transmission Electron Microscopy (TEM)

Polymerization reactions for Chapter 3 were prepared for TEM by methods previously described (*189*). Reactions for ARA were diluted 1:10 and reactions for heparin were diluted 1:5. After dilution, reactions were fixed with a final concentration of 2% glutaraldehyde, placed on formvar-carbon coated grids (Electron Microscopy Sciences), and stained with 2% uranyl acetate (Electron Microscopy Sciences) (*189*). Prepared grids for Chapter 3 were viewed with a JEOL 1200 EXII electron microscope, and images were captured with the MegaViewII imaging system (Soft Imaging System). Tau filament lengths were measured from digitized electron micrographs using the Optimas analytical imaging software (Media Cybernetics). Frequency distributions of filament lengths were generated by placing filament lengths into 50 nm bins with the center of the first bin at 25 nm. The number of filaments per bin was multiplied by the bin center to generate the approximate mass of filaments within a given length of filaments. The mass per bin was then divided by the total filament mass to give a percent of total mass for each range of filament lengths (*189*). Prepared grids for Chapter 4 were diluted 1:10, and were viewed on a Tecnai F20 XT Field Emission TEM (FEI).

2.9 ARA and Heparin induced tau polymerization kinetics (Chapter 3 Part 1)

2N4R tau (0.5-4 μM) was incubated at optimal, limiting and inhibitory ratios of ARA and heparin. Reactions were followed by the fluorescence increases in the presence of 20 μM ThS using a Flexstation II fluorometer microplate reader (Molecular Devices Corporation). The Flexstation automatically adds ARA and reads the reactions immediately to reduce any lag time introduced by human pipetting. Data was fit to a single phase exponential association equation using GraphPad Prism software. The data for optimal ratios of ARA were fit using a mathematical model developed for the kinetics of actin nucleation and polymerization (*190*) by first fitting the 4 μM tau curve for values of n, k^+, and K_{n-1} and then using these values to fit the data from the other protein concentrations.

2.10 Glycogen synthase kinase 3β (GSK-3β) phosphorylation of tau isoforms

GSK-3β (Sigma Aldrich) phosphorylation reactions (25 μL) of each tau isoform contained 16.66 μM tau, 0.018 U GSK-3β per pmol of tau in buffer (40 mM HEPES, pH 7.64, 5 mM EGTA, 3 mM $MgCl_2$, and 2 mM ATP). One unit is defined as the amount of GSK-3β required to catalyze the transfer of 1 pmol phosphate to tau in 1 min at 30°C in a reaction volume of 25 μL. Reactions were incubated for 20 hours at 30°C (*191*). The degree of phosphorylation was determined by examining the reaction products by 10% SDS-PAGE.

2.11 ARA induced polymerization of GSK-3β phosphorylated tau isoforms

25 µL phosphorylation reactions of the individual isoforms (see section 2.10) were diluted into ARA containing polymerization reactions, as previously described in (*191*).

2.12 γ-^{32}P ATP Phosphate incorporation

Tau protein was phosphorylated as detailed in (*191*). Briefly, tau was phosphorylated with 2 µM ATP plus 3.125 µCi [γ-^{32}P] labeled ATP (Perkin-Elmer). Samples were filtered and washed to remove unincorporated γ-^{32}P, then counted in a liquid scintillation counter (Packard 1600TR) (*191*).

2.13 Binding of unphosphorylated tau to microtubules

The binding of tau to microtubules was performed using the commercially available Microtubule Binding Protein Assay Kit (Cytoskeleton, Inc.) using the manufacturer's protocol. Varying concentrations of tau (0 µM–10 µM) were mixed with a constant concentration of paclitaxel stabilized microtubules at a final concentration of 1.6 µM tubulin dimers and 20 µM paclitaxel in a 50 µL reaction with the general tubulin buffer (GTB) supplied with the kit (80 mM PIPES, pH 7.0, 2 mM $MgCl_2$, 0.5 mM EGTA). Samples were incubated at room temperature for 30 minutes, and centrifuged at 23°C in 7 × 20 mm polycarbonate Beckman centrifuge tubes in a

Beckman TLA 100 rotor at 100,000 × g for 5 minutes to sediment both tau-free microtubules and tau-bound microtubules. Pellets were resuspended in 1× SDS sample buffer (0.0625 M Tris, 2% SDS, 10% glycerol, 5% β-mercaptoethanol) and tau bound to microtubules were separated from tubulin by electrophoresis. SDS-polyacrylamide gels were scanned with a Hewlett Packard Scanjet 7400 C and the density of the tau contained in the pellet (bound tau) was determined using Adobe Photoshop and a tau standard curve on the same SDS-polyacrylamide gel. Isoforms 0N3R, 0N4R, 1N3R, and tubulin have similar electrophoretic mobility. In order to distinguish tau from tubulin bands, the protein were transferred to PVDF by standard western blot techniques and probed with tau 46.1 primary antibody (gift from Lester I. Binder) and goat anti-mouse horseradish peroxidase conjugated secondary (Pierce). Amersham ECL Plus Western Blotting Detection System was used to detect the secondary antibody (GE Healthcare). The PVDF membrane was visualized using the Kodak Image Station 4000R (Eastman Kodak Co.). Band intensities were determined by the histogram function of Adobe Photoshop. The amount of free tau left in solution was determined by subtracting the amount of tau in the bound fraction from the total amount of tau added to the reaction and normalized to the band intensity of tubulin. The concentrations of tau free in solution versus bound tau were plotted in GraphPad Prism 4 and fit to a noncooperative single-site binding equation:

$$Free = \frac{B_{\max} * Bound}{k_d + Bound}.$$

Binding reactions were performed in triplicate for all tau isoforms.

2.14 Binding of phosphorylated tau to microtubules

Individual tau isoform phosphorylation reactions (92 μL), containing 18.11 μM final concentration of tau, 0.018 U GSK-3β per pmol of tau in buffer (40 mM HEPES, pH 7.64, 5 mM EGTA, 3 mM $MgCl_2$, and 2 mM ATP) were incubated for 20 hours at 30 °C to achieve maximal phosphate incorporation (*191*). Microtubule binding reactions were subjected to ultracentrifugation as described above and separated by SDS-polyacrylamide gel electrophoresis. 0N3R, 0N4R, and 1N3R were transferred to PVDF by standard western blotting techniques as described above, and PVDF blots were treated with shrimp alkaline phosphatase (Roche) before blocking, to remove the phosphate groups that interfere with tau 46.1 antibody binding. Images of gels and blots were collected and processed by methods described above, except that due to the large concentration of tubulin we were unable to normalize the data to the corresponding band. Due to variable data, 5 outliers were excluded from calculations based upon being more than twice as different as the corresponding trials. These points are 0N4Rp trial 3 1 μM and 2 μM, 1N3Rp trial 1 8 μM and trial 2 10 μM, and 2N3Rp trial 2 10 μM.

2.15 Hsp70 expression and purification

Hsp70 (HSPA1A) (Open Biosystems) was cloned into a pET28b vector (Novagen) with an N-terminal histidine tag and purified by nickel affinity chromatography using Chelating Sepharose Fast Flow (GE Healthcare) followed by size exclusion chromatography on a Superdex 200 column using a ÄKTA FPLC (GE Healthcare).

The concentration of the protein from pooled Superdex 200 fractions was determined by a commercially available BCA kit (Pierce). Purity was determined by running sub-microgram amounts on SDS-PAGE gels and staining with coomassie blue.

2.16 ARA, Congo red, or Heparin induced tau polymerization with Hsp70

ARA (Cayman Chemicals 90010.1, in ethanol) at a final concentration of 150 μM (the concentration of ethanol carrier was kept constant at 3.75% for all reactions), and individual tau isoforms at a final protein concentration of 4 μM, BSA at 0.25 μM (to prevent filament clumping at higher temperatures) were incubated with polymerization buffer containing (10 mM Hepes, pH 7.64, 100 mM NaCl, 0.1 mM EDTA and 5 mM DTT) for 18 hours at 37 °C (*51, 150, 191-194*). Congo Red (CR) (Sigma C6277, dissolved in water) at a final concentration of 10 μM, and 2N4R tau at a final protein concentration of 2 μM were incubated in polymerization buffer containing (100 mM NaCl, 10 mM Hepes, pH 7.64, and 5 mM DTT) for 18 hours at 37 ^{o}C (*195*). Heparin (Sigma H4784 Lot#116K1130, estimated molecular weight between 6-30 kDa dissolved in water) at 6 μg/ml and 2N4R tau at a final protein concentration of 2 μM were incubated in polymerization buffer containing (30 mM Hepes, pH 7.64, 17.74 mM NaCl and 5 mM DTT) for 18 hours at 37 °C (*51, 150*). Reactions with ARA, CR or Heparin were incubated with varying concentrations (0-2 μM) Hsp70 for 18 hours at 37 °C.

2.17 LLS kinetics with Hsp70 and 2N4R tau

4 μM 2N4R tau with 150 μM ARA was incubated in polymerization buffer containing 100 mM NaCl, 10 mM Hepes pH 7.64, and 5 mM DTT and varying concentrations of Hsp70 (0-0.5 μM). Reactions were read using LLS for 6 hours and kept at 37 ^{o}C between readings. Data was fit to the Finke-Watzky model (*196*):

$$Y = a - \left[\frac{\left(\frac{k_1}{k_2} + a \right)}{1 + \left(\frac{k_1}{k_2 * a} \right) e^{((k_1 + k_2 * a)x)}} \right]$$

Where Y equals the LLS intensity (arbitrary units), a is the maximum amount of polymerization (arbitrary units), k_1 is the inverse of the induction period (the time until a signal is observed) (minutes^{-1}), and k_2 is proportional to the rate of polymerization (AU/min).

2.18 ATP involvement in Hsp70 inhibition of ARA induced 2N4R tau polymerization

4 μM 2N4R tau was incubated in polymerization buffer (100 mM NaCl, 10 mM Hepes pH 7.64, 5 mM EGTA, 5 mM DTT) with 150 μM ARA, 0.25 μM BSA and varying conditions of ATP (0 mM- 2 mM), and Hsp70 (0 μM- 4 μM). Reactions were incubated 18 hours at 37 ^{o}C and analyzed by LLS and ThS fluorescence.

2.19 Addition of Hsp70 after 2N4R tau polymerization to determine if tau filaments can be disassembled

4 µM 2N4R tau was polymerized in the presence of 150 µM ARA in polymerization buffer (100 mM NaCl, 10 mM Hepes pH 7.64, 5 mM EGTA, 5 mM DTT, 0.25 µM BSA) for 6 hours at 37 ^{o}C. After polymerization, reactions were incubated with or with (1 µM Hsp70, 2 mM ATP, and 3 mM $MgCl_2$) 18 hours at 37 ^{o}C. EM grids of reactions after 6 hours and after 24 hours were analyzed by Image Pro Plus for length and distribution of tau filaments (see 2.21 for details).

2.20 50% inhibition of tau polymerization values

50% inhibition of tau polymerization was determined by normalizing data from LLS or ThS to 100% as the highest value of polymerization (Y-axis) and 0% as the lowest values of polymerization. The equation for the line between the two points where 50% (Y-axis) would lie was created for each trial. The specific equation for each trial of each isoform was then used to find the concentration of Hsp70 (x-value) by inserting 50 as the y-value (%) and solving for x.

2.21 Analysis of electron microscopy images with Image Pro Plus

TEM images were analyzed for the number of filaments and the length of individual filaments per field using Image Pro Plus 6 (Media Cybernetics). Electron dense material is visualized in the images as black objects on the grey background and represents where uranyl acetate has collected, primarily on assembled tau filaments.

Images were set to a threshold so that electron dense filamentous material was within the range, but any non-specific background material was not included. The program also ignores any dense material that does not meet defined length and area criteria. 0 µM 2N4R tau, 2 µM Hsp70 controls were used to determine background material, which is used as the criteria for quantitation. Analysis showed the average length of the electron dense material to be 25 nm and 15 nm wide. Objects that were longer than 25 nm, and having an area greater than 375 nm^2 (25 nm long and 15 nm wide (average filament width)) were counted, measured for length, and exported to Microsoft Excel. Objects from each image were sorted into three categories. Objects greater than and equal to 25 nm and less than 50 nm are considered "small", objects greater than and equal to 50 nm and less than 100 nm are considered "medium" and objects greater than and equal to 100 nm are considered "large". These cutoffs were chosen based upon previous observations that most tau filaments are between 50 nm and 100 nm. Data for approximately 0%, 50%, and 100% inhibition of tau polymerization by Hsp70 was plotted as the mean ± SEM of 5 images per reaction.

2.22 Microtubule assembly assay and data fitting

Microtubule assembly assays were performed using a commercially available DAPI fluorescence based porcine tubulin polymerization assay kit BK011P (Cytoskeleton), using the manufacturer's protocol for enhancers of tubulin polymerization (no glycerol). Every reaction used the same preparation of tubulin, Hsp70 and tau isoform and was performed in the absence of ATP. Reactions were incubated at 37

^{o}C and were read every minute for an hour using a Molecular Devices Flexstation II plate reader with an excitation of 355 nm and an emission of 455 nm. Tubulin polymerization reactions containing taxol alone, Hsp70 alone, and polymerization buffer alone were used as controls. Data for microtubule assembly reactions was normalized to taxol assembled microtubule reactions that were run at the same time to adjust for any variability in tubulin polymerization. Normalized data was fit to the Gompertz growth curve (*197*), defined as:

$$Y = ae^{-e^{-\frac{x-c}{b}}}$$

where *Y* is the relative fluorescence level, *a* is the maximum amount of fluorescence, *x* is time, *b* is $1/k_{app}$ and k_{app} is proportional to the rate of polymerization, and *c* is the point of greatest increase in *Y*. Lag time to significant polymerization (calculated by *c*-*b*), k_{app} and max were determined from the equation for 3 separate trials with or without Hsp70 and averaged as the mean ± SEM.

Chapter 3- The Effects of Inducer Molecules and Post-translational Modifications on Tau Polymerization

Part 1. ARA and heparin induced 2N4R Tau Polymerization In Vitro

Work on in vitro modeling of arachidonic acid and heparin induced 2N4R tau polymerization was a collaborative effort that I contributed to. It is presented here as data that is not entirely my own. Figures are reproduced from: Carlson SW, Branden M, Voss K, Sun Q, Rankin CA, and Gamblin TC, A complex mechanism for inducer mediated tau polymerization, Biochemistry 2007, 46, 8838-8849. http://www.ncbi.nlm.nih.gov/pubmed/17608454

3.1.1 Introduction

Amyloid polymerization in general is thought to follow a nucleation-elongation mechanism. This means that the protein forming amyloid must first form a nucleus that acts as a source for other monomers to add and elongate. Tau protein is thought to follow a similar mechanism. It has been shown that wild-type tau incubated at high concentration of protein and long incubation times fails to polymerize in vitro (*198*). Therefore, in order to research tau polymerization we must add inducer molecules that reduce the energetic barrier for polymerization to proceed. This energetic barrier for nucleation depends on the hydrophobicity and β-sheet formation properties of the protein (*199*). The energic barrier is defined as the critical concentration of polymerization, below which elongation does not proceed. The physiological inducer(s) of tau polymerization in a neuron are not known, if there are

any. However, addition of ARA or heparin will cause tau to form filaments that are structurally similar (formation of cross β-sheet structure) to those isolated from tau inclusions from the brains of AD patients (*200*). Other similarities between aggregated tau from the brains of AD patients and aggregated tau from in vitro reactions include similar densities, widths of ~15 nm, ThS positive and Alz50 antibody reactivity (*201, 202*). The work presented here describes a different mechanism upon the addition of inducer molecules to alter tau polymerization from the standard nucleation-elongation mechanism to one that depends on the concentration of the inducer molecule that allosterically regulates polymerization. This means that at low inducer levels tau polymerization is low, but increases upon addition of more inducer. After an optimal ratio of inducer to protein, polymerization decreases upon addition of more inducer, indicating the inducer inhibits the formation of filaments. The inducer also lowers the critical concentration of polymerization to nearly zero; meaning formation of nuclei is spontaneous. Here we describe a role ARA and heparin play in formation of 2N4R tau filaments in vitro.

3.1.2 Results

3.1.2.1 ARA and heparin induced formation of tau filaments

The formation of tau aggregates in neurons correlates with cognitive impairment, however, the mechanism of formation is not known. Likewise, modifications to tau could alter how polymerization proceeds. As a first step to understand aggregation, we examined full length wild type 2N4R tau in vitro. Previous studies have

examined tau polymerization using two main inducer molecules. ARA is a poly-unsaturated fatty acid with one negative charged group at one terminus and heparin sulfate is a glycosaminoglycan that has multiple negative charges along the entire molecule. In the absence of inducer, tau fails to polymerize even when tau concentrations are increased (Figure 3.1A, B). In the presence of either ARA (75 μM) (Figure 3.1C) or heparin (0.376 μM) (Figure 3.1E) tau polymerization can be detected by both LLS and ThS. Polymerization of tau with ARA and heparin also increases as the concentration of tau increases (Figure 3.1C, E). There is an obvious difference in the morphology of tau filaments upon polymerization. ARA mediated tau polymerization produces more numerous, but shorter filaments than heparin (Figure 3.1D, F). The pathological or toxic consequences of the morphologies are not known, but the morphologies are similar, as they represent straight filaments seen in AD extracted insoluble tau.

3.1.2.2 Polymerization of 2N4R tau with ARA and heparin produces a biphasic dose response

When 2N4R tau at various concentrations (0-4 μM) was incubated with various concentrations of ARA (0-300 μM) (Figure 3.2A) or heparin (0-2 μM) (Figure 3.2B), and examined by ThS, a biphasic dose response curve resulted. This biphasic response indicates that at low inducer to protein levels the concentration of inducer limits the amount of elongation that can proceed. We know this because the addition of more inducer increases the amount of polymerization. Polymerization at high

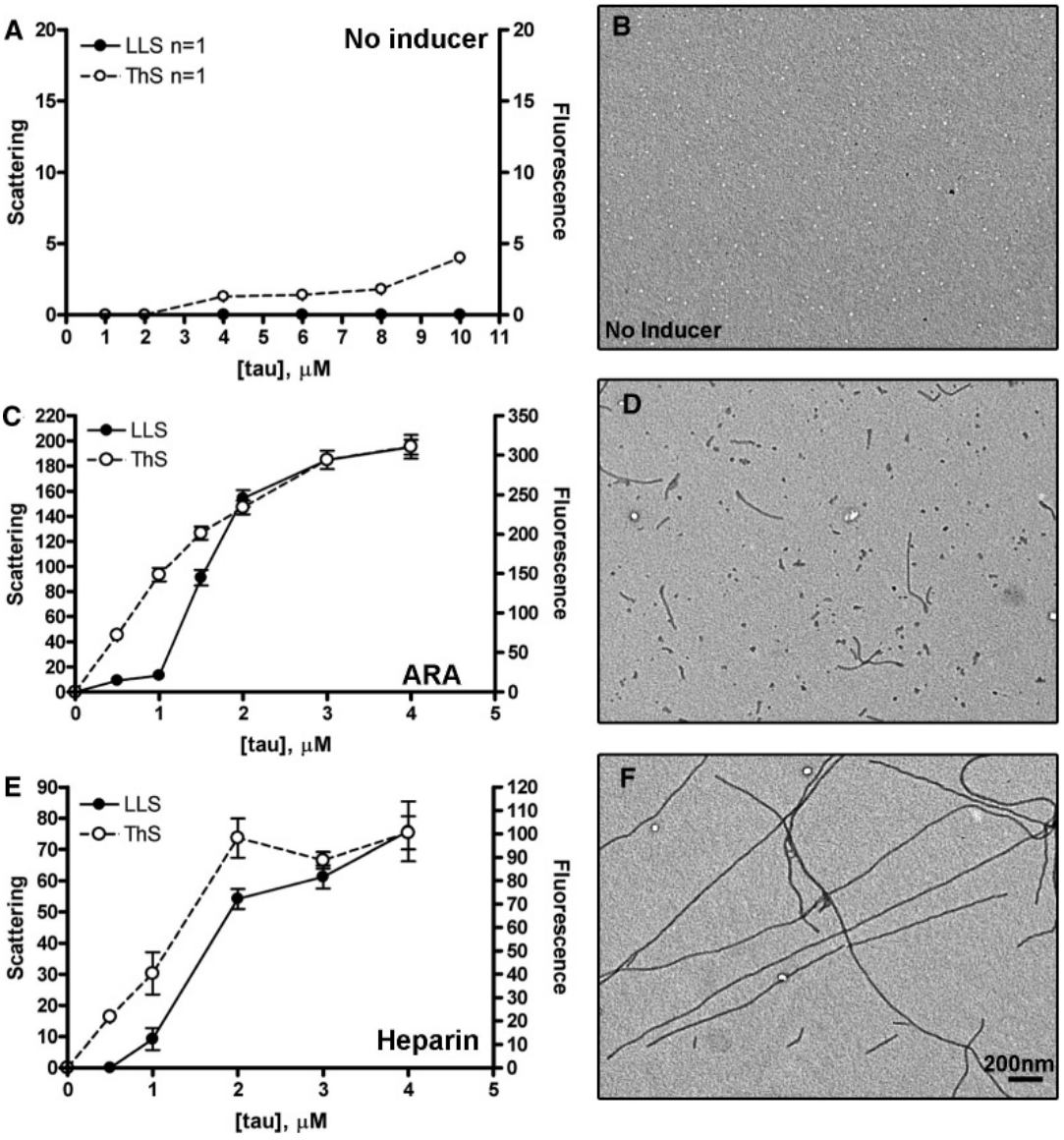

Figure 3.1 Nonlinearity of tau polymerization with regulatory molecules. Tau protein at various concentrations (*x*-axis) was incubated alone (A and B), with 75 μM ARA (C and D), and with 0.376 μM heparin (E and F) for approximately 16 h, and the final extent of polymerization was determined by LLS (●, left *y*-axis) and ThS fluorescence (○, right *y*-axis). The presence or absence of filaments was confirmed by EM (B, D, and F). Note that the scales of the *x*-axes and *y*-axes are different for the different conditions because virtually no polymerization was observed without regulatory molecules, and ARA gave a much stronger signal than did heparin under these conditions. Data in A represent a single experiment. C and E show an average of three experiments ± SEM. The scale bar in F represents 200 nm and applies to each micrograph.

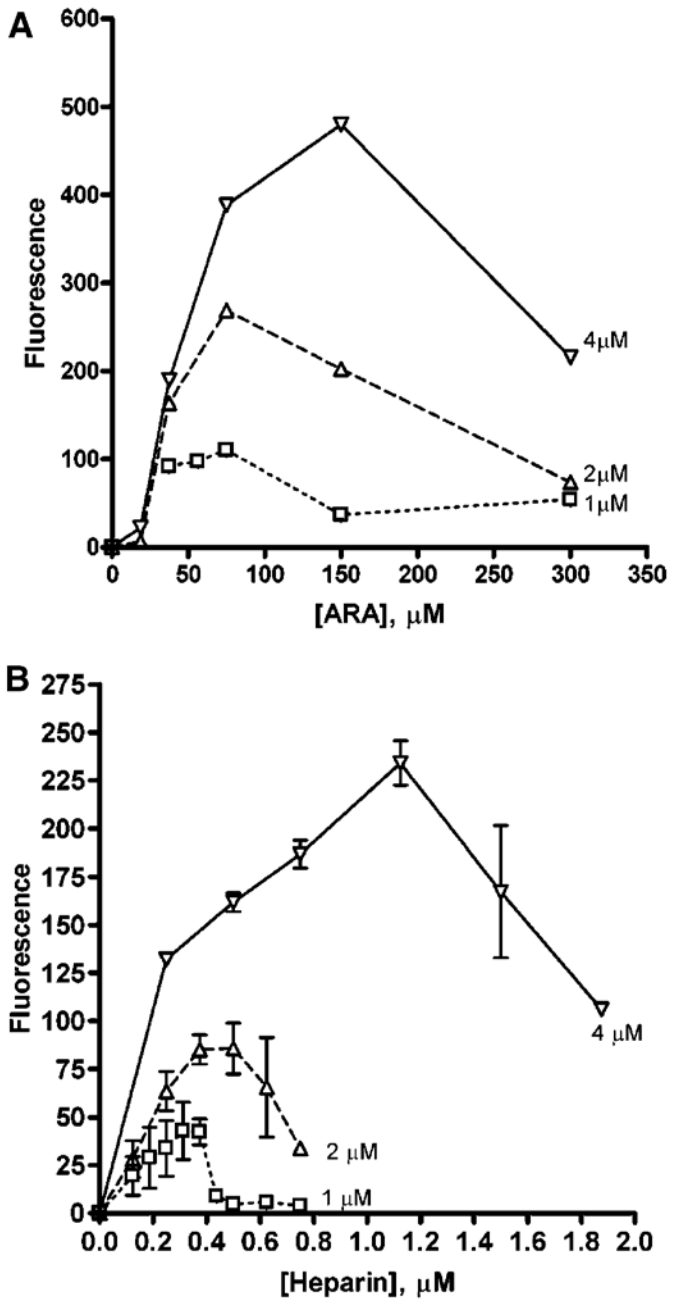

Figure 3.2 Variation of regulatory molecule concentrations in tau polymerization reactions. Tau polymerization reactions at 1 (□), 2 (△), and 4 (▽) μM protein concentration were mixed with various concentrations (x-axis) of (A) ARA or (B) heparin and incubated for approximately 20 h. ThS was added at a final concentration of 20 μM, and the amount of resulting fluorescence was determined. The error bars denote ± SEM.

inducer to protein levels in inhibited by the inducer concentration. We know this because the addition of more inducer results in less polymerization. In between these two parts of the curve lies an optimal amount of inducer to protein at which we achieve the maximum amount of polymerization. The optimal ratio of inducer for ARA: tau was 37.5:1, while for heparin the ratio was 0.188:1. This difference in the optimal ratio indicates that inducer mediated polymerization may follow different mechanisms based upon the inducer used.

The filament morphology of ARA-mediated tau polymerization changes at different ratios (Figure 3.3). At an inhibitory ratio, tau filaments are short (<50nm), similar to what has been described as a potential toxic species of tau isolated from AD neurons (Figure 3.3A, B). As the ratio shifts to the optimal ratio, longer filaments begin to form (Figure 3.3C). Increasing the protein concentration, even more, to shift the ratio to a limiting ratio, results in a shift to even longer filaments (Figure 3.3D, E). Knowing the optimal ratio is important because if reactions are carried out at lower or higher ratios, the results are skewed to what looks like longer or shorter filaments, and more or less polymerization than another form of tau that may have a different optimal ratio. Likewise, in a cell, having a small amount of heparin can polymerize tau, while higher concentrations of ARA would be required for polymerization to proceed. This may indicate that there is interplay of inducers, where small amounts of heparin could initiate formation, but then be inhibited by increasing concentrations of heparin. At this point if the concentration of ARA increased to a level that

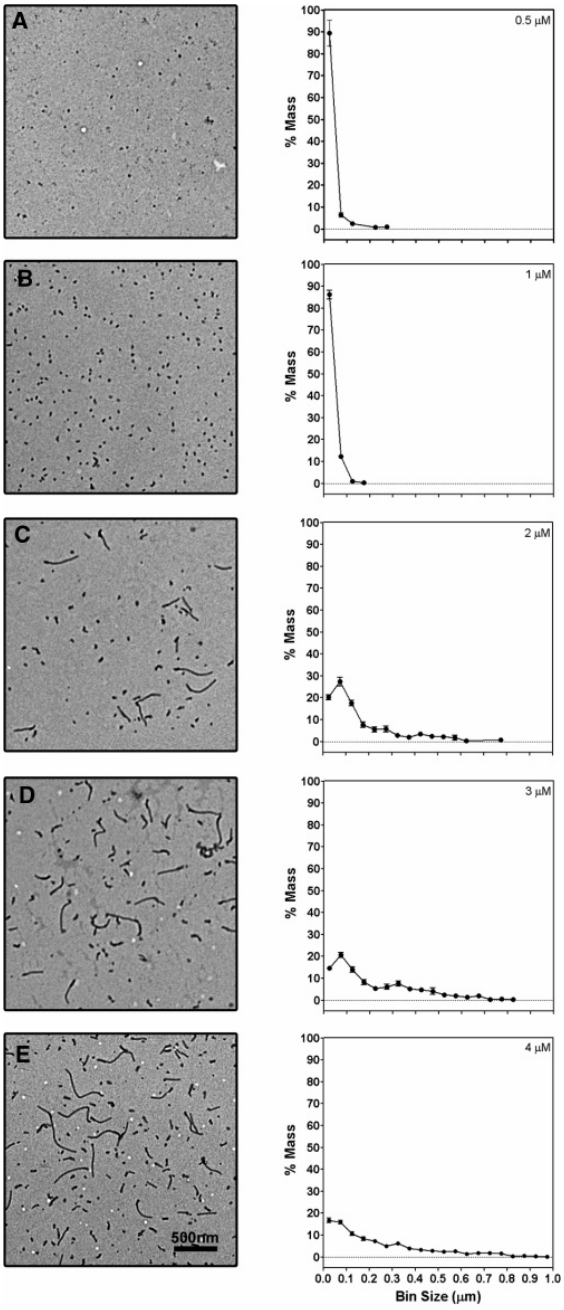

Figure 3.3 Length distribution of tau filaments changes as a function of protein concentration. Representative electron micrographs taken at 20,000x (the bar in E represents 500 nm and is applicable to all images) for polymerization reactions in the presence of 75 µM ARA following approximately 16 h of polymerization are shown for several different concentrations of tau: (A) 0.5 µM; (B) 1.0 µM; (C) 2.0 µM; (D) 3.0 µM; and (E) 4.0 µM. The average mass frequency distributions are shown for each of these concentrations and are plotted as the percent of the total mass that one bin represents (*y*-axis) vs. the center of the bin size (*x*-axis).

promoted filament formation, ARA could take over as an inducer for polymerization.

3.1.2.3 2N4R polymerization kinetics with ARA

By changing the concentrations of inducer at a specific tau concentration, we observe changes in the kinetics of polymerization and filament morphology. Polymerization reactions with ARA (Figure 3.4) were measured over time using ThS fluorescence at a limiting, optimal and inhibitory ratio. Data in Figure 3.4A, C, and D was fit to a one phase exponential association equation:

$$Y = Y_{\max}\left(1 - e^{(-Kt)}\right).$$

Where increases over time t, in polymer from zero to Y_{max}, have a rate constant K. The half time of the reaction to reach equilibrium, $t_{1/2}$, is defined as 0.69/K. With ARA, there was no change in the $t_{1/2}$ or K, for a given ratio, with increasing protein concentration (Figure 3.4E, F). Between ratios, the $t_{1/2}$ decreased significantly for the inhibitory ratio, but was not significantly affected for the limiting ratio as compared to the optimal ratio (Figure 3.4E). The rate of polymerization, K, was unchanged between the optimal and limiting ratios, but significantly higher in the inhibitory ratio (Figure 3.4F). In order to determine the size of the nucleus for polymerization, data for the optimal ratio was also fit to a nucleation equation:

$$\frac{dC}{dt} = K_{n-1}k^{+}\left(T_1\right)^{n-1}\left(T_1 - T_1^{\infty}\right)$$ (Figure 3.4B).

Where C is the polymer addition sites concentration, T_1 is tau monomer concentration, T_1^{∞} is the critical concentration, k^+ is the rate constant for elongation, K_{n-1} is the association constant for nuclei formation, and n is the size of the nucleus. By inserting many combinations of different values for K_{n-1}, k^+, and n we can fit the data at a particular protein concentration, but there is only one combination that allows all protein concentrations to be fit at the same time (*190*). The only nucleus size that fit all protein concentrations was zero, indicating that addition of ARA reduces the nucleation (critical concentration) to zero (Figure 3.4B) When combined with EM data, this kinetics data suggests that the inhibitory ratio blocks elongation of filaments by creating a burst of nucleation of tau, in which not enough tau monomer remains to be incorporated into filaments.

3.1.2.4 2N4R polymerization kinetics with heparin

The kinetics of formation in the presence of heparin was also measured with increasing tau concentrations at optimal, limiting and inhibitory ratios (Figure 3.5A-C). Data was fit to the one phase exponential association equation described above. Again, at a given ratio, the $t_{1/2}$ and K were similar for all protein concentrations. The optimal and limiting ratios had a similar $t_{1/2}$, but the inhibitory ratio had a significantly increased $t_{1/2}$, inverse to what was observed with ARA (Figure 3.5D).

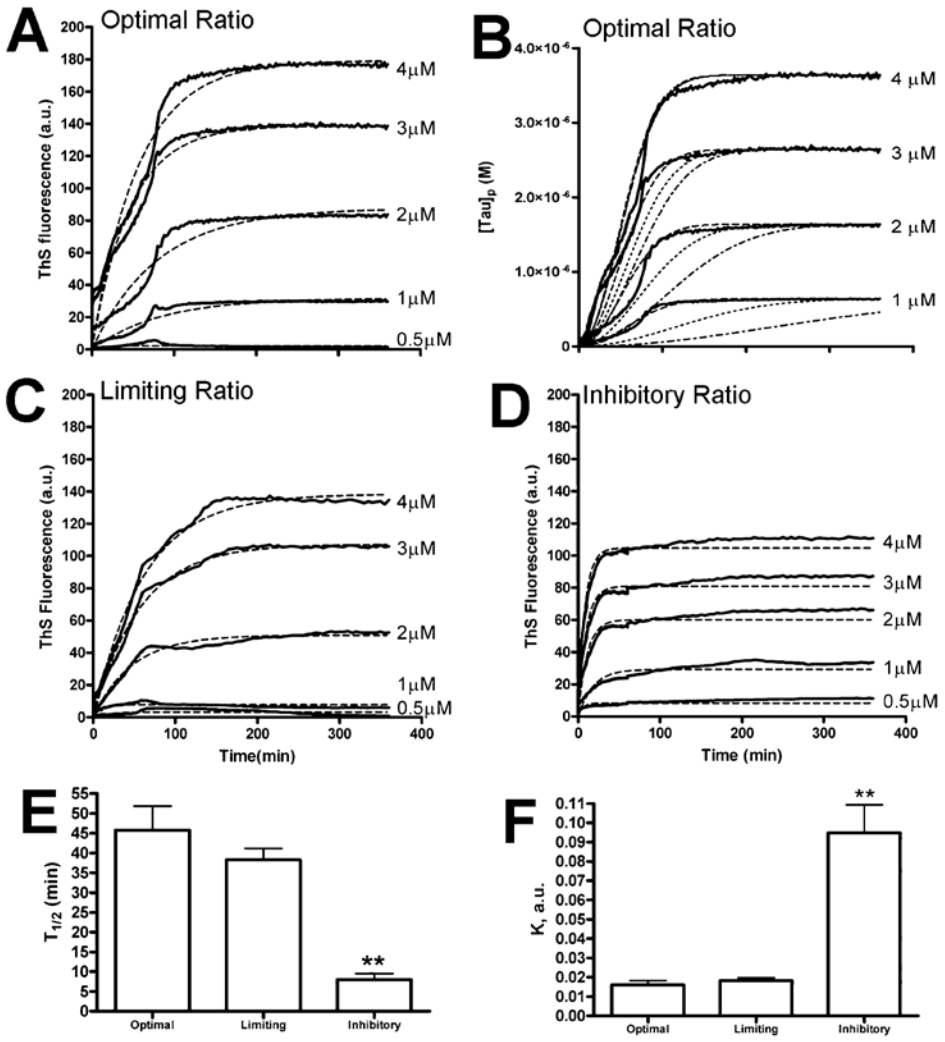

Figure 3.4 Kinetics of ARA induction of tau polymerization. The kinetics of tau polymerization was followed with ThS fluorescence at a constant molar ratio of (A) 37.5:1 (Optimal), (B) 37.5:1 (Optimal), (C) 18.75:1 (Limiting), and (D) 75:1 (Inhibitory) at 0.5, 1, 2, 3, and 4 μM tau (( ), individually labeled on graph) . The data in A, C, and D were fit to a single phase exponential association equation to obtain the values for (E) $t_{1/2}$ and (F) K. The data in E and F are the average values ± SEM for all polymerization reactions that had final polymerization values of more than 10 ThS units. The asterisks denote values that were significantly different from optimal conditions using a t-test ($p<0.01$) The data in (B) was converted to molar concentrations of tau assuming the ThS fluorescence at steady state was equal to the polymer concentration (calculated by subtracting the critical concentration from the total concentration) and fit to equations derived for the kinetics of actin nucleation and polymerization (*190*) using n = 0, $k^+K_{nuc} = 5\text{x}10^{-4}$ $s^{-2}M^{-4}$ (---), n = 1, $k^+K_{nuc} = 1.2\text{x}10^{2}$ $s^{-2}M^{-4}$ (···), and n = 2, $k^+K_{nuc} = 3\text{x}10^{7}$ $s^{-2}M^{-4}$ (·-·-).

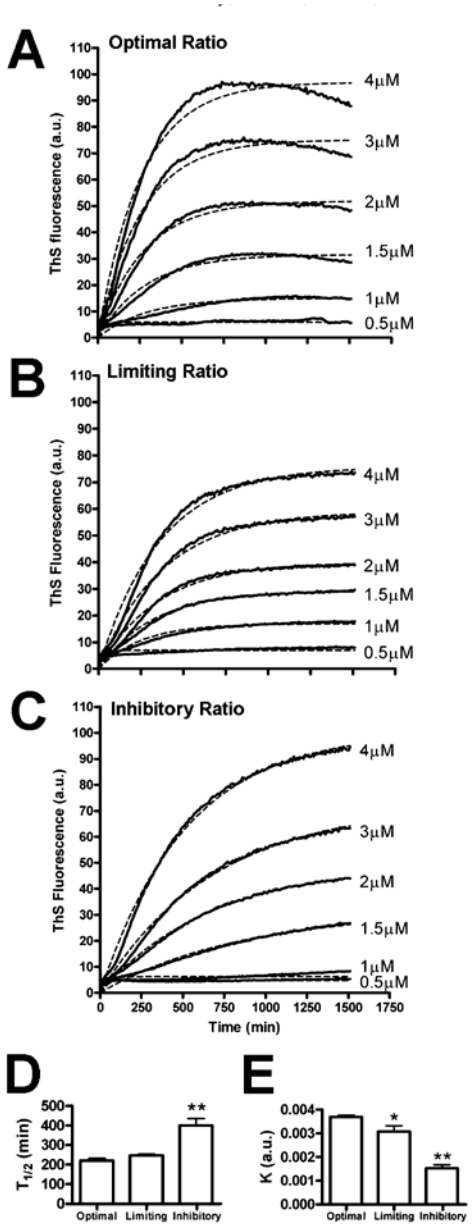

Figure 3.5 Kinetics of heparin induction of tau polymerization. The kinetics of tau polymerization was followed with ThS fluorescence at a constant molar ratio of (A) 0.188:1, (B) 0.094:1, and (C) 0.376:1 at 0.5, 1, 1.5, 2, 3, and 4 μM tau, ((individually labeled on graph). The data were fit to a single phase exponential association equation to obtain the values for (D) $t_{1/2}$ and (E) *K*. The data in D and E are the average values ± SEM for all polymerization reactions that had final polymerization values of more than 10 ThS units. The asterisks denote values that were significantly different from those at optimal conditions using a t-test (* = $p<0.05$, ** = $p<0.01$).

The rate of formation was significantly affected for the limiting ratio, and affected even greater for the inhibitory ratio as compared to the optimal ratio (Figure 3.5E). The rate of formation for heparin was slower than that observed for ARA, and in conjunction with EM data which shows fewer but longer filaments, indicates heparin does not nucleate tau as well.

3.1.3 Conclusions

Understanding the mechanisms by which tau polymerization proceeds provides insight into how progression of tauopathies can occur. The work presented in Chapter 3 Part I has provided insight into these mechanisms for full length wild type tau, under the control of two distinct inducers of polymerization. Our tau polymerization results agree with previous results (*203*) and is enhanced in the presence of both inducers, as compared to no inducer which fails to polymerize even at high protein concentrations and long incubation times. The inducers lower the critical concentration for polymerization to near zero, indicating tau in the presence of inducers does not follow the traditional nucleation-elongation mechanism. This is confirmed with our kinetics analysis of ARA and heparin induced polymerization, where the lag phase characteristic of nucleation is not present. These inducers also act as allosteric regulators of tau polymerization, where at low concentrations of inducer, tau cannot polymerize as effectively as when more inducer is added. Eventually, an optimal ratio is reached, which is different for the two inducers used, and addition of more inducer inhibits the formation of tau polymer. This inhibition

occurs by creating many short filaments that indicates a burst in nucleation that removes enough monomer from the solution that elongation cannot occur. This could have consequences for disease in that local concentrations of ARA could create a burst in short tau polymer that provides a source for later elongation to occur. This research has provided a foundation for examining tau polymerization in vitro. However, tau exists in neurons as six alternatively spliced isoforms that can be phosphorylated. In Chapter 3 Part II, we will examine differences in wild-type and phosphorylated tau isoforms in respect to polymerization and function.

Chapter 3 Part II- GSK-3β Phosphorylation Differentially Affects Tau Isoform Dysfunction and Function

Voss and Gamblin, Mol. Neurodegen., 2009, 4:18, http://www.molecularneurodegeneration.com/content/4/1/18

3.2.1 Introduction

Tauopathies, such as Alzheimer's disease (AD), are characterized by the abnormal aggregation of a hyperphosphorylated microtubule associated protein, tau. The aggregation and phosphorylation of tau correlates with neurodegenerative changes in these diseases (reviewed in (*204*)). It is therefore generally believed that aggregation and phosphorylation changes are causative factors in the etiology of tauopathies. One complicating factor to these observations is that tau mRNA is alternatively spiced to give rise to six protein isoforms. The isoforms are generated by splicing of exons 2, 3 and 10, which encodes for microtubule binding repeat 2, giving rise to isoforms with three microtubule binding repeats (3R) or four (4R) (*5*). The levels of 3R and 4R tau do not differ between normal and AD brains, but in both cases, the levels of alternatively spliced N-terminal exons differ. Isoforms with only exon 2 are the most abundant, followed by isoforms without N-terminal exons and isoforms with both exons 2 and 3 are the least abundant (*11*). In other tauopathies, the ratio of 3R isoforms to 4R isoforms can be altered (reviewed in (*30*)). For example, progressive supranuclear palsy (PSP) can be accompanied by increases in 4R tau, while Pick's Disease is often characterized by an increased amount of 3R isoforms (reviewed in (*30*)). These increases have been explained in part by intronic mutations that promote

or hinder splicing of exon 10, but have no effect on the protein sequence (reviewed in (*205*)). The above observations suggest that a shift in isoform expression may contribute to neurodegenerative changes in tauopathies. However, the individual contributions of tau isoforms to the neurodegenerative process are not well understood. One possibility is that the inherent differences between isoforms are sufficient to cause neurodegenerative changes when their relative levels are altered.

Tau polymerization into filaments similar to those observed in neurodegenerative diseases can be modeled in vitro by the addition of inducer molecules such as arachidonic acid (ARA) and heparin (reviewed in (*203*)) in a complicated fashion (see Chapter 3 Part I) (*51*). It is currently unknown whether different isoforms share ARA and heparin-induced polymerization profiles similar to 2N4R tau.

In addition to being abnormally polymerized, tau has been shown to be hyperphosphorylated in AD pathology. "Hyperphosphorylated" is a loosely defined term used to describe abnormally or inappropriately phosphorylated tau in AD. Although there is not a strict definition, some properties of hyperphosphorylated tau include altered electrophoretic mobility, conformational changes, increased levels of phosphate incorporation, and site-specific inappropriate phosphorylation (*206-208*). While it is not known how hyperphosphorylated tau is generated, glycogen synthase kinase-3β (GSK-3β) is widely believed to play a role in this process (reviewed in (*207*)). In vitro, GSK-3β phosphorylates tau at 14 sites that overlap with AD-tau, as

determined by mass spectrometry, and phosphorylation site-specific antibodies (*191, 193, 209, 210*). In vivo, treatment of transgenic mouse models of tau-induced neurodegeneration with lithium chloride, an inhibitor of GSK-3β, reduces both tau phosphorylation and resulting tau pathology (*211*), (*212*). Phosphorylation of 2N4R tau in vivo by GSK-3β has reduced affinity for microtubules (*213*) and phosphorylation of 0N3R tau in vitro by GSK-3β shows mild changes in affinity of tau for microtubules (*214*). Recombinant 2N4R tau phosphorylated by GSK-3β, upon polymerization with an inducer, forms structures that resemble neurofibrillary tangles in vitro (*51, 193*). However, it is not known how GSK-3β phosphorylation affects the other tau isoforms, and given their differences in primary structure, it is possible that phosphorylation will have differential impacts on their function. We have therefore characterized the polymerization and microtubule binding properties for each isoform, and the effect that phosphorylation by GSK-3β has on these properties. We have found that there are fundamental differences in the functions of 3R and 4R isoforms. These differences are largely determined by the presence or absence of exon 10, with some contributions from exons 2 and 3. Phosphorylation by GSK-3β modulates the function of tau, but only mildly. The data suggest that phosphorylation alters all isoforms to approximately the same degree. These results suggest that the inherent properties of the isoforms are primarily responsible for their variable involvement in disease pathology, rather than the differential effects brought about by GSK-3β phosphorylation.

3.2.2 Results

3.2.2.1 Tau isoforms

The tau transcript is alternatively spliced in humans to form six isoforms. These isoforms (0N3R, 0N4R, 1N3R, 1N4R, 2N3R, 2N4R) are classified by the presence or absence of N-terminal exons 2, 3, and C-terminal exon 10 (containing microtubule binding repeat 2) (see Chapter 1). We expressed and purified each recombinant isoform from *E. coli* (Figure 3.6). The isoform identity was confirmed by molecular weight determination on coomassie stained-sodium dodecyl sulfate polyacrylamide gel electrophoresis (SDS-PAGE) as compared to expected values in the literature (*188*, *208*).

3.2.2.2 Isoform differences in ARA induced polymerization

Because the primary sequences of the tau isoforms are different, the various combinations of exons could influence their interactions with inducer molecules or cause conformational changes affecting tau-tau interactions during the polymerization process. The polymerization characteristics of each isoform was determined by incubating 2 μM protein with a range of ARA concentrations (0–150 μM) and monitoring the extent of polymerization with right angle laser light scattering (LLS, Figure 3.7A) and thioflavine S fluorescence (ThS, Figure 3.7A). We determined that above 100 μM ARA, the results were highly variable and not easily reproducible (data not shown). This is consistent with previously published results showing high variability at the inhibitory ratio of inducer to 2N4R tau (Chapter 3 Part 1 and (*51*)).

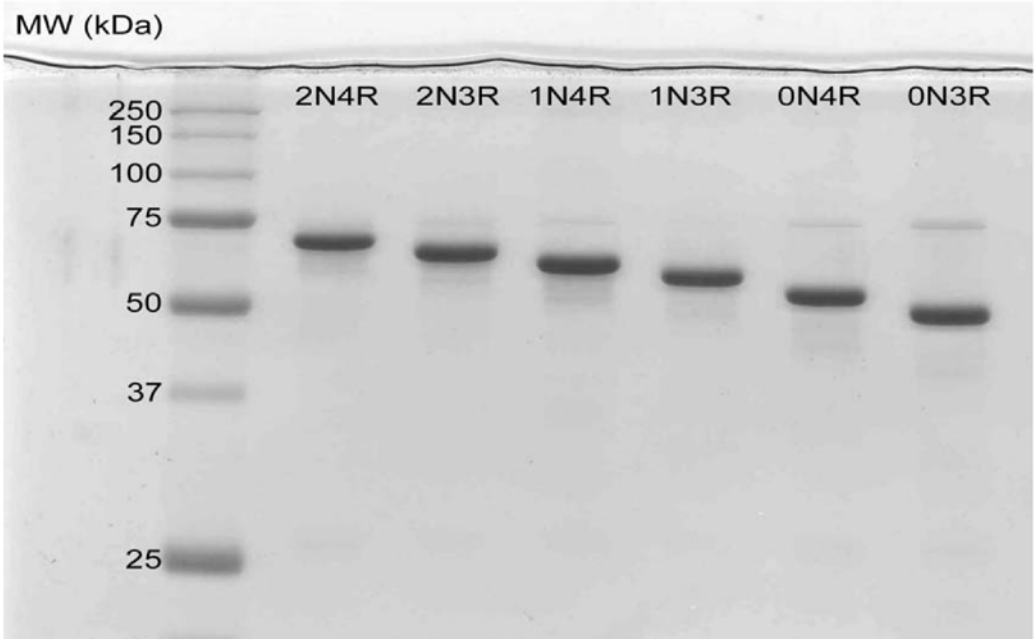

Figure 3.6 Variation between tau isoforms. The six tau isoforms differ in the presence or absence of N-terminal exons 2 and 3 and the presence or absence of exon 10 in the microtubule binding domain. Each lane is labeled with the name of the isoform analyzed. Each isoform migrates a distinct distance on a Coomassie stained 10% SDS-polyacrylamide gel.

The isoforms followed the same general trend of increased amounts of polymerization with increased inducer concentrations. 4R tau isoforms (containing exon 10) polymerized to a greater extent than 3R isoforms (Figure 3.7A, B), indicating that the additional microtubule binding repeat enhances tau polymerization. The resulting filaments from the polymerization reactions above were viewed by transmission electron microscopy (TEM, Figure 3.7C–H). At equivalent ARA concentrations (75 μM), the greatest amount of filament formation was observed with the 1N4R and 2N4R isoforms (Figure 3.7G, H). Fewer filaments were observed for 1N3R and 2N3R (Figure 3.7D, E). Isoforms lacking both N-terminal exons (0N3R and 0N4R, Figure 3.7C, F) tended to form very small filaments (< 50 nm), as has been described previously (*188*), but large aggregates of longer filaments were also observed, albeit infrequently (Figure 3.8). We, and others, have found that while aggregates of tau polymer can be detected by LLS and ThS fluorescence, these aggregates may not be uniformly distributed on a TEM grid, resulting in the user not being able to see these aggregates unless they scan the entire grid.

3.2.2.3 Isoform differences in heparin induced polymerization

Because it is known that some isoforms do not polymerize equally in the presence of heparin (*215*), the polymerization characteristics for all six isoforms were determined under conditions of low ionic strength (*216, 217*). The isoforms (2 μM) were incubated in the presence of various concentrations (0–0.024 mg/ml) of heparin and polymerization measured by LLS (Figure 3.9A) and ThS fluorescence (Figure 3.9B).

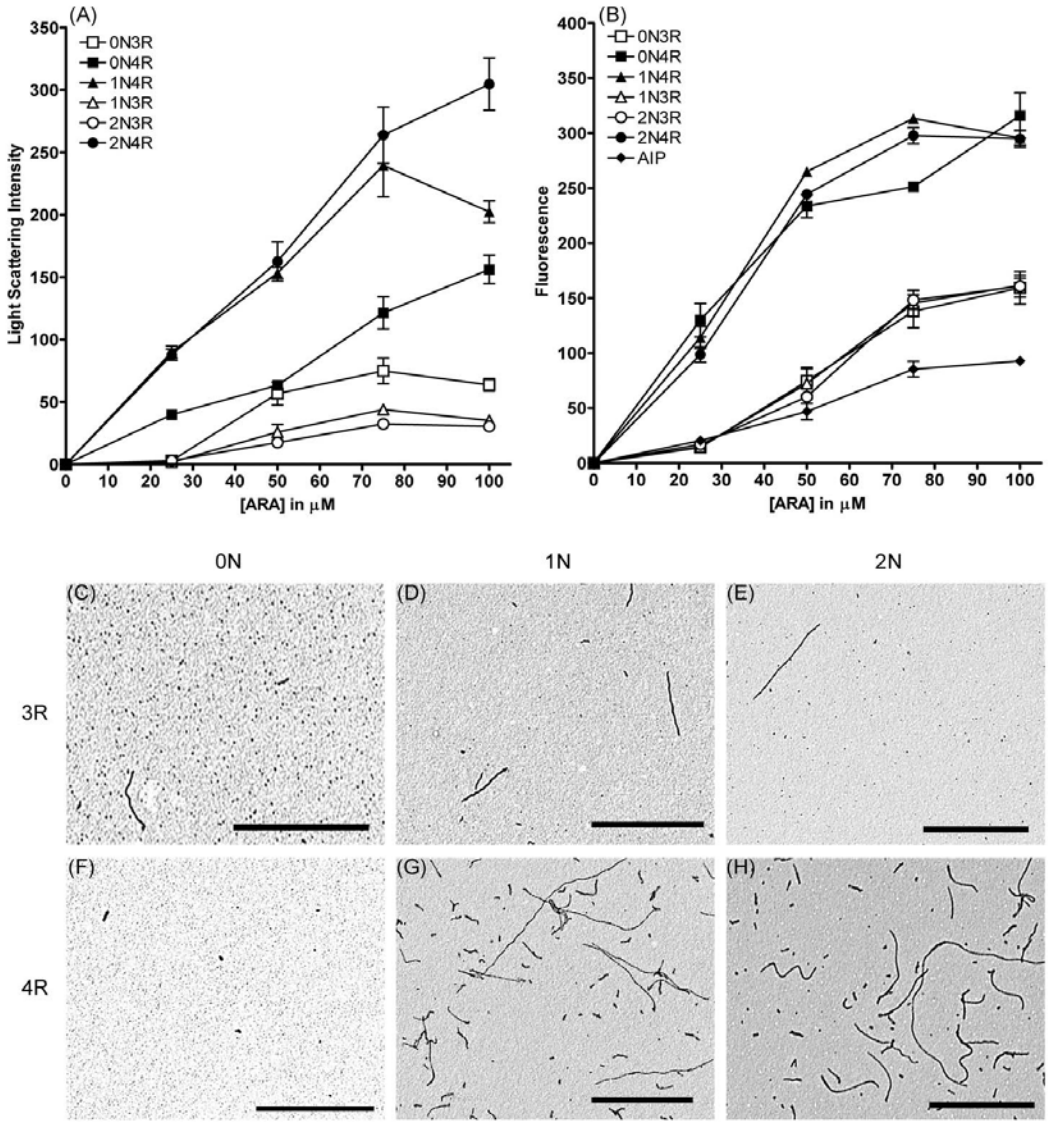

Figure 3.7 ARA induction of tau isoform polymerization. 2 μM tau isoforms were incubated with various ARA concentrations (0 μM to 100 μM) for 18 hrs. Polymerization was measured by (A) LLS or (B) ThS fluorescence. Symbols correspond as follows: (open square) 0N3R, (closed square) 0N4R, (open triangle) 1N3R, (closed triangle) 1N4R, (open circle) 2N3R, (closed circle) 2N4R, and (closed diamond) assembly incompetent protein (AIP (I277, 308P)). Data is in arbitrary units and represents an average of 3 trials ± SEM. After 18 hours, ARA induced polymerization reactions were visualized by TEM at 20,000x magnification. Images are as follows: (C) 0N3R, (D) 1N3R, (E) 2N3R, (F) 0N4R, (G) 1N4R, and (H) 2N4R. Each isoform image is representative of polymerized material at 75 μM ARA. Scale bars represent 1 μm.

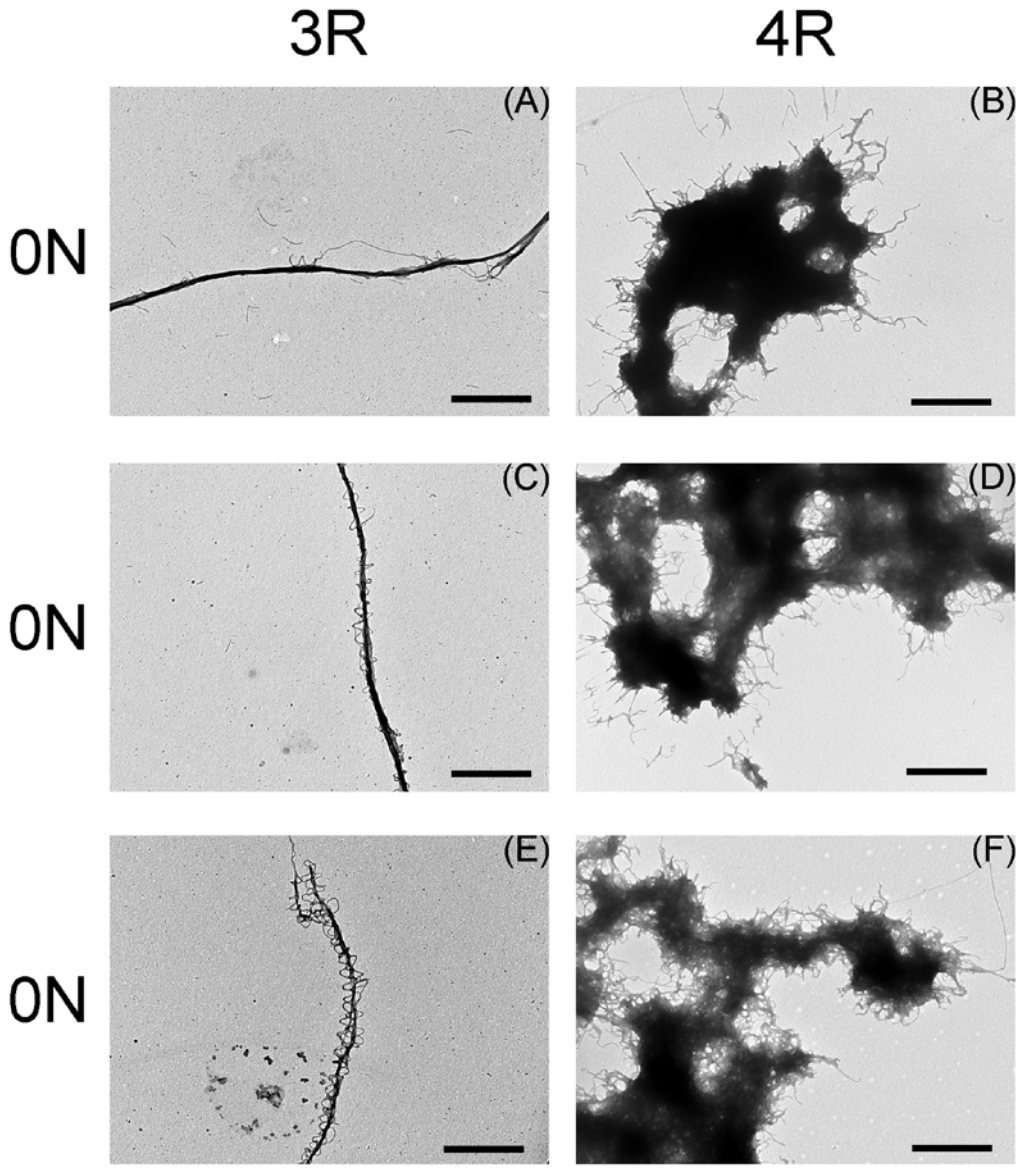

Figure 3.8 Polymerization of 0N3R and 0N4R isoforms with 75 μM ARA into larger aggregates is seen, but infrequent. 0N3R (A, C, E) and 0N4R (B, D, F) isoforms exhibit filament elongation and clustering under nonphosphorylated conditions. Reactions from Figure 3.7 were visualized by TEM at 20,000× magnification. Each image is from a different trial, and was found to occur at about 1–3 times per grid. Scale bars represent 1 μm.

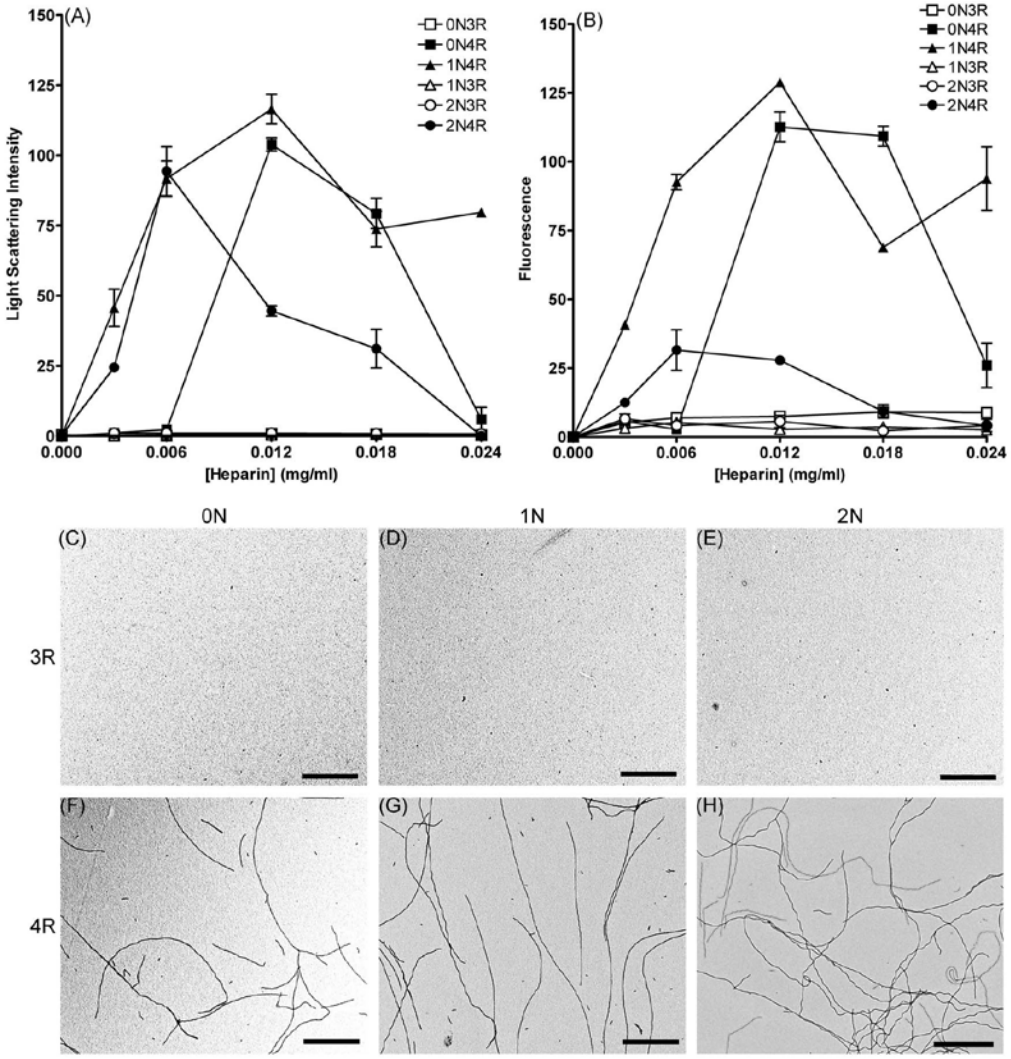

Figure 3.9 Heparin induction of tau isoform polymerization. 2 μM tau isoforms were mixed with various heparin concentrations (0 mg/ml to 0.024 mg/ml) and incubated 18 hrs. Polymerization was measured by (A) LLS or (B) ThS fluorescence. Symbols correspond as follows: (open square) 0N3R, (closed square) 0N4R, (open triangle) 1N3R, (closed triangle) 1N4R, (open circle) 2N3R, (closed circle) 2N4R. Data is in arbitrary units and represents an average of 3 trials ± SEM except for 2N4R with 0.006 and 0.018 mg/ml heparin, 1N4R with 0.024 mg/ml heparin, and 0N4R with 0.018 mg/ml heparin which were 2 trials. After 18 hours, heparin induced polymerization reactions were visualized by TEM at 20,000× magnification. Images are as follows: (C) 0N3R, (D) 1N3R, (E) 2N3R, (F) 0N4R, (G) 1N4R, and (H) 2N4R. Each isoform image is representative of polymerized material at 0.006 mg/ml heparin. Scale bars represent 1 μm.

Polymerization was detected by both methods for the 4R isoforms, and the dose-response curve was biphasic, indicating an optimal inducer concentration for polymerization. 2N4R required a lower concentration of heparin for optimal polymerization than 0N4R and 1N4R. Under these heparin induction conditions, the 3R isoforms failed to polymerize to detectable levels above background (Figure 3.9A and 3.9B). 4R isoforms (Figure 3.9F–H) were induced to form long filaments, but 3R isoforms (Figure 3.9C–E) did not polymerize into any observable filaments by TEM.

3.2.2.4 Tau isoforms are phosphorylated by GSK-3β

All six tau isoforms are abnormally hyperphosphorylated in neurofibrillary tangles found in AD pathology. However, the functional consequences of this phosphorylation are unknown. Previous studies have found that tau phosphorylation, in general, reduces its binding to microtubules (*37*). Likewise, ARA induced filaments of GSK-3β phosphorylated 2N4R tau coalesce into "neurofibrillary tangle-like" structures (*51, 193*). To determine whether GSK-3β exerted similar effects on other tau isoforms, we examined the effects of GSK-3β phosphorylation by measuring the extent of phosphorylation; microtubule binding and ARA induced polymerization. GSK-3β phosphorylation of 2N4R tau results in an upward shift in mobility on SDS-PAGE gels (*51*). The effects of GSK-3β phosphorylation on the electrophoretic mobility of the other isoforms was examined by visualizing phosphorylation reactions of each isoform by SDS-PAGE (Figure 3.10A). All phosphorylated isoforms had an upward shift in electrophoretic mobility compared to

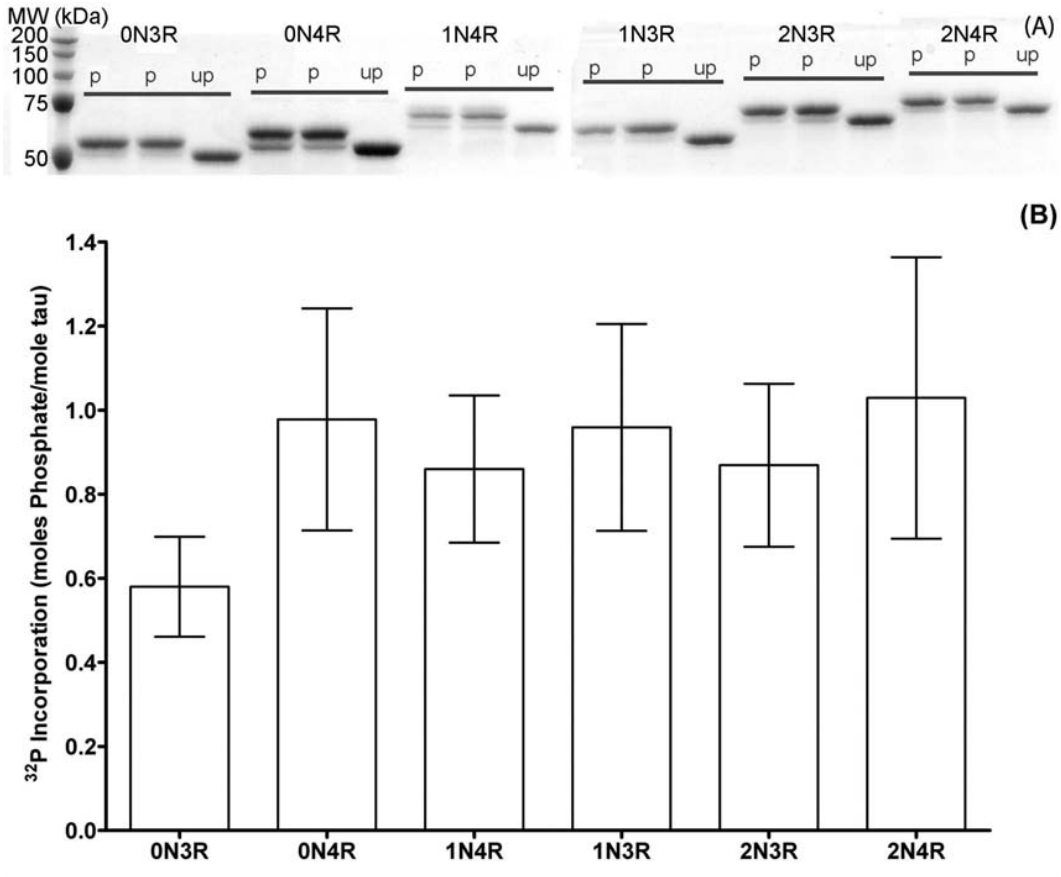

Figure 3.10 GSK-3β phosphorylation of tau isoforms visualized by changes in gel mobility and phosphate incorporation. (A) The migration of GSK-3β phosphorylated tau isoforms (p) was compared to unphosphorylated isoforms (up) by Coomassie-stained SDS-PAGE. The isoforms are labeled above their respective lanes. 2N4R was analyzed on a separate gel and then aligned by its relative migration to molecular weight standards. (B) γ-^{32}P ATP was added to the phosphorylation reaction overnight and moles of phosphate per mole of tau was calculated by averaging 4 trials ± SEM. Each isoform in (B) is individually labeled underneath its respective value.

its non-phosphorylated standard (Figure 3.10B). The quantity of the shifted tau band was unequal for the different isoforms, despite equivalent conditions for phosphorylation. One potential explanation for the differences in quantity could be that the degree of phosphate incorporation is not equal for all isoforms. Therefore, the levels of phosphorylation by GSK-3β were determined directly for each isoform by using γ-^{32}P ATP. An average of approximately 1 mole phosphate was incorporated per mole of tau for each isoform (Figure 3.10B). Only 0N3R showed lower phosphate incorporation, but due to the variability in the reactions, this difference did not reach statistically significant levels. Therefore, the difference in electrophoretic mobility between phosphorylated and non-phosphorylated tau, is not likely due to significant changes in phosphate incorporation, but rather could be due to similar levels of phosphorylation resulting in different levels of SDS-resistant conformational changes in the isoforms. Alternatively, the difference in the quantity could be a result of experimental variability of phosphorylation by GSK-3β.

3.2.2.5 Microtubule binding of tau isoforms changes with phosphorylation by GSK-3β

Tau is a microtubule-associated protein that, when phosphorylated at specific sites in the microtubule binding regions, such as at site S262 by p110^{MARK} (microtubule affinity regulating kinase), promotes strong disassociation (~10×) from microtubules (*218*), while phosphorylation outside of the microtubule binding regions (such as by GSK-3β in the proline rich region) has weaker effects on microtubule binding (*155*).

We therefore determined the effects of phosphorylation by GSK-3β on the microtubule binding affinities of each isoform, using unphosphorylated protein as a control (Figure 3.11A–F). Unphosphorylated 4R isoforms bound more tightly than the unphosphorylated 3R isoforms (Figure 3.11G), which is consistent with previously published results (*26*). Upon phosphorylation, the largest decrease in microtubule affinities occurred in 1N isoforms (~3×) (Figure 3.11G); indicating GSK-3β phosphorylates 1N isoforms at sites that mildly influence microtubule binding. The average K_d of phosphorylated 0N3R, 0N4R, and 2N4R isoforms was higher than the corresponding unphosphorylated K_d, however, these changes did not reach statistically significant levels (Figure 3.11G). 2N3R showed an increase in affinity for microtubules upon GSK-3β phosphorylation. These data indicate that phosphorylation by GSK-3β has mild effects on the microtubule binding of tau isoforms, which is consistent with phosphorylation at the proline rich region or other regions only mildly involved with microtubule binding.

3.2.2.6 Phosphorylation of tau isoforms changes filament polymerization levels

To determine how phosphorylation affects polymerization with ARA, all six isoforms were phosphorylated prior to the induction of polymerization. Heparin was not used because it failed to induce polymerization in non-phosphorylated 3R isoforms (see Figure 3.9). The extent of polymerization at 2 μM tau and 75 μM ARA was

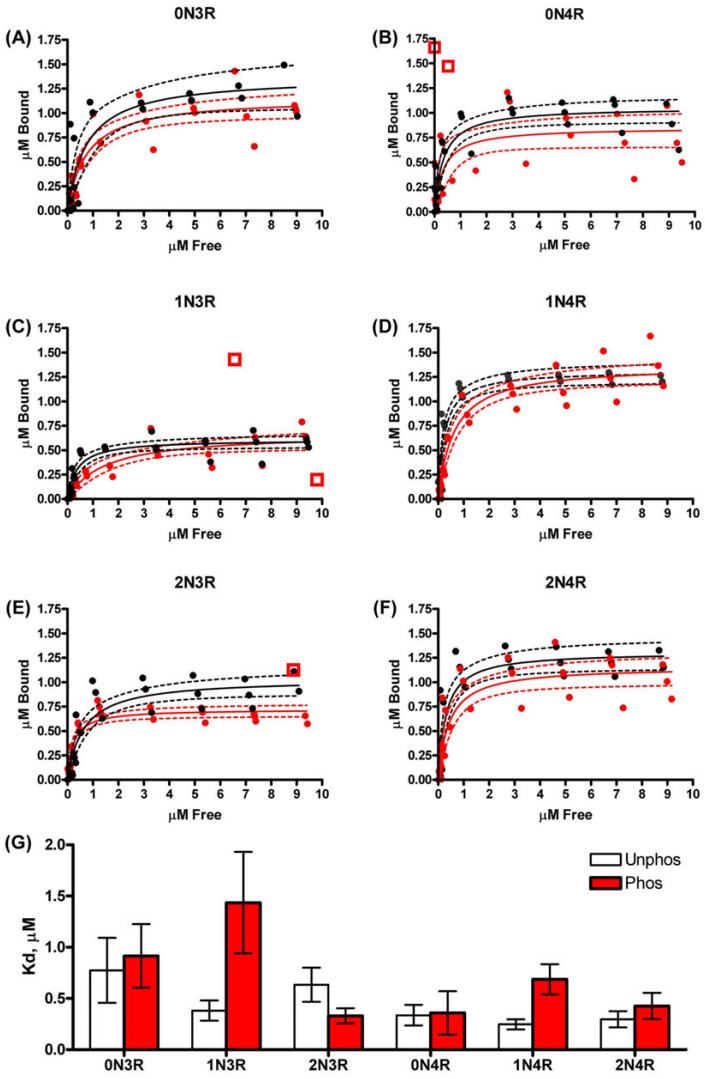

Figure 3.11 Changes in microtubule binding of tau isoforms when phosphorylated with GSK-3β. Microtubule binding reactions were performed at various concentrations of tau (0 µM to 10 µM) and bound vs. free tau (in µM) for both unphosphorylated (black circle) and phosphorylated (red circle) was plotted (A-F). Three separate trials are plotted together to demonstrate the variability in the reactions. The data were fit to a nonlinear single site binding equation for unphosphorylated (black solid line) and phosphorylated (red solid line) tau isoforms (A-F). The 95% confidence intervals of the fits are drawn as dashed lines. Outliers existed for phosphorylated samples, are shown as red open boxes, and were excluded from calculations. (G) The dissociation constant (K_d) (in µM) was determined for unphosphorylated (white bars) and phosphorylated (red bars) isoforms by K_d = the concentration of tau required to reach 1/2 B_{max}. Data represents the average of 3 trials ± SEM.

measured by LLS and ThS fluorescence (Figure 3.12). Non-phosphorylated and phosphorylated assembly incompetent tau (AIP, I277/308P) was used to correct for background scattering as previously described (*219*). 2N3R (Figure 3.12A) and 1N3R (Figure 3.12C) had relatively unchanged ThS values, but 2N3R had decreased LLS upon phosphorylation, while 1N3R had increased LLS. The phosphorylated 2N4R and 1N4R isoforms polymerized less than their unphosphorylated counterparts as measured by both LLS and ThS. Phosphorylated 0N3R had increases in both LLS and ThS, while 0N4R had no change in LLS, and decreased ThS. The data indicate that phosphorylation does not influence the polymerization of isoforms equally, but these changes are mild in comparison to differences between unphosphorylated isoforms.

3.2.2.7 Phosphorylation of tau isoforms changes filament morphology

Because LLS readings can be influenced by the size and length of the particles (*220*) and it is not clear to which molecular species ThS binds (*201, 221, 222*), samples of phosphorylated tau isoform filaments were viewed by TEM to determine whether phosphorylation induces significant changes in filament morphology, as has been observed with 2N4R tau (*51, 193*). Representative micrographs of phosphorylated samples polymerized in the presence of 75 μM ARA indicate distinct morphological changes from unphosphorylated tau isoforms (Compare Figure 3.13 and Figure 3.7). Phosphorylated 0N3R and 0N4R (Figure 3.13A, B) isoforms had increases in the

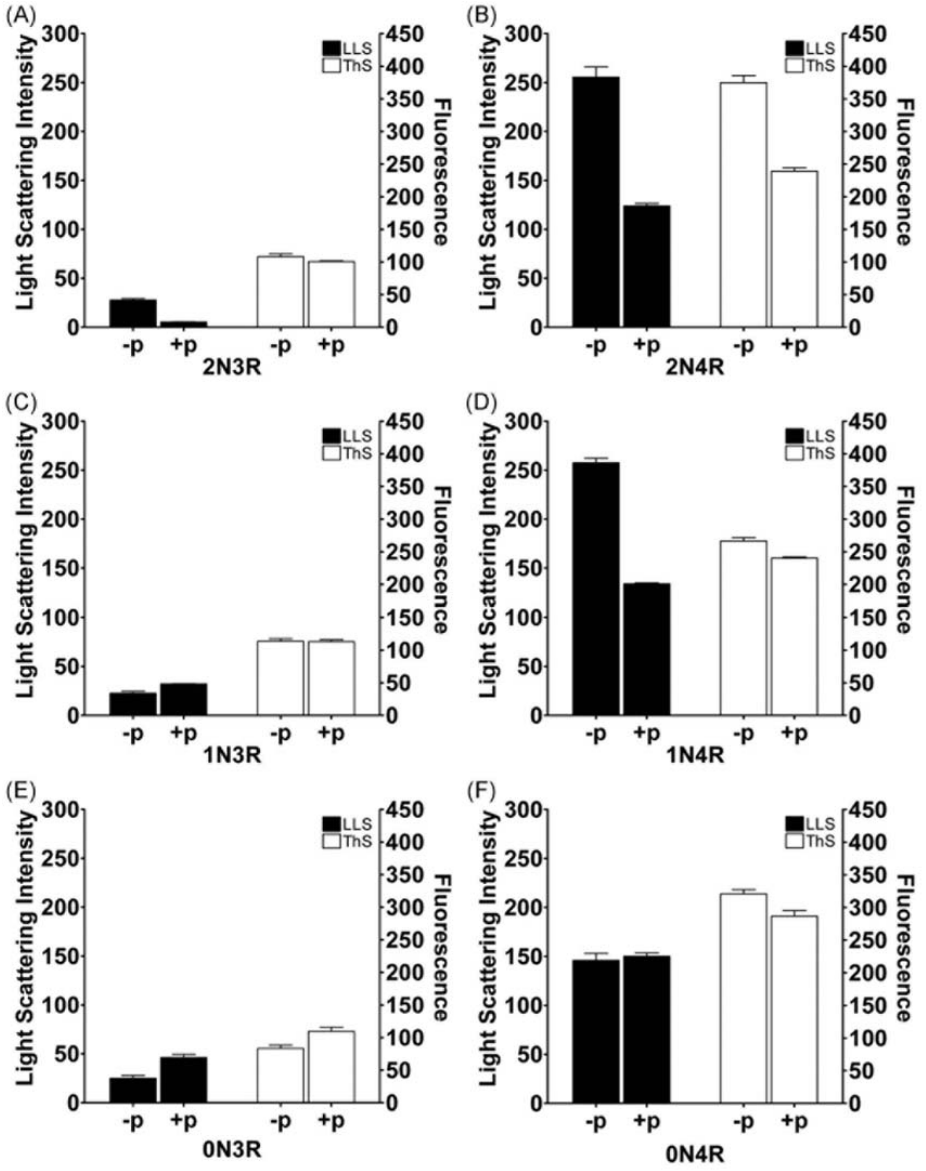

Figure 3.12 Effect of phosphorylation on ARA induced tau isoform polymerization. Each isoform (A) 2N3R, (B) 2N4R, (C) 1N3R, (D) 1N4R, (E) 0N3R, and (F) 0N4R was polymerized with 75 μM ARA after phosphorylation by GSK-3β (+p) or without phosphorylation (-p). Reactions were measured by LLS (black bars and left y-axis) and ThS fluorescence (open bars and right y-axis). All LLS data is background subtracted with AIP for -p and AIPp for +p values respectively. Data is an average of 3 trials ± SEM.

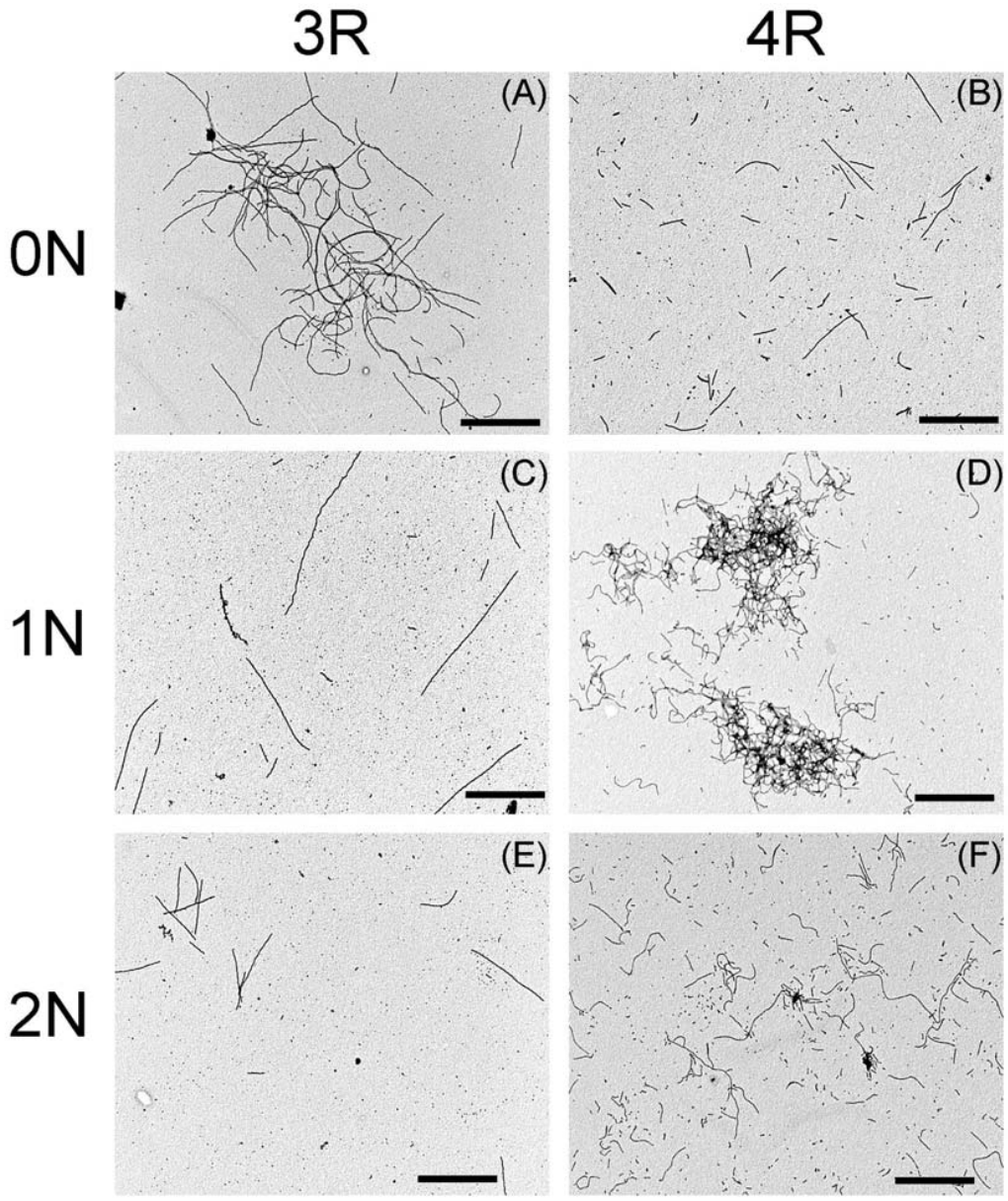

Figure 3.13 TEM images of ARA induction of GSK-3β phosphorylated tau isoforms. Images are as follows: (A) 0N3R, (B) 0N4R, (C) 1N3R, (D) 1N4R, (E) 2N3R, and (F) 2N4R. Images were recorded at a magnification of 20,000× (A-F) and are representative of polymerized material from 75 μM ARA induced-reactions presented in Figure 6. Scale bars represent 1 μm.

relative length and number of filaments formed as compared to non-phosphorylated (Figure 3.7C, F). Filaments formed from phosphorylated 1N3R and 1N4R (Figure 3.13C, D) isoforms also appeared to be relatively more numerous, and longer than non-phosphorylated (Figure 3.7D, G), although these changes were less dramatic than for the 0N isoforms. Phosphorylated 2N3R and 2N4R (Figure 3.13E, F) appeared to be relatively unchanged in the length and number of filaments (Figure 3.7E, H). Filaments from phosphorylated 0N3R, 1N4R, and 2N4R, had an increased tendency to cluster in close association to form "tangle-like" structures, similar to those seen previously with phosphorylated 2N4R induced with lower (25 μM) ARA concentrations (*51, 193*). It is apparent that isoform and inducer concentration, as well as phosphorylation, affect filament interactions promoting "tangle-like" structures.

3.2.3 Discussion

Many studies aimed at understanding the normal and abnormal functions of the microtubule-associated protein tau have focused on only one or two of its isoforms. However, all six isoforms of tau differ in their primary structure and therefore can potentially differ in their functions. In fact it has been shown that significant differences exist between the microtubule binding and microtubule stabilizing capacities of isoforms with three microtubule binding repeats and those with four microtubule binding repeats (*26, 223*). It has also been demonstrated that there are substantial differences between the self-polymerization characteristics of three repeat

isoforms and four repeat isoforms (*188, 215*) and between isoforms with different numbers of N-terminal exons (*188*). We have recently demonstrated that the phosphorylation of the 2N4R isoform of tau by GSK-3β causes arachidonic acid induced filaments to coalesce into larger structures similar to those purified from Alzheimer's disease (*51, 193*). Due to the potential differences between the characteristic functions of tau isoforms, we investigated the effects of GSK-3β phosphorylation on all six isoforms of tau. As a necessary first step for this study, we established baseline parameters for the self-polymerization of non-phosphorylated tau isoforms. This step was necessary because it is clear the type of inducer used and the conditions for polymerization have a large influence on the degree of polymerization of tau isoforms (*51, 215-217*). Using arachidonic acid as an inducer for polymerization, we found several significant differences between the isoforms. First, four repeat isoforms polymerized to a greater extent than three repeat isoforms. Secondly, removal of the two N-terminal exons (exons 2 and 3) increased the concentration of inducer required for maximal polymerization. Lastly, the presence of exon 2 is sufficient to reduce the levels of inducer required for maximal polymerization because the addition of exon 3 to exon 2 containing isoforms does not further reduce inducer concentrations needed for maximal polymerization. The structural involvement of exon 2 and 3 in filament formation is poorly understood, but could be related to the length of the N-terminus that is involved in regulating tau polymerization. By altering the length of the N-terminal domain, tau may be able to adopt only certain conformations leading to an increase or decrease in polymerization.

The inducers may be able to play a role in mediating this difference in length by acting as a linker between the N-terminus and the MTBRs.

A similar biphasic curve was obtained for the heparin induction of four repeat tau isoform polymerization. However, in the presence of heparin, three repeat isoforms failed to polymerize to detectable levels. The N-terminal exons also influenced the concentrations of inducer required to reach maximal polymerization. The 2N4R isoform required less heparin inducer for maximal polymerization than 1N4R and 0N4R. The observation that three repeat isoforms essentially failed to polymerize in the presence of heparin was somewhat surprising because it has been shown that the heparin induced polymerization of 0N3R tau is actually enhanced as compared to 2N4R tau (*215*). It should be noted that the heparin polymerization studies by the other lab were incubated at higher protein and inducer concentrations in solutions with greater ionic strength and for longer time periods than the current study. Our conditions for polymerization are based on previously published conditions of low ionic strength, protein concentration and inducer concentration that result in efficient tau polymerization reaching apparent steady state in 24–48 hours (*216, 217*). These results indicate that the local environment has a large impact on how individual tau isoforms self-polymerize, which could have an impact on isoform specific regulation of tau in the cell. Our results and those of others strongly suggest that most isoforms of tau have distinct polymerization characteristics. The local environment is a major determinant of the amount of polymerization observed, and the isoforms do not

respond equally to changes in environment. GSK-3β has been shown to phosphorylate tau in transgenic mice and cause neurodegeneration (*135*), which can be abolished with lithium treatment to inhibit GSK-3β (*211*). Based on these observations, we examined GSK-3β phosphorylation of tau isoforms.

The levels of GSK-3β phosphorylation of the isoforms were similar at an average of approximately 1 mole of phosphate per mole of tau, although there was a large degree of variability in the amount of phosphate incorporation in repeated experiments. On average, the 0N3R isoform was phosphorylated to a lesser degree than the other isoforms, but not at statistically significant levels. One explanation for the low amount of phosphate incorporation could be that either the kinase or the γ-^{32}P ATP did not work as effectively as it should, which could also explain the large variability among the three trials. While the tau isoforms were not phosphorylated at ~8 moles of phosphate per mole of tau, similar to hyperphosphorylated tau found in tau pathologies, we do see a corresponding band shift, characteristic of hyperphosphorylated tau. This could be explained by site specific phosphorylation, at T231, inducing an SDS-resistant conformational change. Phosphorylation at T231 is recognized by the prolyl isomerase, Pin1, to reverse conformational and functional changes that would otherwise result in increased polymerization and decreased microtubule binding (*224, 225*). Since previous results have shown T231 phosphorylation of 2N4R by GSK-3β in vitro (*191, 193*), we believe this site could be phosphorylated on all isoforms, although we did not examine the specific

phosphorylation sites for each isoform. Based upon these same previous papers showing multiple sites phosphorylated over an entire monomer population, despite only having 2 moles of phosphate per mole of tau (*191, 193*), we believe phosphorylation occurs on the tau isoforms at multiple sites as well. Based on these data, it would be difficult to conclude that GSK-3β preferentially phosphorylates any particular isoform in vitro. More discussion on GSK-3β phosphorylation of the tau isoforms can be found in Chapter 5.

Although the level of GSK-3β phosphorylation was approximately equal, there were differences in the effects on isoform functions. As expected, four repeat tau isoforms bound more tightly to microtubules than did three repeat isoforms. Phosphorylation by GSK-3β decreased the average K_d of 0N3R, 0N4R and 2N4R, but not at statistically significant levels due to the variability in the data. The 2N3R isoform bound more tightly to microtubules upon phosphorylation, which is not unprecedented for the effects of phosphorylation on tau-microtubule interactions (*153*). The largest differences were observed for the 1N isoforms. Both 1N3R and 1N4R had approximately 3- fold reductions in microtubule binding following GSK-3β phosphorylation. While phosphorylation with GSK-3β affects microtubule binding differently for each isoform, these effects are small as compared to kinases (such as $p110^{MARK}$ at S262) which cause a complete loss in microtubule binding of tau (*218*). Loss of microtubule binding by increased phosphorylation is thought to play a role in the progression of AD.

The effect of GSK-3β phosphorylation on the ARA induction of tau polymerization also differed between isoforms. In general, phosphorylation decreased the amount of detectable polymerization by ThS fluorescence for the 4R isoforms and had little effect on the polymerization of 3R isoforms. It is difficult to assess the amount of polymerization detected by LLS since the phosphorylation process seemed to increase the tendency of several isoforms to cluster into larger structures. These larger structures can potentially result in aberrant scattering (*120, 194, 219, 220*). The largest changes observed due to phosphorylation occurred with filament morphology as viewed by TEM. When compared to the unphosphorylated state, each isoform tended to increase in length and some showed increased affinities between polymers. However, the physiological relevance of such changes in morphology is unknown. GSK-3β phosphorylation influences each of the tau isoforms differently, although these changes appear to be small in comparison to the inherent differences in the non-phosphorylated proteins. For example, GSK-3β phosphorylation reduces the ARA induced polymerization of the 4R isoforms, but the phosphorylated versions still polymerize to a greater degree than the non-phosphorylated 3R isoforms. GSK-3β phosphorylation of tau isoforms does alter their microtubule binding in a variable manner, but these changes are small, with the greatest effect on binding being an approximate 3-fold reduction in binding.

In conclusion, GSK-3β phosphorylation has different impacts on the functions of the six isoforms of tau. However, the effect of GSK-3β phosphorylation on tau function

appears to be less significant than the pre-existing differences in isoform function based on their primary structure. These inherent differences in the isoforms seem to react differently to the local environment that appears to be the major determinant of the amount of polymerization. Increasing a localized concentration of hyperphosphorylated tau along the axon could drive aggregation, as shown previously, where increased concentrations of proteins that form amyloid show increased filament formation in vivo (*226-228*). It is unlikely however, that GSK-3β is the only kinase involved in this process as we only saw mild effects on microtubule binding. This work is therefore a vital first step in understanding the effects of phosphorylation and hyperphosphorylation on the functional biochemical properties of tau isoforms.

Chapter 4- Hsp70 Differentially Affects Tau Isoforms

4.1 Introduction

The microtubule associated protein tau exists as six alternatively spliced isoforms (*5*). Alzheimer's disease (AD) is the most prevalent tauopathy. However, AD is unique in that tau is neither mutated nor is there any change in the relative levels of tau isoform expression as compared to aged matched controls (*11*). This indicates post-translational modifications and interactions with other cellular proteins could play a major role in AD pathogenesis. We have shown previously that tau isoform polymerization is affected by the buffer conditions, the type of inducer for polymerization used and post-translational modifications (*150*). The polymerization differences caused by changes in the local environment indicate each may have a distinct role in the progression of neurodegeneration.

Molecular chaperones have multiple roles which include: preventing inappropriate aggregation of hydrophobic regions of misfolded proteins, targeting proteins to subcellular compartments, and assisting in degradation of proteins (reviewed in (*160*)). Heat shock protein 70 kDa (Hsp70) is the 70 kDa inducible form of a class of proteins that are upregulated in response to stress, termed heat shock proteins (reviewed in (*171*)). Hsp70 levels are normally low in central nervous system neurons, but can be increased in response to stress (reviewed in (*229*)). Hsp70 acts by binding hydrophobic regions of a substrate protein in its substrate binding domain and using internal ATPase activity to hydrolyze ATP to ADP, creating a tighter

interaction with the substrate (reviewed in (*230*)). Hsp70 then can independently assist in refolding, transfer the protein to the Hsp90 system, or transfer the protein the chaperonin system for refolding (reviewed in (*230*)). Chaperonins are larger complexes that provide an isolated environment where the misfolded protein can refold in the absence of other misfolded proteins. Therefore, Hsp70 reduces protein misfolding and aggregation under conditions that would favor protein misfolding.

AD patients show an elevated level of stress response proteins. Therefore, recent work has focused on elucidating the role of chaperones in AD. AD hippocampal sections show elevated expression of Hsp70/90, as compared to aged matched controls (*183*, *187*). In specific hippocampal neurons there is an inverse relationship of tau aggregation and Hsp70/90 levels (*183*). Hsp70 has been shown to reduce abnormal tau by increasing its degradation and dephosphorylation (*183*, *185*). Also, increased levels of Hsp70/90 promote tau solubility and microtubule binding in cellular models (*183*). Both the constitutively active (Hsc70) and inducible (Hsp70) forms of Hsp70 have been shown to bind tau directly (*186*). Inhibition of Hsp70 ATPase activity has been show to increase proteasomal degradation of tau in cell culture (*231*). Finally, previous studies have shown that heparin induced 2N4R tau polymerization with Hsp70 and Hsp40 is lowered compared to tau only controls (*187*).

The previous work on Hsp70/tau interactions has shown Hsp70 could be used to reduce abnormal tau polymerization. For example, there is an inverse relationship of

Hsp70 and tau levels in specific AD hippocampal neurons (*187*). Also, previous results show tau isoforms do not respond similarly to changes in the local environment (*150*). Finally, tau has been shown to have an increased affinity for microtubules in the presence of Hsp70 in COS-1 cells (*183*). Therefore, we hypothesize that in vitro Hsp70 would differentially affect the polymerization and microtubule assembly properties of tau isoforms. This hypothesis was examined by assaying inducer-mediated tau polymerization using arachidonic acid, heparin sulfate, and Congo Red, in vitro, using right angle laser light scattering (LLS), thioflavine S fluorescence (ThS) and transmission electron microscopy (TEM) for extent and morphology of filament formation, as previously described (*51, 150, 189, 191-195, 203*). Microtubule assembly was examined using a commercially available fluorescence kit in the presence and absence of Hsp70. We found that Hsp70 inhibits inducer mediated tau polymerization in an isoform specific manner, differentially affects the rate and total amount of tubulin polymerization and can affect both polymerization and microtubule assembly.

4.2 Results

4.2.1 Hsp70 inhibits ARA induced 2N4R tau polymerization

Because it has been shown that Hsp70 binds tau and prevents heparin induction of polymerization, we sought to determine whether Hsp70 can inhibit ARA induction of 2N4R tau polymerization. The reactions were incubated 18 hours and the resulting amount of polymerization was assayed by LLS (Fig 4.1A) and ThS (Fig 4.1B). At

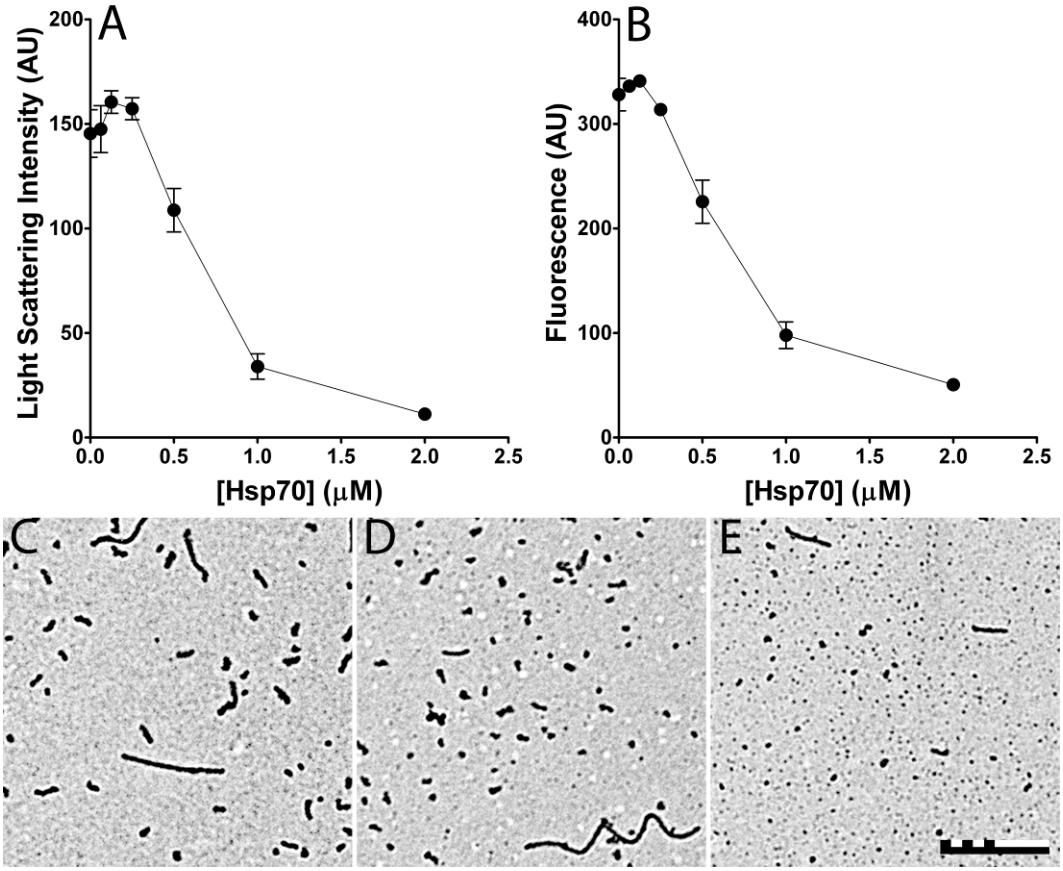

Figure 4.1. Hsp70 inhibition of ARA induced 2N4R tau polymerization. 4 μM 2N4R tau and 150 μM ARA was incubated in the presence of various amounts of Hsp70 (0-2 μM) for 18 hrs at 37 ^{o}C. Polymerization was measured by (A) LLS and (B) ThS fluorescence. Data is in arbitrary units and represents the average of 3 trials ± SEM. After 18 hrs, polymerization reactions for (C) 0 μM, (D) 0.5 μM, and (E) 1 μM Hsp70 were visualized by TEM at 3600x magnification, as they correspond to approximately 0, 50, and 100% inhibition. Representative images are shown, scale bar represents 500 nm.

low concentrations of Hsp70 there was little observable effect. Increasing concentrations of Hsp70 reduced the amount of tau polymerization observed. At a 2:1, tau: Hsp70 ratio, polymerization of tau was nearly completely inhibited. Data was normalized as 100% equal to the highest observable value, and 0% as the lowest observable value, and the concentration of Hsp70 needed to reduce the y-value to 50% was estimated by creating the equation of a line between the two points where 50% would lie and inserting 50 for the y-value. The concentration of Hsp70 needed to reduce ARA induced 4 μM 2N4R tau polymerization to 50% of the highest value was approximately 0.60 ± 0.07 μM as measured by ThS fluorescence and 0.64 ± 0.08 μM as measured by LLS. To further determine if Hsp70 inhibits tau polymerization, samples of the 2N4R reactions were taken and visualized by transmission electron microscopy (TEM) (Fig 4.1C-E). Compared to the control reaction without Hsp70 (Fig 4.1C), increasing concentrations of Hsp70 showed a noticeable decrease in filament lengths longer than 25 nm (Fig 4.1D, E). While there was also an increase in electron dense material shorter than 25 nm with increasing concentrations of Hsp70, a similar increase was observed by TEM in the absence of tau (data not shown). Density smaller than 25nm were therefore not included in any quantitative analysis of TEM data.

4.2.2 Other inducers of tau polymerization

The ability of Hsp70 to inhibit the polymerization of tau in the presence of other inducers, such as Congo Red (CR) and heparin sulfate, was also investigated. CR

induced tau polymerization reactions were analyzed by LLS (Fig 4.2A) and TEM (Fig 4.2B-D). ThS analysis was not performed because CR obscures ThS fluorescence. The concentration of Hsp70 required to reduce tau polymerization by 50% was approximately 0.25 ± 0.01 μM. Samples of reactions were visualized by TEM (Fig 4.2B-D). Upon addition of Hsp70, a decrease in filament lengths and an increase in the number of filaments were observed (Fig 4.2C, D) as compared to reactions without Hsp70 (Fig 4.2B). The ability of Hsp70 to suppress heparin sulfate induction of tau polymerization was examined by incubating 2N4R tau with varying concentrations of Hsp70 in the presence of heparin. Reactions were analyzed by ThS (Fig 4.3A) and TEM (Fig 4.3B-D). Reactions were not analyzed by LLS because LLS of reactions in the absence of tau, but the presence of Hsp70, had similar scattering as those reactions in the absence of Hsp70. The concentration of Hsp70 required to reduce tau polymerization by 50% was approximately 0.76 ± 0.04 μM. Visualization of samples by TEM without Hsp70, revealed only very long filaments (Fig 4.3B). These filaments were so long that the ends did not fit into a 6 μm by 6 μm field of view. Upon addition of Hsp70, filament lengths decreased and the number of filaments increased (Fig 4.3C, D).

When comparing inhibition curves, 50% inhibition values and TEM images of polymerization reactions, it is evident that Hsp70 has similar effects on blocking tau polymerization induced by ARA, CR and heparin. These three compounds are structurally distinct. ARA is a fatty acid, CR is a planar aromatic dye, and heparin is

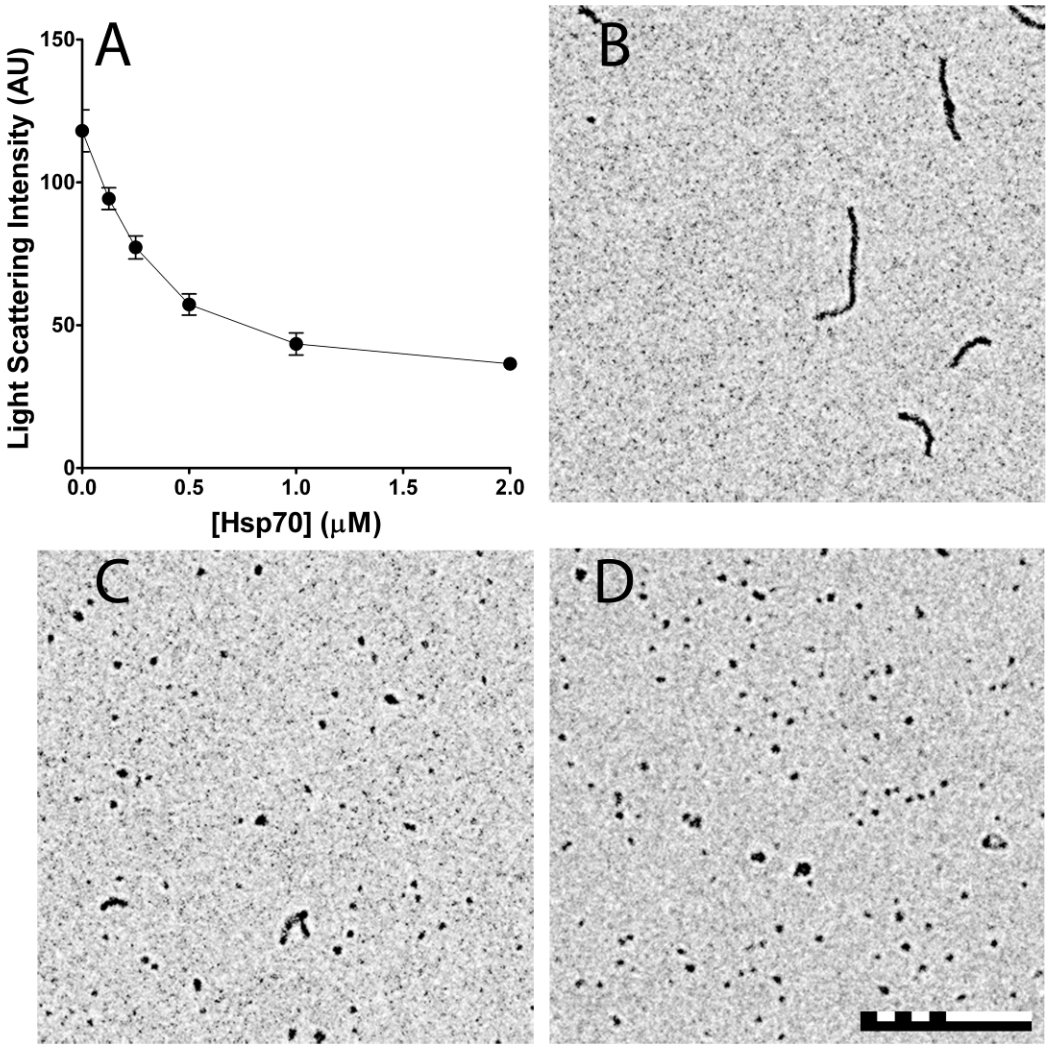

Figure 4.2. Hsp70 inhibition of Congo red (CR) induced 2N4R tau polymerization. 2 μM 2N4R tau and 10 μM CR was incubated in the presence of varying amounts of Hsp70 (0-2 μM) for 18 hrs at 37 ^{o}C. Polymerization was measured by (A) LLS only because Congo red interferes with ThS fluorescence. Data is in arbitrary units and represents the average of 3 trials ± SEM. After 18 hrs, polymerization reactions for (B) 0 μM, (C) 0.5 μM, and (D) 1 μM Hsp70 were visualized by TEM at 3600x magnification as they correspond to approximately 0, 50, and 100% inhibition. Representative images are shown, scale bar represents 500 nm.

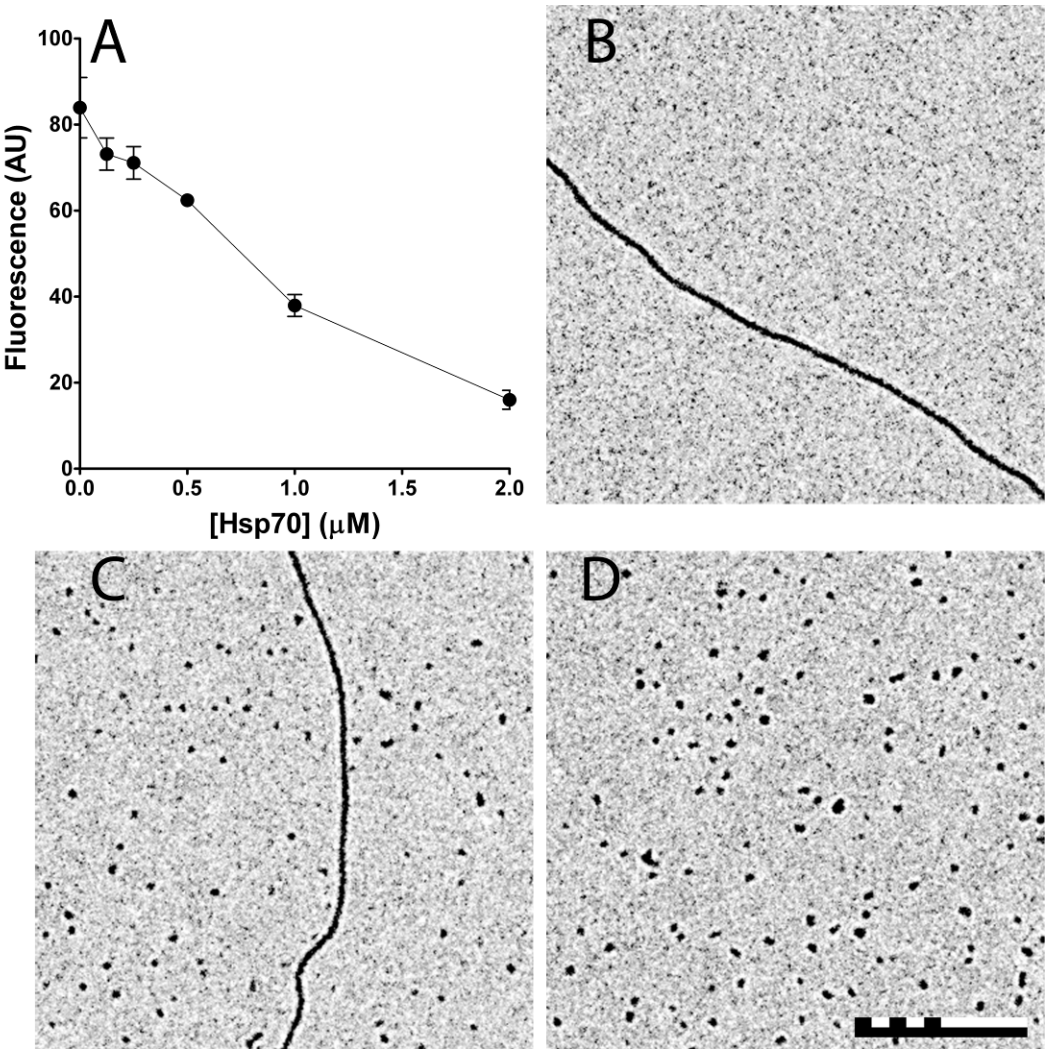

Figure 4.3. Hsp70 inhibition of heparin induced 2N4R tau polymerization. 2 μM 2N4R tau and 6 μg/ml heparin was incubated in the presence of varying amounts of Hsp70 (0-2 μM) for 18 hrs at 37 ^{o}C. Polymerization was measured by (A) ThS fluorescence. Data is in arbitrary units and represents the average of 3 trials ± SEM. After 18 hrs, polymerization reactions for (B) 0 μM, (C) 0.5 μM, and (D) 1 μM Hsp70 were visualized by TEM at 3600x magnification as they correspond to approximately 0, 50, and 100% inhibition. Representative images are shown, scale bar represents 500 nm.

a proteoglycan. Therefore, the ability of Hsp70 to suppress the induction by all three inducers suggests that the observed inhibition is not inducer specific, but rather specific to tau.

4.2.3 Hsp70 acts by slowing the elongation of 2N4R tau

To determine how Hsp70 is affecting tau polymerization, ARA induced polymerization reactions of 2N4R tau and Hsp70 at various concentrations were examined over 6 hours using LLS (Fig 4.4). ThS kinetics were not used as ThS binds Hsp70 weakly and also enhances tau polymerization. When the data were fit to an improved model for tau polymerization, we found that the initial nucleation rate did not change, but rather the rate of elongation was slowed, as indicated by a less steep slope, so that overall the total amount of tau polymerization was lowered with increasing Hsp70 concentrations (Table 4.1). This suggests that Hsp70 would bind tau and remain in close association with tau to prevent monomer from adding onto filaments.

4.2.4 ATP does not affect Hsp70 inhibition of 2N4R tau polymerization

Experiments were carried out to determine the role of ATP in the Hsp70 mediated inhibition of ARA induced tau polymerization (Figure 4.5). The concentration of Hsp70 was varied in the reactions, at a constant amount of ATP. 4 μM 2N4R tau and 150 μM ARA was incubated with 0, 1, 2, or 4 μM Hsp70 in the presence (0.5 mM) or absence (0 mM) of ATP. We found that both the LLS intensity and ThS fluorescence

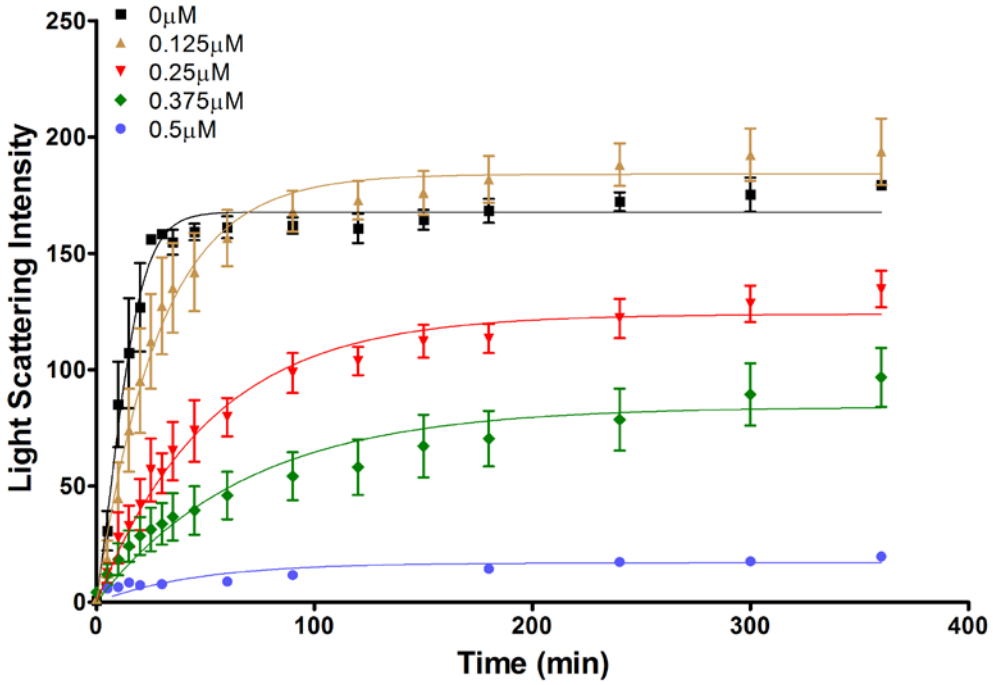

Figure 4.4 Hsp70 inhibits ARA induced tau polymerization by slowing the elongation rate. 4 μM 2N4R was incubated in the presence of 150 μM ARA and varying concentrations of Hsp70 (0-0.5 μM) at 37 ^{o}C. LLS readings of each reaction were taken at various time points over 6 hours. Data was fit to the F-W equation (defined in Chapter 2). Data is shown as the average of 3 trials ± SEM.

[Hsp70] (μM)	Lag Time (min^{-1})	Rate of Assembly (AU^{-1} min^{-1})	Extent of Assembly (AU)
0	0.027 ± 0.012	1.002E-3 ± 4.376E-5	167.800 ± 5.083
0.125	0.030 ± 0.011	1.773E-4 ± 1.008E-4	186.000 ± 12.430 **
0.25	0.019 ± 0.005	7.117E-16 ± 5.792E-16 **	125.400 ± 6.281 ***
0.375	0.014 ± 0.004	1.903E-16 ± 1.466E-17 **	86.270 ± 8.204 ***
0.5	0.023	1.710E-15 **	16.900***

Table 4.1 LLS kinetics of ARA induced 2N4R polymerization with varying Hsp70 concentrations. Data from fitting Figure 4.4 to F-W equation. Data is shown as the average of 3 trials ± SEM, and asterisks denote significant differences (* = $p<0.05$, ** = $p<0.01$, *** = $p<0.001$) from the 0 μM Hsp70 control as determined by an unpaired two-sided t-test.

decreased with increasing concentrations of Hsp70 and that the addition of ATP did not influence Hsp70 inhibition of tau polymerization. A possible explanation of the data could be that 4 μM Hsp70 exhaust the ATP pool quicker than the 1 μM Hsp70. To examine this possibility we kept the ratio of ATP to Hsp70 constant. 4 μM 2N4R tau was incubated in the presence of either no ATP/Hsp70, 0.5 mM/1 μM ATP/Hsp70, 1 mM/2 μM ATP/Hsp70, or 2 mM/4 μM ATP/Hsp70. We found that with increasing concentrations of Hsp70 there was no difference between the 500:1 ATP/Hsp70 ratio and just adding 500 mM ATP. These results indicate the addition of ATP has no effect on Hsp70 inhibition of tau polymerization.

4.2.5 Addition of Hsp70 after filament formation slightly decreases filament lengths

We have shown that Hsp70 can inhibit inducer mediated tau polymerization when added to the reaction at the beginning; however, Hsp70 and other chaperones also have an ability to disassemble aggregates. Hsp70 is not known to disassemble large aggregates. Hsp104 forms a hexamer that accomplishes this. However, Hsp70 could aid in the process. 2N4R tau was polymerized in the presence of ARA and in the absence of Hsp70 overnight at 37 ^{o}C (Fig 4.6A). Hsp70 at 1 μM was then added for 18 hours (Fig 4.6B), visualized by TEM and filament lengths were analyzed by Image Pro Plus (Fig 4.6C, D). The number and mass of small filaments increased in the presence of Hsp70, while the number and mass of medium length filaments decreased and long filaments were not significantly changed. We did not observe complete

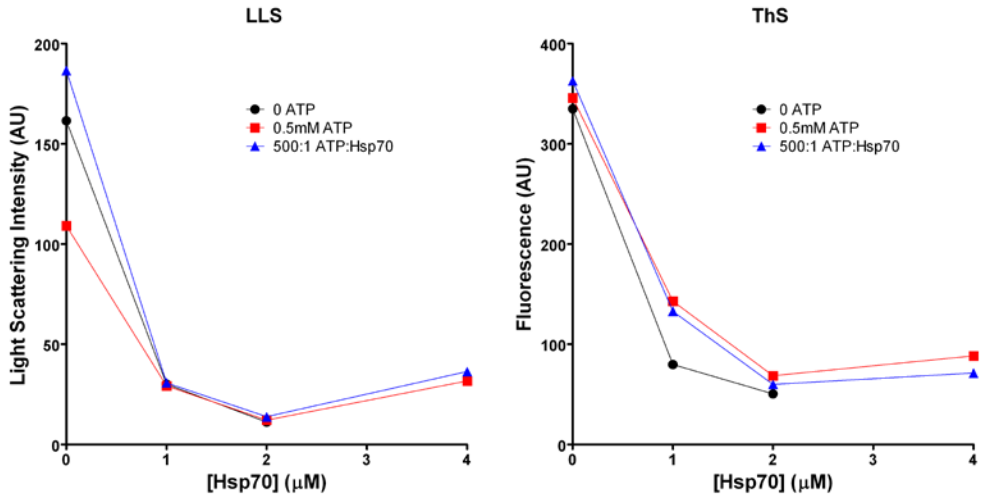

Figure 4.5 The contribution of ATP to Hsp70 inhibition of tau polymerization. ATP at various concentrations was added to Hsp70 at varying concentrations and 150 µM ARA induced 4 µM 2N4R tau reactions. Reactions without ATP (black), with 500 mM ATP, or keeping the ATP/Hsp70 ratio at 500:1 were examined by LLS (left) and ThS fluorescence (right).

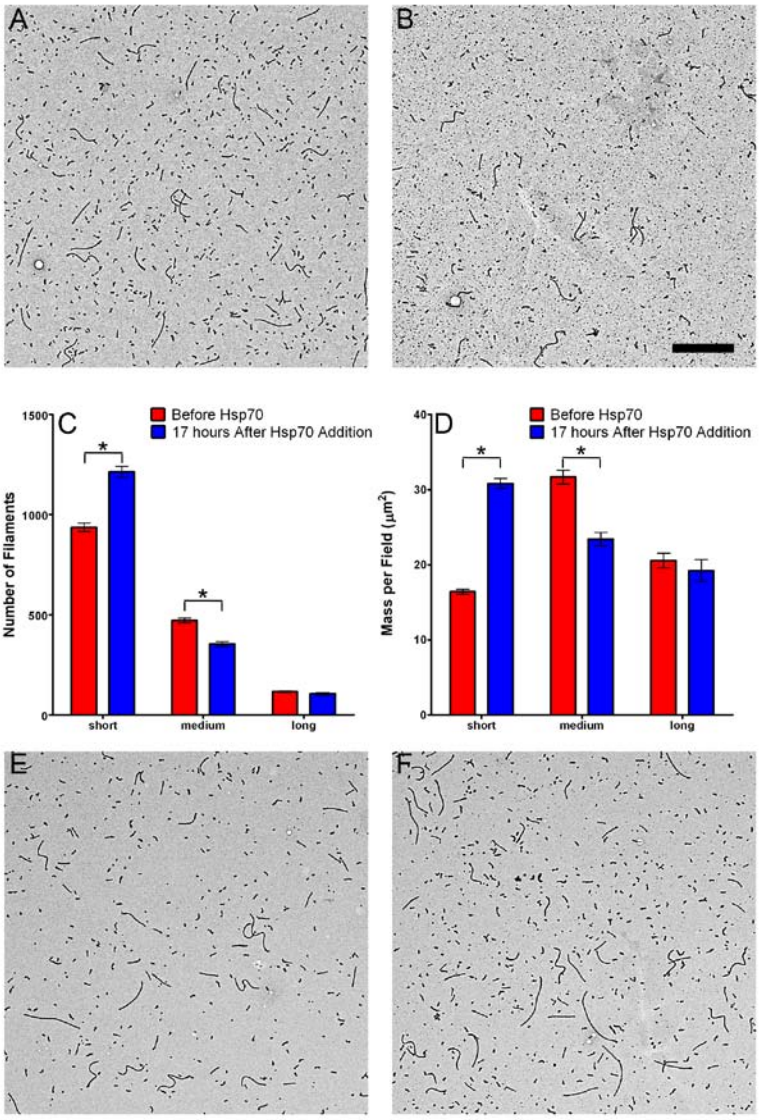

Figure 4.6 Hsp70 partially disassembles ARA induced tau filaments in the presence of ATP. Pre-formed ARA (150 μM) induced 2N4R tau (4 μM) filaments without Hsp70 (A) and with 1 μM Hsp70 (B), in the presence of 2 mM ATP, were incubated 18 hours. Images were analyzed using Image Pro Plus to determine filament lengths with a minimum size of 25 nm. Data for each image was then counted for inclusion in one of the following ranges: short (between 25 nm and 50 nm), medium (between 50 nm and 100 nm), or long (greater than 100 nm). The mean ± SEM of 5 fields is displayed for each range for length (C) and total filament mass of that range (D). TEM images of pre-formed ARA induced 2N4R tau filaments without ATP and without Hsp70 (E) or without ATP and with 1 μM Hsp70 (F), incubated 18 hours. Asterisks indicate significant differences ($p<0.05$) between with and without Hsp70.

disassembly of filaments, however. Similar reactions in the absence of ATP were performed, however, no difference in filament length was observed. This indicates that Hsp70 can partially disassemble tau filaments, indicating that increasing Hsp70 levels in a cell that has tau pathology could potentially reverse the effects of aggregation.

4.2.6 Hsp70 differentially inhibits other ARA induced tau isoform polymerization

Tau exists as alternatively spliced isoforms that differ greatly in primary sequence, with differences from 29 to 89 amino acids as compared to full length 2N4R. While 89 amino acids are only 20% differences, this includes the removal of a known functional unit, microtubule binding repeat 2. The absence of repeat 2 (3R isoforms) has been shown to have a marked decrease in microtubule binding ability and overall polymerization potential as compared to the presence of the repeat (4R isoforms) (*150*). Therefore, it is possible that Hsp70 will affect tau isoforms polymerization differently. To test this, tau isoforms were incubated with ARA and varying concentrations of Hsp70 for 18 hours. The extent of polymerization was determined by LLS (Fig 4.7A) and ThS (Fig 4.7B). Hsp70 inhibited ARA induced polymerization of each tau isoform in a dose dependent manner similar to 2N4R.

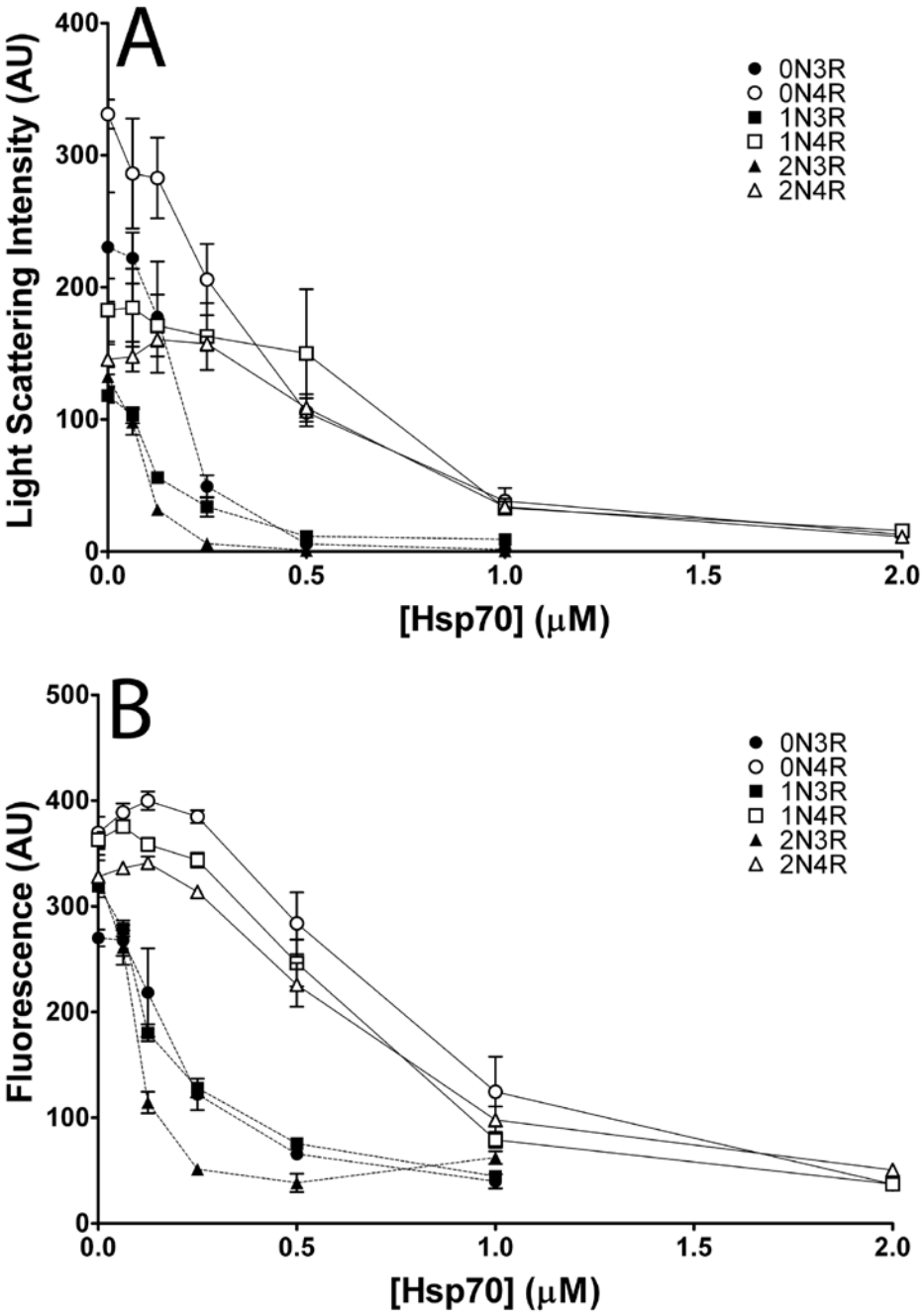

Figure 4.7. Hsp70 inhibition of ARA induced tau isoform tau polymerization. 4 μM tau isoforms and 150 μM ARA were incubated in the presence of varying amounts of Hsp70 (0-2 μM) for 18 hrs at 37 ^{o}C. Polymerization was measured by (A) LLS and (B) ThS fluorescence. Data is in arbitrary units and represents the average of 3 trials ± SEM.

[Hsp70] (μM) for 50% tau polymerization		
	ThS	LLS
0N3R	0.19 ± 0.03	0.16 ± 0.03
1N3R	0.13 ± 0.01	0.12 ± 0.01
2N3R	0.10 ± 0.01	0.09 ± 0.01
0N4R	0.71 ± 0.08	0.31 ± 0.03
1N4R	0.61 ± 0.05	0.66 ± 0.06
2N4R	0.60 ± 0.07	0.64 ± 0.08

ThS 50% values
Newman-Keuls Multiple Comparison Test

	Mean Diff.	q	Significant? P < 0.05?
2N3R vs 0N4R	-0.61	12.24	Yes
2N3R vs 1N4R	-0.51	10.23	Yes
2N3R vs 2N4R	-0.5	10.03	Yes
2N3R vs 0N3R	-0.09	1.806	No
2N3R vs 1N3R	-0.03	---	No
1N3R vs 0N4R	-0.58	11.64	Yes
1N3R vs 1N4R	-0.48	9.632	Yes
1N3R vs 2N4R	-0.47	9.431	Yes
1N3R vs 0N3R	-0.06	---	No
0N3R vs 0N4R	-0.52	10.43	Yes
0N3R vs 1N4R	-0.42	8.428	Yes
0N3R vs 2N4R	-0.41	8.227	Yes
2N4R vs 0N4R	-0.11	2.207	No
2N4R vs 1N4R	-0.01	---	No
1N4R vs 0N4R	-0.1	---	No

LLS 50% values
Newman-Keuls Multiple Comparison Test

	Mean Diff.	q	Significant? P < 0.05?
2N3R vs 1N4R	-0.57	12.75	Yes
2N3R vs 2N4R	-0.55	12.3	Yes
2N3R vs 0N4R	-0.22	4.919	Yes
2N3R vs 0N3R	-0.07	1.565	No
2N3R vs 1N3R	-0.03	---	No
1N3R vs 1N4R	-0.54	12.07	Yes
1N3R vs 2N4R	-0.52	11.63	Yes
1N3R vs 0N4R	-0.19	4.249	Yes
1N3R vs 0N3R	-0.04	---	No
0N3R vs 1N4R	-0.5	11.18	Yes
0N3R vs 2N4R	-0.48	10.73	Yes
0N3R vs 0N4R	-0.15	3.354	Yes
0N4R vs 1N4R	-0.35	7.826	Yes
0N4R vs 2N4R	-0.33	7.379	Yes
2N4R vs 1N4R	-0.02	0.4472	No

Table 4.2. Concentration of Hsp70 (in μM) required to inhibit the maximum ARA induced tau isoform polymerization by 50% and p-values comparing each data set. Data given in the top part is the mean ± SEM of 3 trials. Comparisons were done using a one way ANOVA with a Newman-Keuls multiple comparison test.

While all tau isoform polymerization was inhibited with increased Hsp70 concentrations, differences between isoforms were observed. In the absence of Hsp70, 3R and 4R, isoforms have approximately the same ThS values (Fig 4.7B), while LLS values of reactions without Hsp70 are more varied (Fig 4.7A). At low Hsp70 concentrations (less than 0.25 μM), there was a dramatic decrease in polymerization for 3R isoforms, while 4R isoforms had no change. At 0.5 μM Hsp70, polymerization reactions containing 4R isoforms began to decrease while reactions containing 3R isoforms were completely inhibited. 2N3R was inhibited at lower concentrations of Hsp70 as compared to 0N3R and 1N3R. There were no discernable differences between the numbers of N-terminal exons in the 4R isoforms. The concentration of Hsp70 required to inhibit tau polymerization 50% from the maximum LLS or ThS value for each tau isoform and the results of a one-way analysis of variance (ANOVA) to determine if the means of the isoforms are significantly different is reported in Table 4.2. The only significant difference for ThS values when comparing the concentration of Hsp70 required for 50% inhibition of tau polymerization is that the 3R isoforms are inhibited at a lower concentration than 4R isoforms. For LLS, the 3R isoforms are significantly different from the 4R isoforms, and 0N4R is significantly different from the other 4R isoforms. TEM analysis of the reactions will determine how morphology of the filaments is affected by Hsp70.

4.2.7 TEM analysis of tau isoform inhibition

Reactions of ARA induced tau isoform polymerization with Hsp70 were visualized by TEM (Fig 4.8). TEM revealed a shortening of filaments indicating the decrease in LLS and ThS values correspond to a decrease in filament lengths. TEM images of polymerization reactions were quantitated using a 25 nm cutoff filter to account for Hsp70 background (Fig 4.9). Hsp70 reduced the overall number and length of all of the tau isoform filaments, but the patterns of inhibition were not the same. For example, upon addition of Hsp70 to 0N3R and 0N4R there is a decrease in the number of short and medium length filaments while the number of long filaments stay about the same.

The data for 0N4R fits this model if 0.5 µM is used as the start point instead of 0 µM because large aggregates described previously (*150*) seen in the absence of Hsp70, and are difficult to quantitate because we can not determine filament ends, form less well in the presence of increasing Hsp70, creating an artificial increase in filament number (Fig 4.10). For 1N3R and 2N3R, the number of short filaments increases, the number of medium length filaments stays about the same and the number of long filaments decreases. 1N4R and 2N4R, which requires more Hsp70 than their 3R counterparts to reach complete inhibition, showed relatively no change in the number of short filaments, but a decrease in the number of medium and long filaments. These data indicates that as Hsp70 concentrations are increased, the elongation of tau isoforms is differently affected.

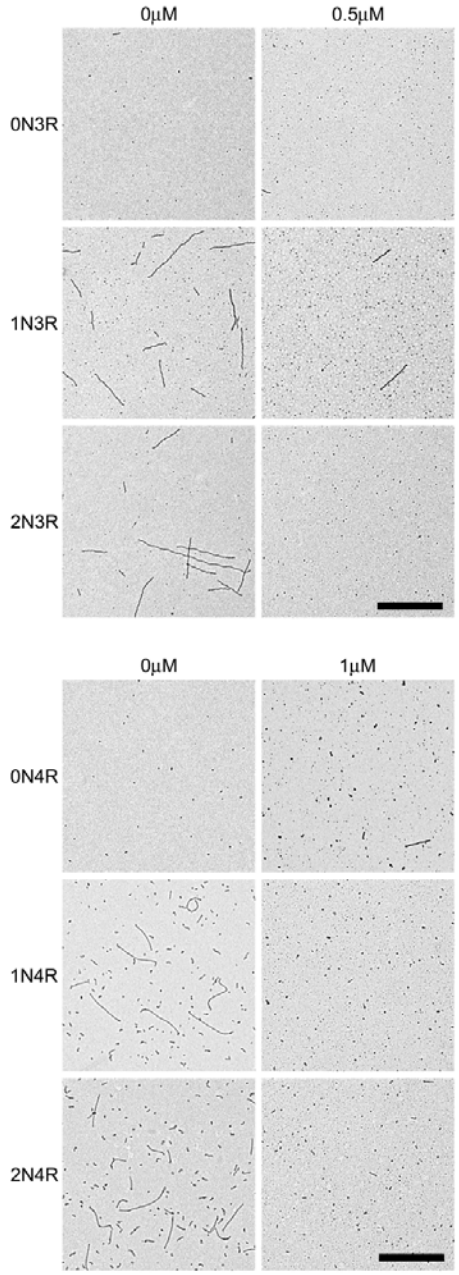

Figure 4.8. Electron micrographs of Hsp70 inhibited tau isoform polymerization with ARA. After 18 hrs, polymerization reactions from Figure 4.7 were visualized by TEM at 3600x magnification. Representative images at 3600x magnification of 3R isoforms are shown of (left column) 0 μM, and (right column) 0.5 μM Hsp70, and 4R isoforms of (left column) 0 μM, and (right column) 1 μM Hsp70. Scale bars represent 1 μm.

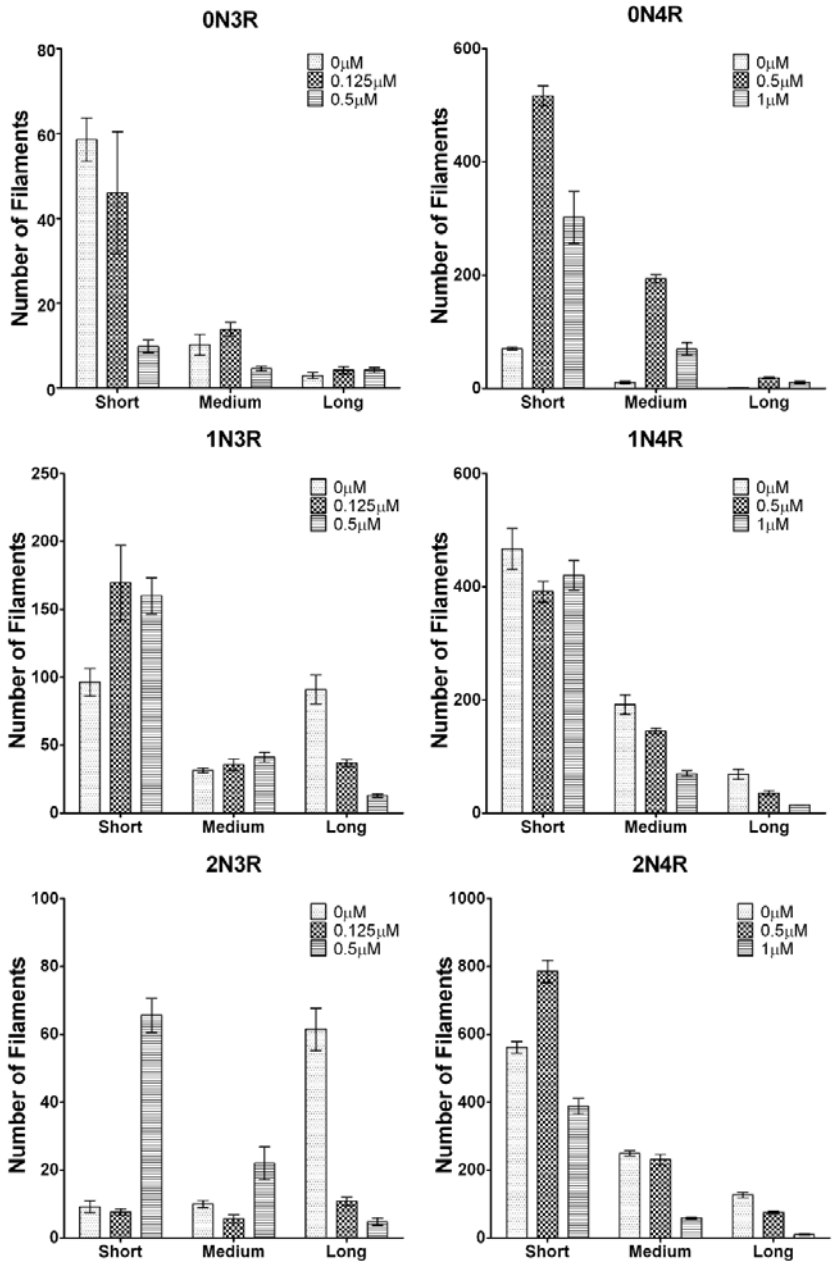

Figure 4.9. Electron micrograph filament length distributions of Hsp70 inhibited tau isoform polymerization with ARA. Images of polymerization reaction from Figure 4.7 were analyzed using Image Pro Plus to determine filament lengths with a minimum size of 25 nm. Data for each image was then counted for inclusion in one of the following ranges: short (between 25 nm and 50 nm), medium (between 50 nm and 100 nm), or long (greater than 100 nm). The mean ± SEM of 5 fields is displayed for each range.

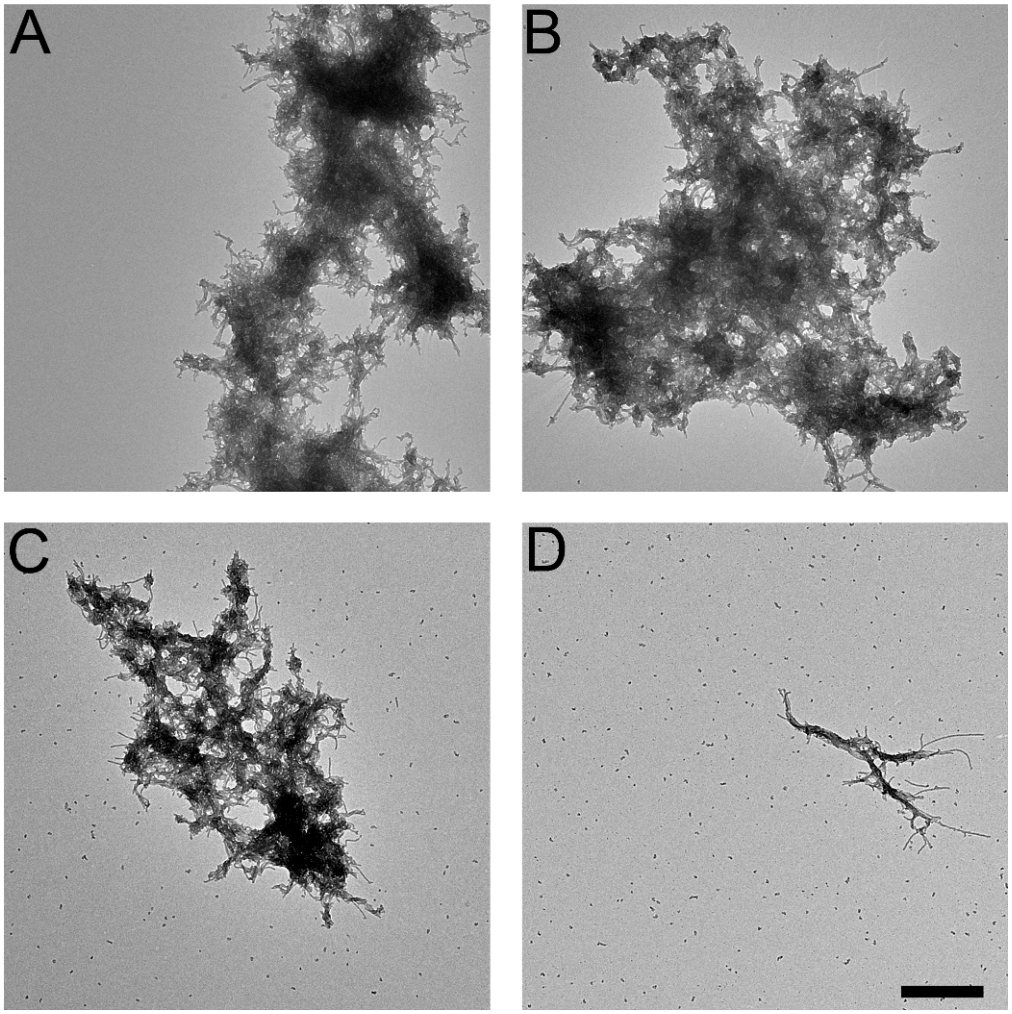

Figure 4.10. 0N4R aggregates artificially skew quantitation of electron microscopy data. After 18 hrs, polymerization reactions of ARA induced 0N4R tau polymerization with varying concentrations of Hsp70 were visualized by TEM at 3600x magnification. (A) 0 µM Hsp70 (B) 0.0625 µM Hsp70 (C) 0.125 µM Hsp70 and (D) 0.5 µM Hsp70. As the concentration of Hsp70 is increased, the size of infrequent large aggregates seems to decrease and filaments seem to become distributed more evenly across the grid. This suggests the data for quantitation of 0N4R filament lengths is skewed due to large aggregates. Scale bar represents 1 µm.

4.2.8 Hsp70 affects tau associated microtubule assembly

Because tau is a microtubule associated protein, and previous work has shown that Hsp70 increases tau protein affinity for microtubules in cells (*183*), the influence of Hsp70 on the microtubule assembly rate of the different tau isoforms was examined. A commercially available fluorescence based microtubule assembly assay was used (Cytoskeleton). Each tau isoform was incubated with and without Hsp70 (at a 1:1 ratio) and tubulin. This ratio of tau to Hsp70 is enough to completely inhibit tau polymerization in vitro. Microtubule assembly reactions were run concurrently with taxol, Hsp70 and buffer only controls. The taxol control was used to normalize data sets from different trials (Fig 4.11). Microtubules assembled in the presence of taxol and all tau isoforms. The addition of Hsp70 or buffer alone to tubulin reactions failed to increase tubulin assembly to detectable levels. In general, tau reactions that lack Hsp70 assembled tubulin to a higher steady state, and usually at a faster rate as compared to reactions that included tau and Hsp70. The data was fit to a nonlinear Gompertz function to determine lag, apparent rate of polymerization and maximum polymerization (*192, 197, 219*). 0N3R and 1N4R showed significant differences ($p<0.05$) for all three attributes upon addition of Hsp70 (Table 4.3). Hsp70 shortened the lag time, slowed the rate of microtubule assembly, and reduced the total extent of microtubule assembly in the presence of 0N3R. Hsp70 shortened the lag time, and reduced the total extent of assembly, but increased the rate of microtubule assembly for 1N4R. Hsp70 significantly affected the overall extent of microtubule assembly with 0N4R, 1N3R and 2N3R. Hsp70 also significantly affected the rate of 1N3R.

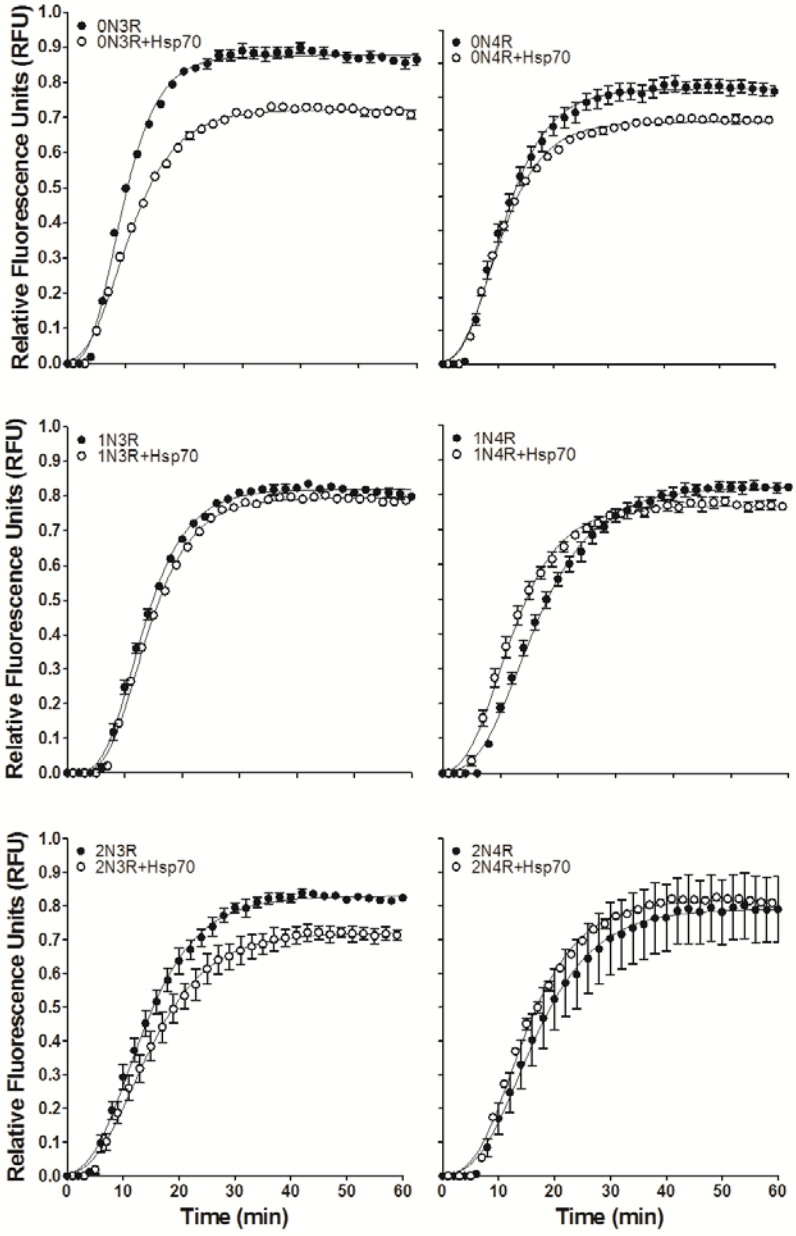

Figure 4.11. Microtubule assembly with tau isoforms and Hsp70. 1 µM tau isoforms were incubated with tubulin in the presence or absence of 1 µM Hsp70 at 37 ^{o}C for 1 hr. Fluorescent readings at 355 nm excitation and 460 nm emission were taken every minute. A taxol only control was used to normalize data from different runs, but the tau isoform and its corresponding tau +Hsp70 was always in the same run. Data shown is every other minute for ease of viewing and is the mean ± SEM of 3 trials.

	Hsp70	Y_{max} (RFU)		k_{app} (min^{-1})		lag (min)	
0N3R	-	0.88 ± 0.01	***	0.24 ± 0.01	**	3.72 ± 0.03	**
	+	0.72 ± 0.01		0.19 ± 0.00		3.27 ± 0.05	
1N3R	-	0.82 ± 0.01	*	0.20 ± 0.00	***	6.18 ± 0.42	
	+	0.79 ± 0.00		0.19 ± 0.00		6.76 ± 0.06	
2N3R	-	0.83 ± 0.01	**	0.15 ± 0.01		4.25 ± 0.41	
	+	0.72 ± 0.02		0.14 ± 0.01		4.66 ± 0.37	
0N4R	-	0.82 ± 0.02	*	0.19 ± 0.01		3.58 ± 0.22	
	+	0.72 ± 0.01		0.19 ± 0.01		3.19 ± 0.13	
1N4R	-	0.82 ± 0.01	*	0.14 ± 0.00	*	6.05 ± 0.13	**
	+	0.77 ± 0.01		0.18 ± 0.01		4.21 ± 0.30	
2N4R	-	0.79 ± 0.10		0.13 ± 0.01		6.19 ± 0.34	
	+	0.82 ± 0.00		0.15 ± 0.00		5.59 ± 0.14	

Table 4.3. Statistics of microtubule assembly with tau isoforms and Hsp70. Microtubule polymerization data were fit to the Gompertz growth curve to analyze the lag time, k_{app} (proportional to rate), and maximum polymerization. Statistical significance (* = $p<0.05$, ** = $p<0.01$, *** = $p<0.001$) as determined by an unpaired t-test is denoted by an asterisk for differences between with and without Hsp70 for each isoform.

4.3 Discussion

Hsp70 levels are increased in AD brains, most likely in response to oxidation and inflammation, known to be associated with AD (*232-236*). The inverse relationship of Hsp70 levels and tau pathology in specific hippocampal neurons indicates the cell could respond to a specific signal to upregulate Hsp70 to increase its ability to respond to the presence of abnormal tau and prevent aggregation. Previously published cell culture results showed an interaction between Hsp70 and 0N3R or 2N4R tau, resulting in decreased insoluble tau and an increase in tau association with microtubules (*183*). Due to the Hsp70 and tau interactions previously reported, we hypothesized that Hsp70 would affect tau protein dysfunction by inhibition of inducer mediated tau polymerization in vitro. 2N4R tau polymerization with various inducers of polymerization, arachidonic acid, Congo red and heparin was inhibited upon addition of Hsp70. This indicates that Hsp70 is a general inhibitor of tau polymerization and not dependent upon the inducer used. This is significant since the physiological inducer of tau polymerization is unknown. However, our data suggests that Hsp70 will inhibit any inducer because inhibition is likely protein specific and not inducer specific. We also determined that Hsp70 inhibits tau elongation, not nucleation.

We found that Hsp70 can act independently of ATP binding, which has been previously described (*237*). This ATP independent binding of Hsp70 is interesting as in a cell there is an abundance of ATP. However, we are describing an interaction of

Hsp70 and tau and not a refolding mechanism. In the ADP bound state, Hsp70 has a higher affinity for its substrate and a slower exchange rate. Therefore, in our in vitro system we conclude Hsp70 interacts with tau in a high affinity state in the absence of ATP. With the addition of ATP to the reactions, Hsp70 will hydrolyze ATP, but remain bound to tau similar to a reaction without ATP. In a neuron, there would be other factors such as co-chaperones and continuous cycling of ATP and ADP states. While we are not replicating what is most likely happening in a neuron, we show Hsp70 can bind tau in the absence of ATP and prevent aggregation.

Finally, we found tau filaments can be partially disassembled by Hsp70 in the presence of ATP although complete disassembly was not observed. Similarly, ATP is most likely required for partial disassembly as reactions without ATP had little observable effect. These data suggest increasing Hsp70 levels in a neuron before 2N4R tau polymerization takes place could increase the amount of inhibition of tau polymerization, and there is a potential to reverse the effects of tau polymerization by increasing the levels of heat shock proteins.

The alternative splicing of tau isoforms could influence the global hairpin structure commonly believed to be adopted by tau in solution (Fig 4.12) (*238*). These differences in structure could allow Hsp70 to interact with different residues of different tau isoforms (see Fig 5.1 for predicted Hsp70 binding sites). Therefore, we hypothesized that Hsp70 would differentially affect the polymerization inhibition of

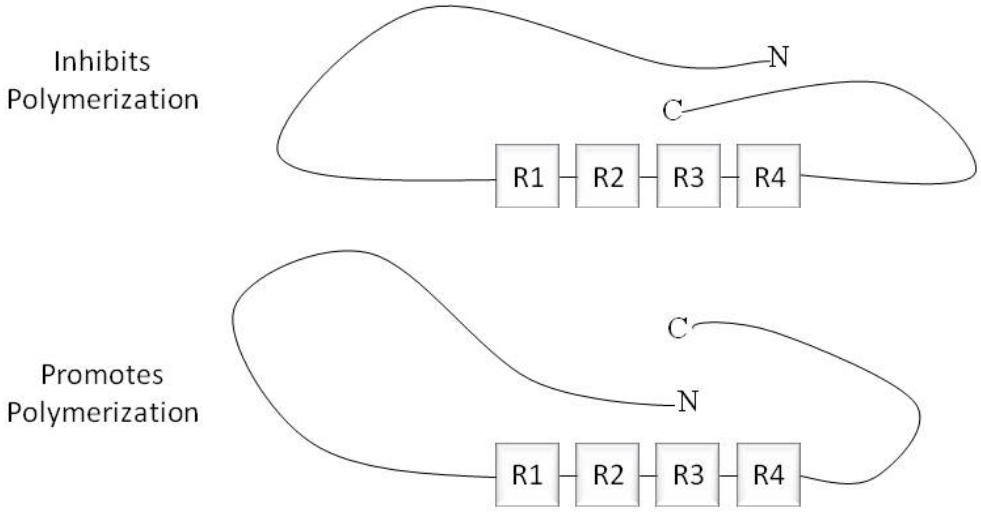

Figure 4.12 The global hairpin configuration of tau. Tau is thought to adopt a global hairpin conformation in solution. When the C-terminus is in close contact with microtubule binding repeat 3, tau is thought to be in its soluble form. When the N-terminus is in close contact with microtubule binding repeat 3, tau can form filaments. This later specific conformation is confirmed by the Alz50 and MC1 antibodies that bind to amino acids in both the N-terminus and amino acids in repeat 3, and only bind insoluble tau, not monomeric tau.

tau isoforms. 3R isoforms were found to be inhibited at lower concentrations of Hsp70 than 4R isoforms. Previous results have shown that a constitutively active heat shock protein, Hsc70, which shares a 86% sequence identity with Hsp70, can bind to tau isoforms (*186*). Hsc70 bound to 3R isoforms with a lower K_D than 4R isoforms. This difference in binding is thought to be due to the site of binding of Hsc70 to tau. ^{275}VQIINK^{280} and ^{306}VQIVYK^{311} are regions flanking microtubule binding repeat 2, which is alternatively spliced as exon 10 in 3R isoforms, and are thought to play a role in tau polymerization. Hsp70 therefore, could bind to the one available site on 3R isoforms, while it has two options on 4R isoforms. Thus, at low concentrations of Hsp70, 3R isoforms are inhibited perhaps because more tau protein has Hsp70 bound than 4R isoforms that may have a polymerization site still available. We also observed that 2N3R tau were inhibited 50% of maximum polymerization at a lower Hsp70 concentrations as compared to 0N3R and 1N3R, indicating that perhaps exon 3 is also involved in Hsp70 inhibition of tau polymerization. This could be due to the longer N-terminus affecting the global hairpin conformation and perhaps allows the ^{306}VQIVYK^{311} site to be more accessible. We did not observe a dramatic difference between the 4R isoforms that supports the idea that having two polymerization sites allows tau to polymerize in the presence of Hsp70 bound at one site.

Since the predicted site of Hsp70 binding is near the microtubule binding repeat regions, Hsp70 could inhibit the normal functions of tau through steric hindrance.

Previous results show increased Hsp70 levels in cell culture result in increased tau associated with microtubules. This indicates Hsp70 is not interfering with the microtubule binding function; however, Hsp70 could affect the microtubule assembly function of tau by removing the ability of one or more microtubule binding repeats to bind to assembling microtubules. This phenomenon has been described previously for tau where phosphorylation at certain sites changes the assembly properties, but not the microtubule binding properties of tau (*156*). We hypothesized that Hsp70 would differentially affect the tau isoforms ability to assemble microtubules in vitro, due to differences in primary sequence between isoforms. Even in the presence of equimolar concentrations of Hsp70, tau isoforms robustly assembled microtubules. However, Hsp70 significantly affected all three assembly properties (lag, k_{app}, and max) of 0N3R and 1N4R, but to various degrees. 0N4R and 2N3R were also affected significantly in terms of maximum assembly. This indicates that Hsp70 acts specifically on certain isoforms to change their ability to assemble microtubules, however assembly can still occur. Because 0N3R is the fetal form, increases in Hsp70 levels could play a role in microtubule formation in developing neurons.

We have shown that increased Hsp70 concentrations inhibit tau isoform polymerization. This inhibition is independent of polymerization inducer used, and independent of ATP. However, ATP could be useful in disassembling preformed tau filaments as reactions without ATP had little observable effect. Hsp70 also was shown to allow robust microtubule assembly, but was able to alter certain tau

isoforms ability to assemble microtubules slightly. These data, and previous results, indicate that increasing Hsp70 levels can inhibit the dysfunction of tau (polymerization) while allowing the normal microtubule assembly and binding function to remain intact. However, alterations in post-translational modifications, such as phosphorylation, could play a role in how Hsp70 interacts with tau isoforms. Changes in the post-translational modification of tau isoforms can alter the global hairpin conformation and potentially increase or decrease Hsp70 binding. These data could also explain the inverse relationship of molecular chaperones to tau pathology in AD affect hippocampal neurons, and could in part explain differences seen between tauopathies where the ratio 3R to 4R isoforms is altered.

Chapter 5-Conclusions and future directions

Alzheimer's disease was first described in 1907. Tau protein, which forms neurofibrillary tangles, a pathological hallmark of AD, was not discovered until 1975. Even then, tau was not implicated to play a role in neurodegeneration until the 1980s. Given this, the tau field is relatively new at about two decades. Further, research of tau is hampered by the lack of structural data to determine how tau undergoes the transition from natively unfolded to an amyloid form. Techniques that have been employed as ways to investigate tau folding include using small fragments of tau, or looking at lower resolution such as FRET studies that examine if two regions of the protein come in close contact with each other upon folding. An even more basic question exists as prior to this dissertation work, little was known about how alterations to tau affected filament formation. For instance, the physiological inducers for tau polymerization in neurons remain unknown, if there are any. Also, prior to this work, differences between tau isoforms were rarely compared. Most research is performed on 2N4R tau, as it includes all the exons missing from other tau isoforms. This makes comparison of the results between isoforms easier as differences between an isoform and 2N4R tau could be attributed to the missing exons. 2N4R also produces robust filaments upon polymerization with inducer molecules, and binds well to microtubules, making it an attractive isoform to work with. This work was endeavored upon to support a concept that tau research should take into account differences between isoforms.

Because the six tau isoforms differ largely in their primary sequence, it follows that there should be differences in both how they function normally by binding to tubulin, and how they polymerize and cause disease. The results presented in Chapter 3 show that 3R isoforms are not able to polymerize to the same extent as 4R isoforms. This is thought to be due to the absence of ^{275}VQIINK^{280} that is present in exon 10. This sequence has been shown to be important in tau polymerization as it is a minimal component of amyloid fiber formation (*121, 239, 240*). Also in Chapter 3, we show that the optimal ratio of inducer to tau isoform differs between isoforms and in fact, under certain conditions, heparin fails to induce polymerization of 3R isoforms. This suggests that in a cell, at a given inducer concentration, certain tau isoforms can polymerize at different rates than others. This also indicates that the local cellular environment plays a large role in tau dysfunction. The environment refers to the local concentration of an inducer between neurons. While we do not know what the physiological inducer is, it is difficult to assess how the relative levels change over time. Also, the environment refers to the local concentration of tau, which can vary from the cell body to the end of the axon, and if hyperphosphorylated could lead to changes in distribution along the axon (see section 1.5). Chapter 3 also demonstrated that even though all six isoforms can be phosphorylated by GSK-3β, they do not alter their filament morphologies, or even polymerization to the same degree. What we determined as the more important factor in regulating tau polymerization was the primary sequence, rather than GSK-3β phosphorylation. Finally, GSK-3β had various effects on tau isoform microtubule binding. In general, GSK-3β decreased

microtubule binding of tau isoforms, however in the case of 1N4R, microtubule affinity was increased. What this chapter indicates overall is that the six tau isoforms are not equal, and in order to model how tau dysfunction causes neurodegeneration, investigating specific effects of all six isoforms is required. It will not be sufficient to investigate just one isoform and apply that model to the others. GSK-3β has been shown to accumulate near NFTs in the cell body in transgenic mice models, but not in aged matched controls, indicating the localization of GSK-3β adds to the environmental complexity of tau aggregation (*241*). Our results indicate that GSK-3β, the kinase widely believed to play the major role in hyperphosphorylation of tau, cannot most likely act alone. We believe this is because GSK-3β failed to induce major changes in microtubule binding or tau aggregation into NFTs. It is possible that upon phosphorylation with multiple kinases, larger changes may occur.

The original rationale for performing the experiments in Chapter 3 Part 2 was to extend previous work performed in our lab on GSK-3β phosphorylation and pseudophosphorylation of 2N4R to the other tau isoforms (*191-193*). While we cannot directly compare all the tau isoform results to this work, we can compare our 2N4R results, and if similar to the previous results, make the assumption that the isoform results we observe are significant. The results of GSK-3β phosphorylation with 2N4R prior to and after polymerization showed that 2N4R was able to form what are termed "tangle-like" aggregates (*191, 193*). We see similar structures upon GSK-3β phosphorylation of 2N4R in our results where tau filaments start to bundle

into clusters, indicating phosphorylation of tau plays a role in the aggregation of filaments into larger structures such as NFTs. However, we note that not all tau isoforms were found to aggregate into these clusters, indicating that perhaps if phosphorylation by GSK-3β can accomplish this for some, there are perhaps other kinases that can accomplish clustering for the other tau isoforms. This clustering is despite slightly lower levels of phosphorylation in our results (~1 mole of phosphate per mole of tau) as compared to the previous results which saw ~3 moles of phosphate per mole of tau (*191*). We also saw a similar shift in the 2N4R band by SDS-PAGE upon phosphorylation, despite the lower phosphate incorporation. This most likely indicates a less efficient phosphate incorporation rate, but at similar sites as to induce a conformational change. We did not investigate the site specificity of the tau isoforms, however with similar levels of phosphate incorporation and a corresponding band shift upon phosphorylation between isoforms, we speculate that phosphorylation is occurring at similar sites on the various tau isoforms. We can attempt to correlate our GSK-3β phosphorylation data to the pseudophosphorylation data by examining which mutants are similar in properties to the 2N4R phosphorylation form. Based upon the pseudophosphorylation data examining which forms created an SDS-resistant mobility shift, our data is similar to the S396/404E and the 6- (199, 202, 205, 231, 396, 404) and 7-phos (199, 202, 205, 231, 235, 396, 404) mutants, which include the S396/404E mutations (*192*). These were the only pseudophosphorylation mutants that showed a SDS-resistant mobility shift similar in shift to our data. Our microtubule binding analysis showed that unphosphorylated

WT 2N4R tau had a similar K_d for both studies and upon phosphorylation with GSK-3β, 2N4R decreased in affinity to ~0.4 μM where the 6-phos pseudophosphorylation mutant decreased the microtubule binding affinity to ~0.4 μM as well. What is interesting is that single and double site mutations of the 6-phos (205, 199+202+205, 231, 393+404) all had similar K_d values, indicating that GSK-3β may phosphorylate any of these sites. Phosphorylation at any of these sites is possible because we believe that in solution, the tau monomer phosphorylated by GSK-3β is a mixture of many sites based upon the previous work (*191*, *193*). Likewise, upon comparison of overall polymerization between GSK-3β phosphorylated and pseudophosphorylation mutants, in general, most of the pseudophosphorylation mutants had decreased LLS values as compared to WT, similar to our observations. Differences between the two studies are observed when examining filament morphologies. Despite increased filament lengths for both studies, the pseudophosphorylation mutants did not show a tendency to cluster into tangle-like structures. This is despite the 6- and 7-phos mutant filaments on average being longer than GSK-3β filaments. However, in a set of unpublished data by Qian Sun and T. Chris Gamblin, mixtures of pseudophosphorylation mutants did lead to clustering, indicating the various phosphorylation states of tau monomers is important for clustering. Based upon our data for GSK-3β phosphorylation of 2N4R tau, we can conclude that we recapitulated previous results and that the observations of the other tau isoforms are representative of real differences upon phosphorylation with GSK-3β. Further studies investigating pseudophosphorylation of the tau isoforms may be able to elucidate the mechanisms

of phosphorylation changes affecting functional and dysfunctional properties of tau protein.

Over 30 kinases are known to be able to phosphorylate tau under normal and physiological conditions. We have examined GSK-3β phosphorylation of the tau isoforms in Chapter 3. GSK-3β, however, is known to be a kinase that works more effectively at primed sites (*242*). Primed sites are phosphorylated residues that are recognized by GSK-3β, for instance, to signal phosphorylation at a nearby site. So what we describe as mild effects of GSK-3β on tau isoforms could in fact be enhanced if tau undergoes phosphorylation by priming kinases such as CDK 5 and ERK 1. In fact, an entire dissertation could be devoted to examining the effects of phosphorylation by priming kinases alone and in conjunction with GSK-3β phosphorylation. Similarly, our lab has shown that by making mutations from serine and threonine to glutamic and aspartic acid, we can create pseudophosphorylation mutants that behave similarly to phosphorylated tau (*192*). By using this method, we can investigate residue specific changes to tau isoforms. Each method has its drawbacks though. If we were to use kinases exclusively, the phosphorylation process proceeds rapidly, however, we cannot control which residues the kinases will phosphorylate on tau. To this end, our lab has shown that phosphorylation of 2N4R tau with GSK-3β phosphorylates tau at about 1-4 moles of phosphate per mole of tau, however, up to 11 sites can be phosphorylated by use of phosphorylation site specific antibodies (*191, 193*). This indicates that not every tau monomer is phosphorylated

the same creating a problem of heterogeneous mixtures. By using kinases to investigate phosphorylation in vitro, determination of which sites are phosphorylated will be important to understand the results. Alternatively, if we were to use the pseudophosphorylation mutants, there is a long setup time in making mutations in all the isoforms at various combinations and then purifying each construct. We would have a more homogeneous mixture of tau monomer when looking at a specific mutation of residues; however, in a cell it is unlikely this exists. The best way to approach the question of how phosphorylation by multiple kinases plays a role in tau polymerization and loss of function, may be to employ both techniques where pseudophosphorylation mutants of priming sites are created and then phosphorylation with GSK-3β in vitro occurs. By doing this we can make sure we examine each priming site individually and in combination and then examine how priming affects GSK-3β phosphorylation of tau, using site specific phosphorylation antibodies that our lab has procured. Using this technique, we can more precisely examine the role phosphorylation plays in regulating tau function and dysfunction.

Chapter 4 provided a different angle on regulation of tau function and dysfunction. Instead of looking at post-translational modifications, we examined the role of a molecular chaperone, Hsp70, in the mediation of tau polymerization and microtubule assembly. Hsp70 is upregulated in response to stress, such as heat shock, oxidative stress, or inflammation and has been found to correlate inversely to the level of tau aggregation in hippocampal neurons (*183*). Therefore, we proposed that Hsp70 could

act directly on tau in vitro and prevent its aggregation. Our data showed that Hsp70 acts on tau directly, not by binding the inducer, preventing tau polymerization. Similar results of 2N4R tau polymerization inhibition with Hsp70 has been shown to occur in vitro, supporting our idea that Hsp70 acts direct on tau (*187*).

Likewise, Hsp70 can act through an ATP independent mechanism to prevent tau aggregation as the addition of ATP to polymerization reactions showed similar characteristics as reactions without ATP. The exact mechanism by which this occurs is an interesting topic for future studies examining structural changes of Hsp70 and tau upon Hsp70 and tau binding. Previously, ATP independent binding has been described in which the substrate binding domain (SBD) of DnaK, the *E. coli* homologue of Hsp70, was shown to bind a peptide in the presence or absence of ATP and/or the presence or absence of the ATPase domain (*237*). This indicates the substrate binding domain can exist in a high affinity state for substrate. Whether this happens in the cell is unknown as the cellular environment contains large amounts of ATP.

We found all tau isoform polymerization was inhibited by Hsp70, to varying degrees. Most notably the 3R isoforms were inhibited at a lower concentration of Hsp70 than the 4R tau isoforms. The mechanism for how this occurs is speculative at this point, but Hsp70 is thought to bind to the two hexapeptide regions (275-280 and 306-311), similar to what has been reported for Hsc70 (*186*). 4R tau contains both regions,

therefore two Hsp70 would need to bind one tau in order for polymerization to be inhibited, and if only one Hsp70 was bound, the unbound hexapeptide could still be involved in polymerization. Conversely, 3R tau only has one hexapeptide and if Hsp70 binds this, there is not a compensatory hexapeptide to allow polymerization to still proceed, and is thus inhibited at a lower concentration of Hsp70. What was also of interest is that 2N3R tau was inhibited at a lower concentration of Hsp70 than the other 3R isoforms. This indicates Hsp70 also has an impact on exon 3 as 0N and 1N isoforms lack exon 3. This also indicates that future uses of Hsp70 as a therapeutic may need to involve isoform specific interactions as Hsp70 seems to influence isoform polymerization differently. The exact role Hsp70 plays in 2N3R polymerization inhibition is unknown. Based upon what is known about tau polymerization however, we can speculate as to a mechanism. The N-terminus of tau is thought to be involved in promotion of tau polymerization, as a truncation of the N-terminus decreases the polymerization of tau in vitro (*243-245*). Based upon a Kyte-Doolittle hydropathy plot of tau isoforms (Fig 5.1) the 2N isoforms have a patch of hydrophobic residues in exon 3, a potential binding site of Hsp70. If Hsp70 binds to the N-terminus and the 275-280 hexapeptide, which could only occur with 2N isoforms, then this would mimic N-terminal truncation and potentially explain why 2N3R is inhibited at a lower Hsp70 concentration than other 3R isoforms. We also found Hsp70 acts on tau to alter the microtubule assembly properties of tau, although there is still a large amount of microtubule assembly. Only two tau isoforms were significantly affected for all three parameters measured, but 4 isoforms had a

significantly lowered overall amount of microtubule assembly. In order to determine why there is a difference between the isoforms more information would need to be determined about the specific interactions of Hsp70 and the individual tau isoform by examination of binding affinities for the various tau isoforms.

The results of Chapter 4 are a good indicator that Hsp70 could be a good therapeutic target for control of tau aggregation in neurons. Hsp70 inhibits tau polymerization, while still allowing robust microtubule assembly. However, more information about the Hsp70 and tau interaction needs to be determined, most notably where Hsp70 can interact on tau. This proposed interaction, based upon previous studies examining Hsc70 and tau interactions (*186*), would indicate Hsp70 binds to the two hexapeptides flanking MTBR 2. However, it seems that in the case of 2N3R, Hsp70 could bind to a part of exon 3 as well. Examination of a Kyte-Doolittle hydropathy plot of the tau isoforms shows potentially large hydrophobic regions where Hsp70 could bind (Fig 5.1). Investigation into Hsp70 binding of 2N4R using a variety of techniques has resulted in uninterpretable results (see Appendix). The reason for these results is most likely due to technical difficulties, as both Hsp70 and tau are very "sticky" proteins that can bind non-specifically to the materials used. For example, the first experiment to test the binding affinity of Hsp70 and 2N4R tau was to bind 2N4R tau and Hsp70 to Protein G beads coupled with anti-tau and Hsp70 antibodies (Fig A.1). The protein however, was unable to stay bound to the beads. The second attempt used magnetic nickel agarose beads with histidine tagged tau, and adding non-

histidine tagged Hsp70 (Fig A.4). However, Hsp70 was able to bind to the nickel agarose beads in the absence of tau, despite the fact that Hsp70 with no histidine tag did not react with an anti-histidine antibody via western blot (Fig A.3). The next technique to measure binding was isothermal titration calorimetry; however we were never able to consistently produce a normal isotherm (Fig A.5-A.8). We believe this is due to the high protein concentrations required to run the experiment, and possible dimerization of Hsp70, which upon dilution would result in dissociation and heat changes. We finally tried using the BIAcore surface plasmon resonance technique that uses an immobilized ligand on a chip and flows an analyte over the surface; any change in the mass on the surface of the chip is measured as a change in the reflection of light. We tried a variety of immobilization combinations (tau antibody, Hsp70 antibody, 2N4R tau, and histidine tag antibody) and flowed the corresponding analyte over the surface. While we were able to generate results, our control channel (no protein coupled to the chip) showed interactions, with both tau (Fig A.9) and Hsp70 (data not shown), but not with a peptide that can bind to Hsp70 (Fig A.10). Despite the issues with the control panel, we did find the Hsp70 bound a larger amount of 2N4R tau than 2N3R tau, or a deletion mutant of residues I277, I278, I308, and V309, which are hydrophobic residues in the two hexapeptide regions (Fig A.11-13). This verifies that Hsp70 and tau interact with each other and that the two hexapeptide regions are targets of Hsp70. Despite the technical difficulties with the control channel, a future direction for this project would be to make peptides, of roughly 11 amino acid lengths (similar in size to the substrate binding peptide used in the

BIAcore experiments), that span the regions determined by the hydropathy plot to be potential Hsp70 binding sites (Fig 5.1). These peptides should have less non-specific binding to the control channel as seen with the Hsp70 substrate binding domain peptide (Fig A.10).

Despite a lack of understanding of how Hsp70 and tau interact, investigation into how modifications to tau affect Hsp70 binding is critical to understanding how to prevent tau aggregation in a neuron. Our lab has the resources to test a wide variety of mutations and post-translational modification states of tau isoforms. Because hyperphosphorylated tau is so widely involved in the pathogenesis of AD and other tauopathies, and having pseudophosphorylation constructs readily available for all the isoforms, we can examine how phosphorylation at various sites changes Hsp70 polymerization inhibition. The substitution of glutamic and aspartic acid for serine and threonine would make these regions less hydrophobic, especially for regions that have multiple serines and threonines like the C-terminus. We would predict that by making these regions more negative and decreasing hydrophobicity, tau would still potentially be inhibited in its polymerization. We would also predict that because of the decreased hydrophobicity, inhibition of inducer mediated tau polymerization would require a larger concentration of Hsp70, consistent with upregulation of Hsp70 during stress. In addition, once the residues of tau that Hsp70 can bind to are determined, the next interesting question is to ask how Hsp70 inhibits tau polymerization. For instance, does Hsp70 bind tau and because of steric hindrance

prevent interactions with other tau monomers? Alternatively, does Hsp70 create a folding intermediate of tau that is unable to polymerize because the hexapeptides are buried? Hsp70 is a good target for modulation of tau dysfunction as Hsp70 levels are increased during stress and most likely increases in Hsp70 levels will have a minimal impact on other cellular functions as Hsp70 will only bind abnormally folded proteins. However, Hsp70 may not be the best candidate for targeting tau. It would be interesting to determine how much better or worse other chaperones, such as Hsp40 (the co-chaperone of Hsp70), Hsp90, or Hsp104, might be at regulation of tau dysfunction. In addition, within neurons, multiple heat shock proteins work in conjunction to regulate protein misfolding. Examination of the interplay of these chaperones in vitro would provide better insight into how to improve tau aggregation inhibition.

This dissertation is the culmination of work performed during my graduate school tenure. It has demonstrated that tau isoforms respond differently to their environment (summarized in Table 5.1). It has shown that by focusing on one specific tau isoform the whole picture is obfuscated, as the tauopathies involve the aggregation and modification of various tau isoforms. This dissertation has shown that the natural cell response to prevent aggregation by increased molecular chaperone involvement works, but is somehow evaded in AD. Perhaps in the other tauopathies the misregulation of heat shock proteins can result in the variety of tau isoforms found the insoluble inclusions. This work advances the field by providing a step toward

understanding how tau isoforms are differentially regulated and involved in tauopathies. Since Hsp70 is a natural stress responder, this work points toward the use of inducible cellular proteins, to treat neurodegenerative diseases as a potential future therapeutic. Such therapies could make use of chemical modifiers of Hsp70, such as geldanamycin analogues, that have been shown to upregulate Hsp70 in cells. These cells, which the current literature suggests have a defective stress response, may need help through the use of the analogues, while normal cells would hopefully sense a normal state and not respond.

	Region 1	Region 2
0N3R	41-AGLKAEEAGIG-51	
0N4R	41-AGLKAEEAGIG-51	
1N3R		
1N4R		
2N3R		70-PTAEDVTAPLVDEGAP-85
2N4R		70-PTAEDVTAPLVDEGAP-85

	Region 3	Region 4
0N3R	60-AAGHVTQARMVS-71	185-LQTAPVPMPDLKNV-198
0N4R	60-AAGHVTQARMVS-71	185-LQTAPVPMPDLKNV-198
1N3R	89-AAGHVTQARMVS-100	214-LQTAPVPMPDLKNV-227
1N4R	89-AAGHVTQARMVS-100	214-LQTAPVPMPDLKNV-227
2N3R	118-AAGHVTQARMVS-129	243-LQTAPVPMPDLKNV-256
2N4R	118-AAGHVTQARMVS-129	243-LQTAPVPMPDLKNV-256

	Region 5	Region 6
0N3R		214-GGKVQIVYKPVDLSKVTSKCGSLGNI-239
0N4R	217-VQIINKKLDLSNV-229	241-HVPGGGSVQIVYKPVDLSKVTSKCGSLGNI-270
1N3R		243-GGKVQIVYKPVDLSKVTSKCGSLGNI-268
1N4R	246-VQIINKKLDLSNV-258	270-HVPGGGSVQIVYKPVDLSKVTSKCGSLGNI-299
2N3R		272-GGKVQIVYKPVDLSKVTSKCGSLGNI-297
2N4R	275-VQIINKKLDLSNV-287	299-HVPGGGSVQIVYKPVDLSKVTSKCGSLGNI-328

	Region 7	Region 8
0N3R	261-VQSKIGSLDNITHVP-275	300-GAEIVYKSPVVSGD-313
0N4R	292-VQSKIGSLDNITHVP-306	331-GAEIVYKSPVVSGD-344
1N3R	290-VQSKIGSLDNITHVP-304	329-GAEIVYKSPVVSGD-342
1N4R	321-VQSKIGSLDNITHVP-335	360-GAEIVYKSPVVSGD-373
2N3R	319-VQSKIGSLDNITHVP-333	358-GAEIVYKSPVVSGD-371
2N4R	350-VQSKIGSLDNITHVP-364	389-GAEIVYKSPVVSGD-402

	Region 9
0N3R	318-HLSNVSSTGSIDMVDSPQLATLADEVSASLAKQGL-352
0N4R	349-HLSNVSSTGSIDMVDSPQLATLADEVSASLAKQGL-383
1N3R	347-HLSNVSSTGSIDMVDSPQLATLADEVSASLAKQGL-381
1N4R	378-HLSNVSSTGSIDMVDSPQLATLADEVSASLAKQGL-412
2N3R	376-HLSNVSSTGSIDMVDSPQLATLADEVSASLAKQGL-410
2N4R	407-HLSNVSSTGSIDMVDSPQLATLADEVSASLAKQGL-441

Figure 5.1 Predicted hydrophobic regions of tau isoforms. Hsp70 binds primarily to exposed hydrophobic patches of proteins. Tau isoforms were analyzed using ProtScale on ExPASy (http://expasy.org/cgi-bin/protscale.pl) using the Kyte-Doolittle (*246*) hydrophobicity scale at a window size of 11 amino acids. Regions of hydrophobic patches were aligned for each isoform. Numbers denote amino acid residue for the specific tau isoform. The three regions that differ are 41-51 for the 0N isoforms, 70-85 for the 2N isoforms and Region 5 that contains VQIINK (only present in 4R isoforms, and a previously described Hsc70 binding site).

	0N3R	1N3R	2N3R	0N4R	1N4R	2N4R
Polymerization changes upon increasing [ARA]	increases, lower extent than 3R	increases, lower extent than 3R	increases, lower extent than 3R	increases, higher extent than 3R	increases, higher extent than 3R	increases, higher extent than 3R
Polymerization changes upon increasing [Heparin]	no polymerization	no polymerization	no polymerization	polymerization, but inhibited at higher [Heparin]	polymerization, but inhibited at higher [Heparin]	polymerization, but inhibited at higher [Heparin]
Phosphate incorporation with GSK-3β	about 0.5 moles phophate per mole tau	about 1 mole phophate per mole tau	about 1 mole phophate per mole tau	about 1 mole phophate per mole tau	about 1 mole phophate per mole tau	about 1 mole phophate per mole tau
Change in microtubule binding affinity upon phosphorylation with GSK-3β	no significant change	decreased affinity	increased affinity	no significant change	decreased affinity	no significant change
Change in morphology upon phosphorylation with GSK-3β	increased length, clustering	increased length	increased length	increased length	increased length, clustering	increased length, clustering
Change in polymerization upon increasing [Hsp70]	decreased	decreased	decreased	decreased	decreased	decreased
50% polymerization inhibition concentration of Hsp70 (μM) (ThS)	0.19 ± 0.03	0.13 ± 0.01	0.10 ± 0.01	0.71 ± 0.08	0.61 ± 0.05	0.60 ± 0.07
Change in morphology upon increasing [Hsp70]	decreased filament lengths	decreased filament lengths	decreased filament lengths	decreased filament lengths	decreased filament lengths	decreased filament lengths
Change in microtubule assembly lag time with Hsp70	decreased lag time	no significant change	no significant change	no significant change	decreased lag time	no significant change
Change in microtubule assembly rate with Hsp70	decreased rate of assembly	decreased rate of assembly	no significant change	no significant change	increased rate of assembly	no significant change
Change in overall extent of microtubule assembly with Hsp70	decreased overall extent of assembly	decreased overall extent of assembly	decreased overall extent of assembly	decreased overall extent of assembly	decreased overall extent of assembly	no significant change

Table 5.1 Summary of tau isoform differences determined in this dissertation.

Appendix- Hsp70 and tau binding studies to date

This appendix is a record of Hsp70 and tau binding studies that have failed to produce useable data. We have tried (in order) using Protein G beads with tau (Tau12) or Hsp70 (SPA810) antibodies to capture tau and Hsp70, and then bind the corresponding protein. Next, we tried using nickel agarose beads to bind histidine tagged tau, and capture non-histidine tagged Hsp70. Next, we tried using isothermal titration calorimetry to measure the heat of binding between tau and Hsp70, but could not reproduce good data. Finally, we tried using surface plasmon resonance to measure binding of Hsp70 and tau, but found both Hsp70 and tau bind in the empty reference channel. This means we cannot account for non-specific binding in the test channels, and results in unreliable data. The images shown are in support of why we chose to use the next set of techniques. This is meant to be a record for future experiments and what not to do.

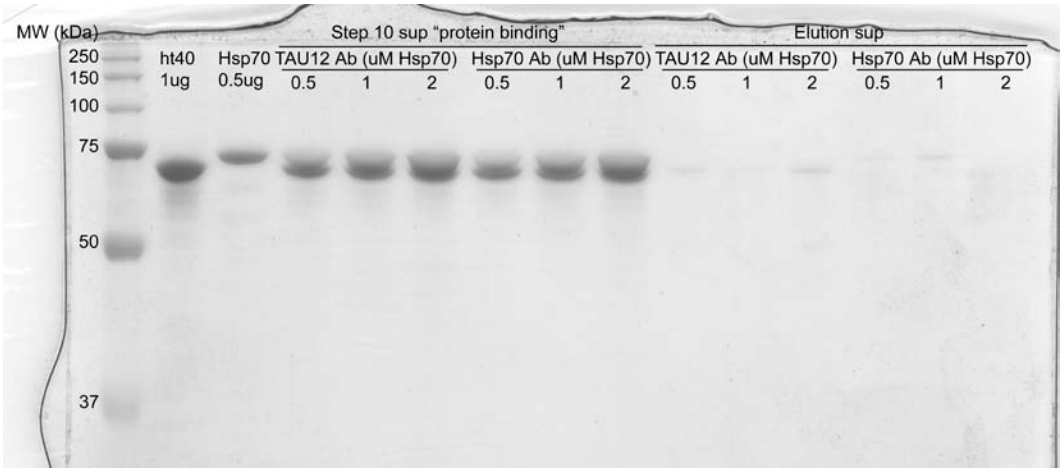

Figure A.1 Hsp70 and 2N4R tau bound to antibodies do not stay bound to Protein G beads. 100 µl of Tau12 (anti-tau) or SPA810 (anti-Hsp70) was incubated with 50 µl of magnetic Protein G beads for 10 minutes at room temperature. Beads were attracted to one side of tube by a magnet and washed before addition of 2 µM tau and 0.5, 1 or 2 µM Hsp70 that had been preincubated at 37 ^{o}C for 10 minutes. After incubation of proteins with beads for 10 minutes, beads were again attracted to one side of the tube, and the supernatant (labeled step 10 sup above) was collected. The beads were washed three times and the remaining protein was eluted (labeled elution sup above). Both supernatants, 1 µg of 2N4R tau, and 0.5 µg Hsp70 with a molecular weight marker were run on 10% SDS-polyacrylamide gels, stained with Coomassie blue and scanned. The data shows that tau and Hsp70 bind weakly to both antibodies, and that very small amounts remain bound by time the elution of proteins occurs.

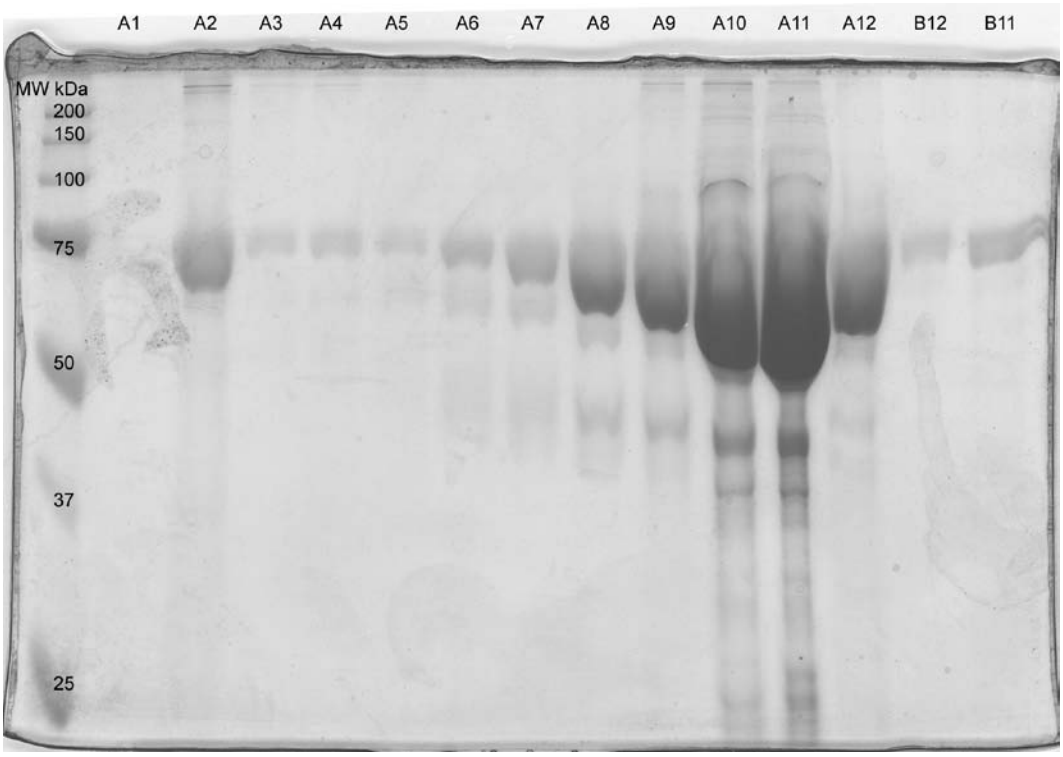

Figure A.2 SDS-PAGE of thrombin cleavage of Hsp70 to remove histidine tag for use in nickel agarose bead precipitation. Purified Hsp70 was subjected to thrombin cleavage to remove the N-terminal histidine tag and run over a Nickel column. Hsp70 without the histidine tag did not bind to the column as indicated by the large protein bands around A8-A12 on the 10% SDS-polyacrylamide gel.

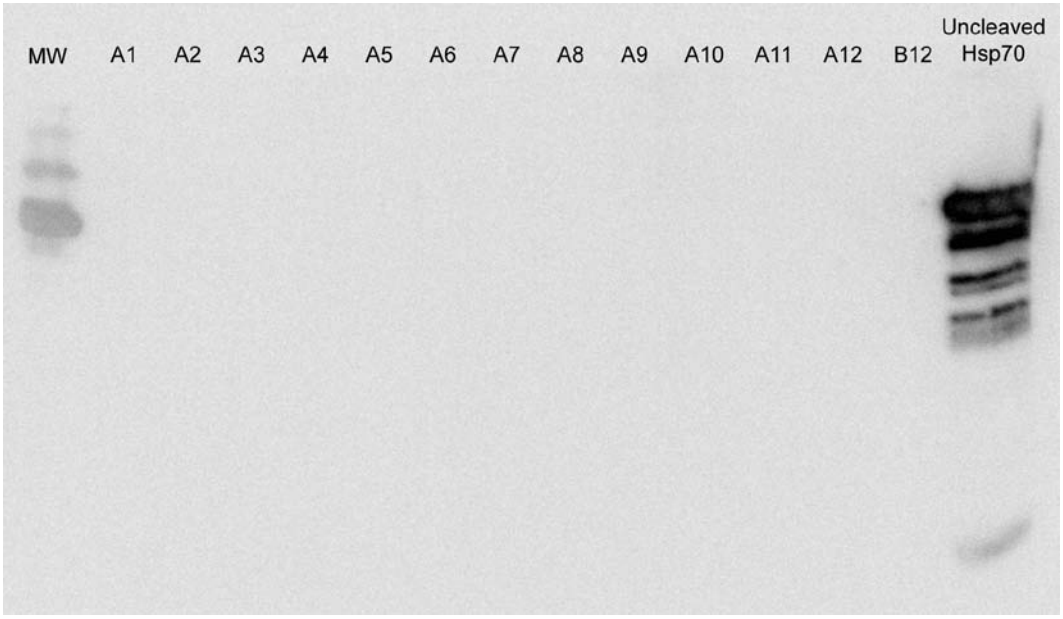

Figure A.3 Western blot for the anti-histidine tag of thrombin cleaved Hsp70 to remove histidine tag for use in nickel agarose bead precipitation. The fractions from Fig A.2 were run again on a 10% SDS-polyacrylamide gel and transferred to a PVDF membrane. Anti-histidine antibody was used to detect the presence of His-tagged Hsp70. As seen, no immunoreactivity was present in A1-B12, but was present in a sample of uncleaved Hsp70. This indicates thrombin cleavage of Hsp70 worked and without a histidine tag.

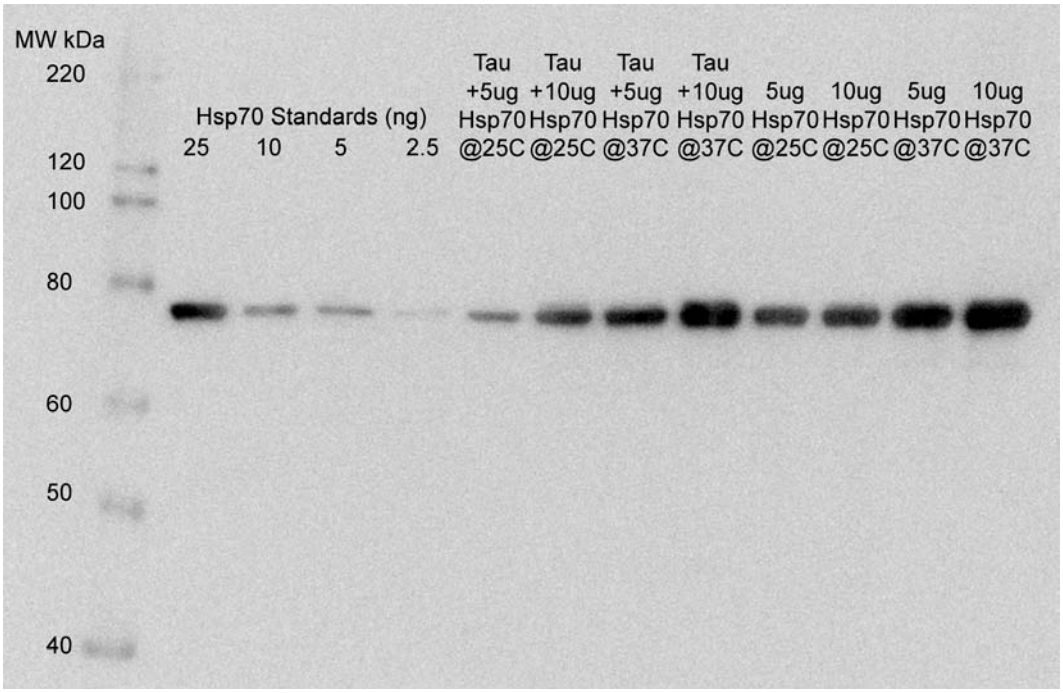

Figure A.4 Tau and non-his-tagged Hsp70 immunoprecipitation with magnetic nickel agarose beads. 0 µg and 5 µg of 2N4R tau and 5 or 10 µg of Hsp70 was incubated at 25 ^{o}C or 37 ^{o}C for 1 hour and then bound to magnetic nickel agarose beads. The elution supernatants (eluted by 250 mM Imidazole) were analyzed by western blot for Hsp70 bound to tau. The anti-Hsp70 western shows that Hsp70 bound to the beads independent of tau (see last four lanes without tau). In addition, Hsp70 seemed to bind better to the beads at 37 ^{o}C than 25 ^{o}C, indicating future experiments may need to be done at 37 ^{o}C.

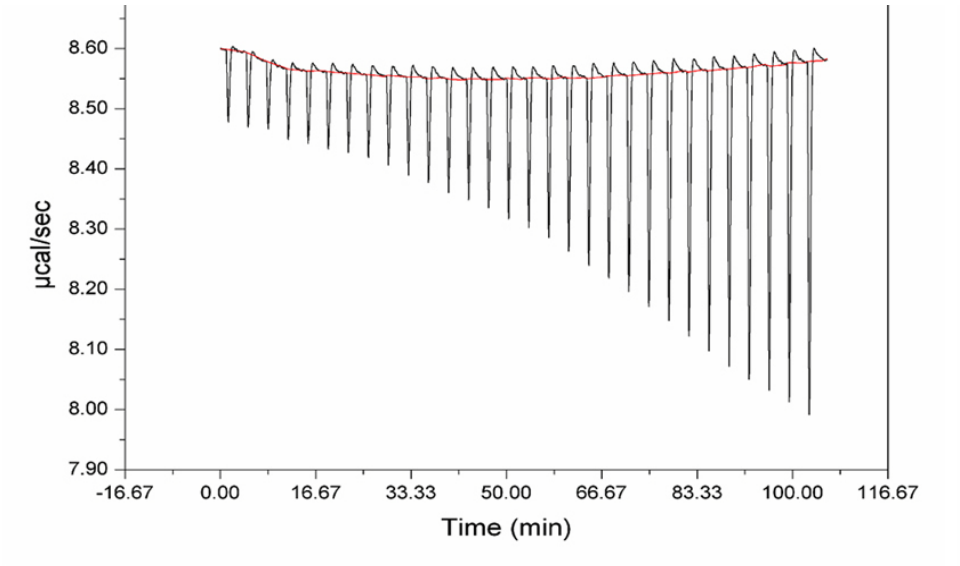
8.60
8.50
8.40
8.30
8.20
8.10
8.00
7.90
µcal/sec
-16.67
0.00
16.67
33.33
50.00
66.67
83.33
100.00
116.67
Time (min)

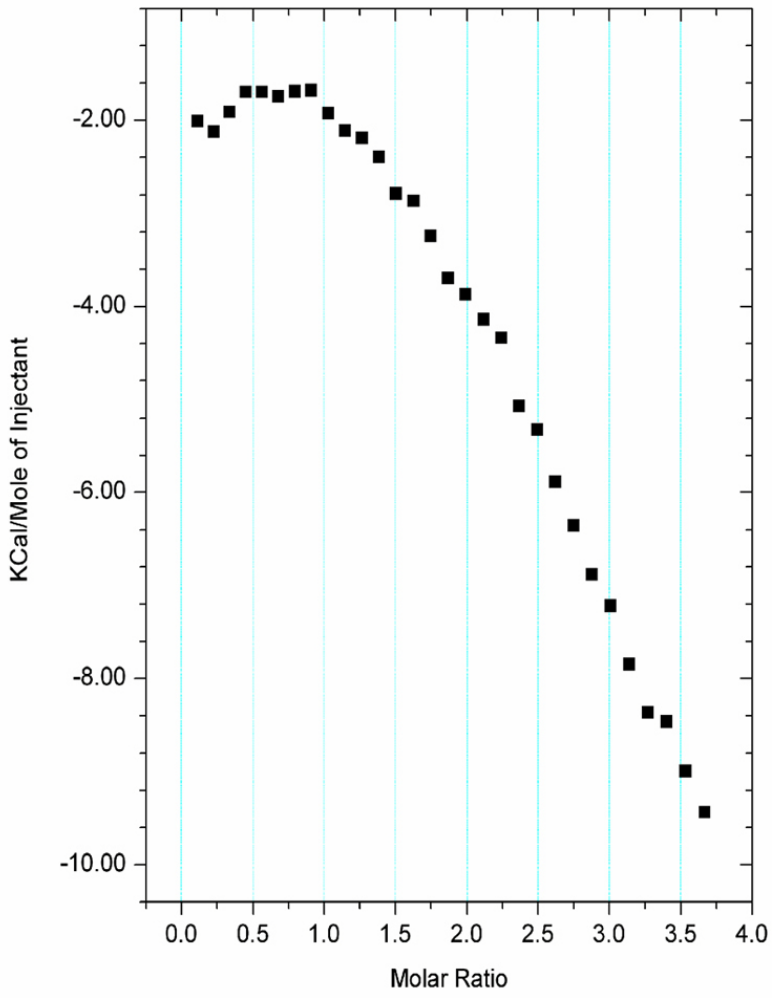
-2.00
-4.00
-6.00
-8.00
-10.00
KCal/Mole of Injectant
0.0
0.5
1.0
1.5
2.0
2.5
3.0
3.5
4.0
Molar Ratio

Figure A.5 Isothermal titration calorimetry (ITC) of Hsp70 and 2N4R tau to determine binding constants. (from 5-24-10) Hsp70 and 2N4R tau were dialyzed with three buffer changes (45 minutes at room temp., 1 hour at room temp., and overnight at 4 ^{o}C) in 100 mM NaCl, 10 mM Hepes pH 7.64, 0.1 mM EDTA, and 1% β-mercaptoethanol. Protein was aliquoted into single use (5 ml tau at 9.3 µM and 500 µl Hsp70 at 147.64 µM). Using a MicroCal VP-ITC, the jacket temperature was set to 37 ^{o}C, tau was loaded into the cell, and Hsp70 was loaded into the syringe. The following are the settings for injections: 30 injections (2 µl initial and 10 µl rest), reference power 10 µcal/sec, 310 rpm stirring speed. The raw data (top image, black line) shows a consistent baseline (top image, red line), however, increasing heats with each injection. The processed data (bottom image, black squares) which accounts for the baseline shows that as Hsp70 is injected into the cell containing tau, more heat is given off each injection. This is the opposite of what should happen if two proteins bind to each other, as the injected protein will eventually bind all the protein in the cell and the heat given off each injection will be less.

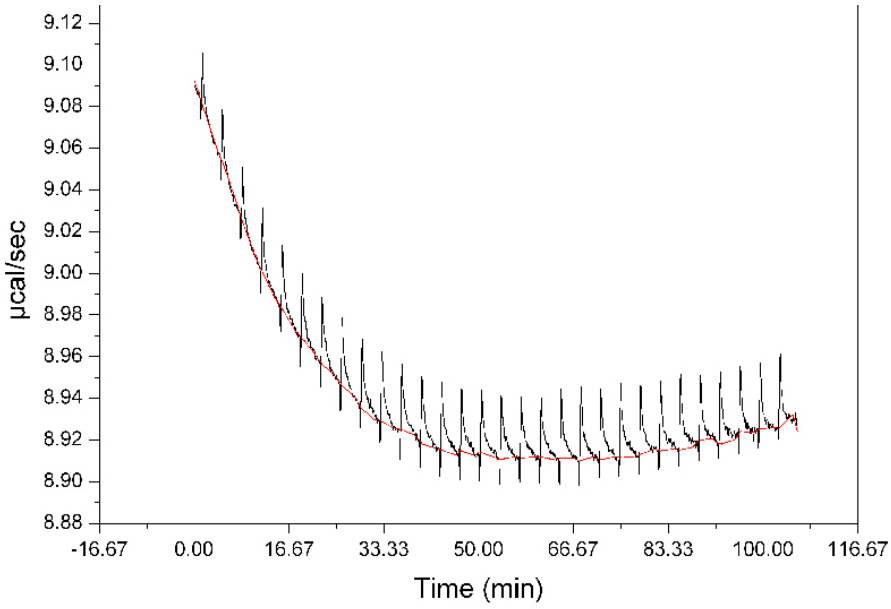
9.12
9.10
9.08
9.06
9.04
9.02
9.00
8.98
8.96
8.94
8.92
8.90
8.88
µcal/sec
-16.67
0.00
16.67
33.33
50.00
66.67
83.33
100.00
116.67
Time (min)

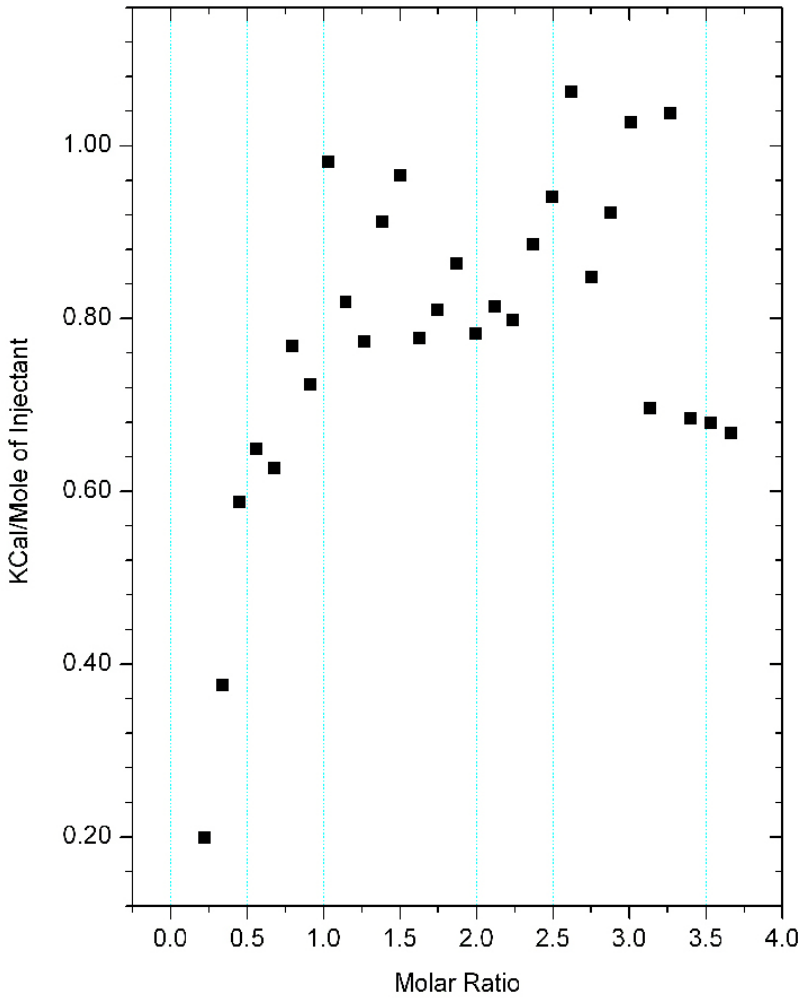
1.00
0.80
0.60
0.40
0.20
KCal/Mole of Injectant
0.0
0.5
1.0
1.5
2.0
2.5
3.0
3.5
4.0
Molar Ratio

Figure A.6 ITC of Hsp70 injection into buffer. (from 5-25-10) Hsp70 at 147.64 µM was injected into buffer at 37 ^{o}C using the same parameters as Figure A.5. The raw data (top image, black line) shows that as more Hsp70 is injected into the cell the heat given off does not change, however the baseline (top image, red line) drifts significantly. A normal dilution of injectant into buffer should have a flat baseline. The processed data (bottom image, black squares) shows a slight increase in the heat given off each injection, indicating possible dimers coming apart upon dilution.

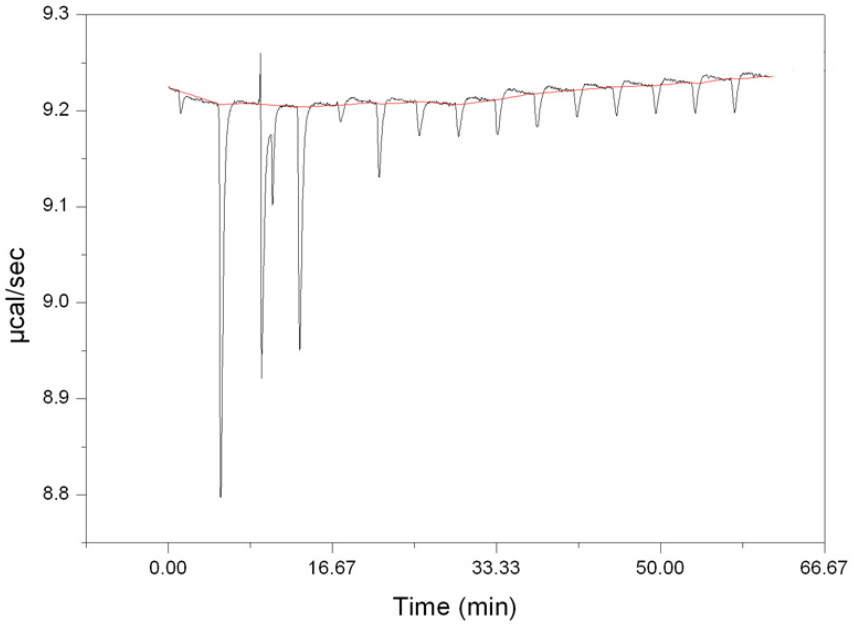
9.3
9.2
9.1
9.0
8.9
8.8
µcal/sec
0.00
16.67
33.33
50.00
66.67
Time (min)

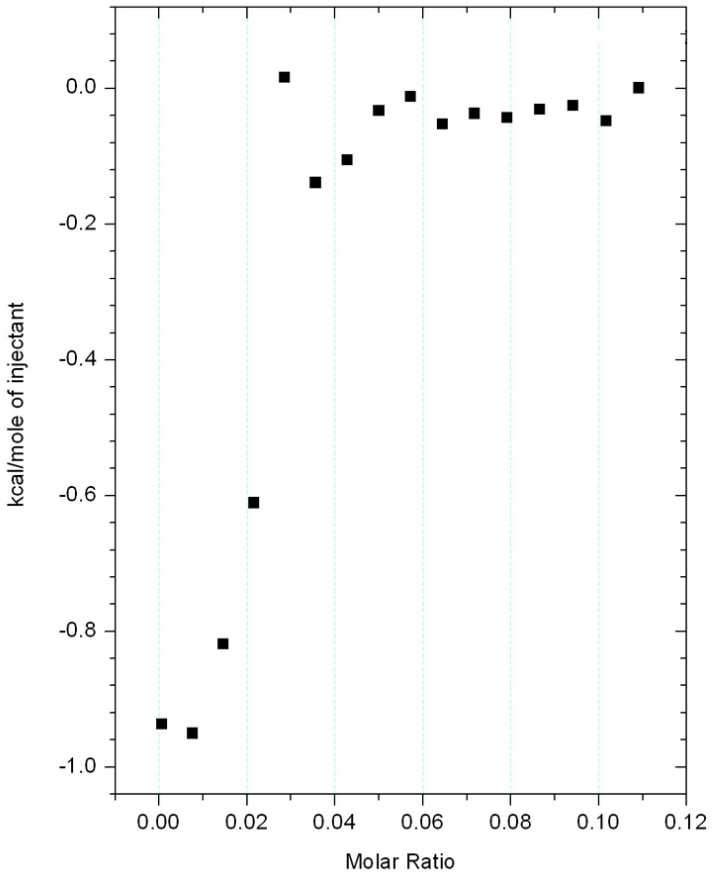
0.0
-0.2
-0.4
-0.6
-0.8
-1.0
kcal/mole of injectant
0.00
0.02
0.04
0.06
0.08
0.10
0.12
Molar Ratio

Figure A.7 ITC was run using an automated version of the VP-ITC. (from 8-12-10) Data shown is of Hsp70 (147.64 µM) and 2N4R tau (10.372 µM) at the settings used in Fig A.5 and A.6, however the system automates everything from cleaning to injecting. The raw data (top image, black line) indicates a decreasing amount of heat as more Hsp70 is added to the system and a steady baseline (top image, red line). The processed data (bottom image, black squares) shows that saturation was reached very soon in the experiment and lower concentrations of protein would shift the curve to where a bottom (no Hsp70 binding tau) could be detected.

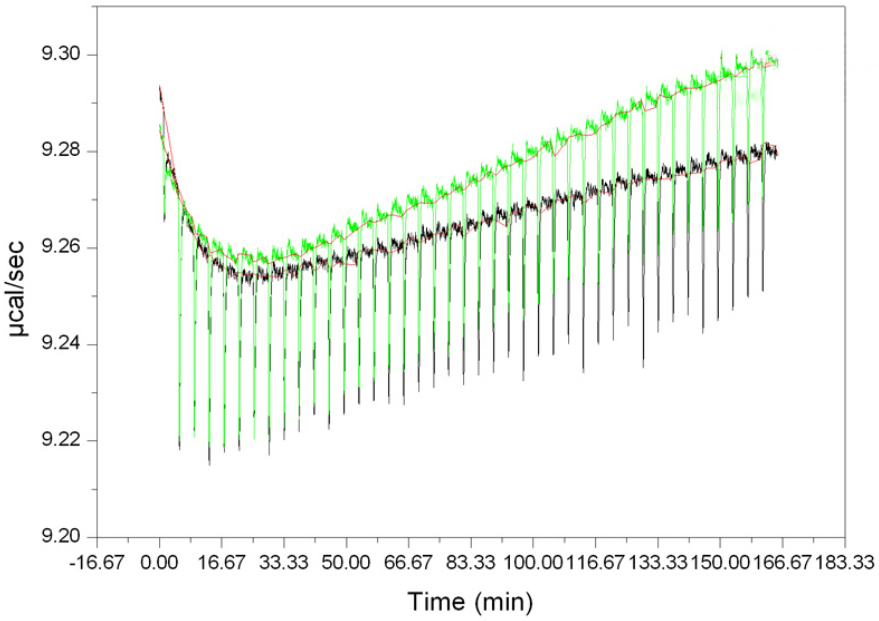
9.30
9.28
9.26
9.24
9.22
9.20
µcal/sec
-16.67 0.00 16.67 33.33 50.00 66.67 83.33 100.00 116.67 133.33 150.00 166.67 183.33
Time (min)

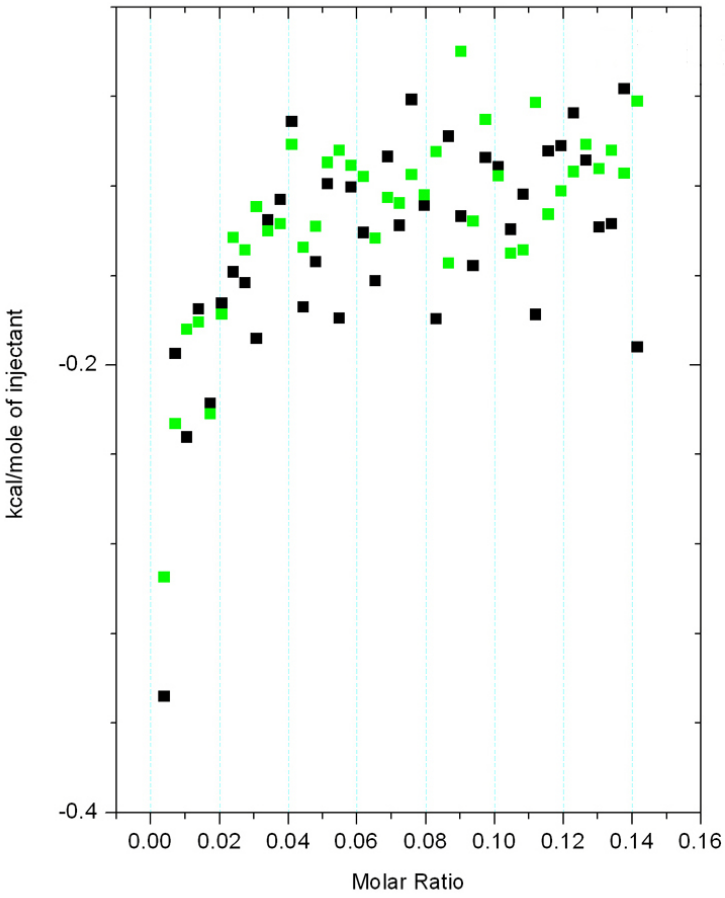
-0.2
-0.4
kcal/mole of injectant
0.00 0.02 0.04 0.06 0.08 0.10 0.12 0.14 0.16
Molar Ratio

Figure A.8 ITC of Hsp70 and 2N4R tau shows results are difficult to reproduce. (from 8-18-10) Hsp70 (125 µM (black) and 147.64 µM (green) with 2N4R tau (10.372 µM) was run at 37 ^{o}C, 5 µl injections, 56 injections. The raw data (top image, black and green lines) did not show reproduce results to those from Fig A.7. We also saw a drifting baseline (top image, red lines). The processed data (bottom image green and black squares) shows an almost random scatter of points. These data indicate ITC is not a good method for determining the interactions of Hsp70 and tau.

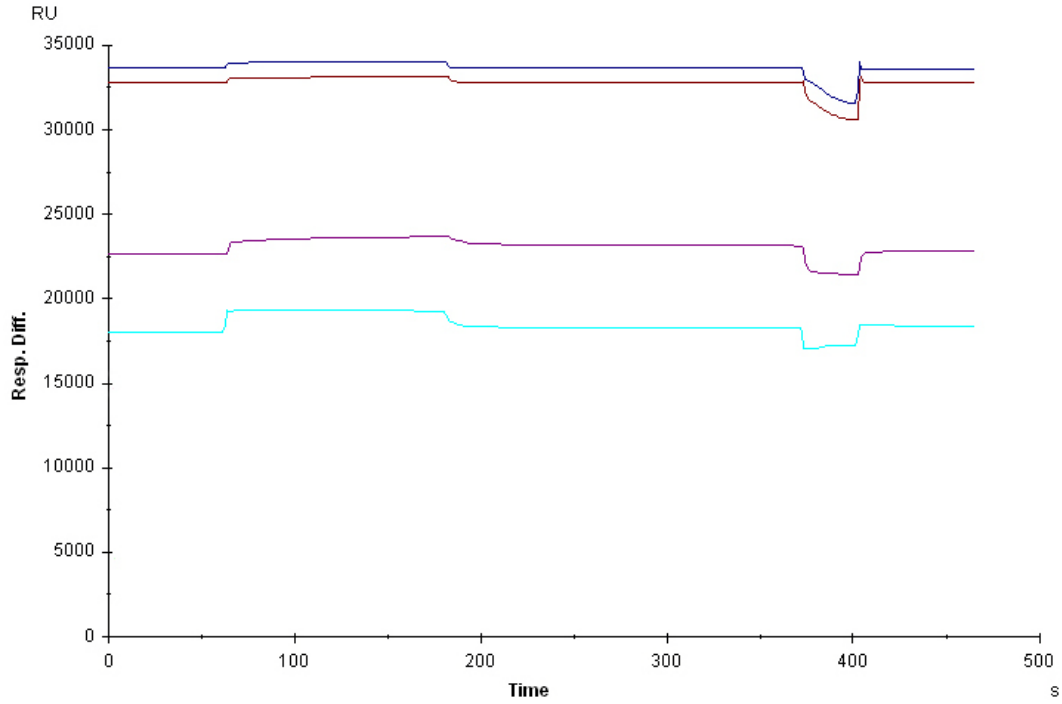

Figure A.9 Surface plasmon resonance (SPR) using the BIAcore. A CM-5 chip, used for immobilizing primary amines of the immobilized protein, was used to examine the binding of Hsp70 and tau. Flowcell (Fc) 1 is a control channel that was activated and blocked with ethanolamine. Fc2 contains immobilized Hsp70 (no his tag) recombinantly purified in our lab. Fc3 contains immobilized commercially purified and purchased Hsp70. Fc4 contains immobilized Tau12 antibody. SPR is a phenomenon where changes in the refractive index of an immobilized protein in contact with a sensor chip are detected. Upon binding of analyte to the immobilized protein, a change in the angle of reflection occurs and is measured by a sensor as a response unit (RU) over time (sec). 2N4R tau at 10 μM (analyte) was flowed over all four flow cells individually. The highest response was from Fc1 which contains nothing, the second highest was from Fc4 with contains immobilized Tau12 antibody, and equal responses occurred from Fc2 and Fc3 which have Hsp70 immobilized. Lines on the graph from top to bottom, Fc2, Fc3, Fc4, Fc1.

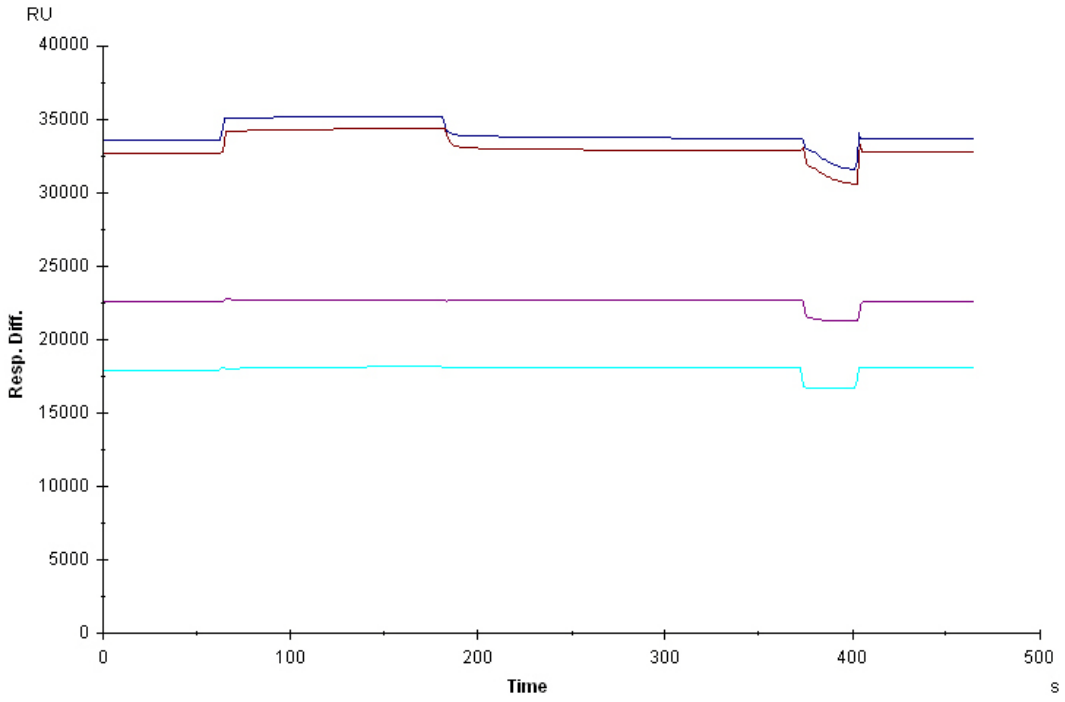

Figure A.10 A substrate binding domain (SBD) peptide for Hsp70 binds to Hsp70, but not to Tau12 antibody or the reference channel. A peptide shown to have a high affinity for the substrate binding domain of DnaK (*247*) the *E. coli* homologue of Hsp70, was used to determine whether the binding of tau to Fc1 was something that would occur for every protein we might use to test the interaction of Hsp70 and tau. The 11-mer peptide (VDKLY-(D-cyclohexylalanine)-LPRPT) was flowed over all four Fc at a concentration of 10 μM. Only responses from Fc2 and Fc3, which contain immobilized Hsp70, were detected. This indicates that tau binding to the reference channel is not a general phenomenon and perhaps we should use tau peptides in future experiments. Lines on the graph from top to bottom, Fc2, Fc3, Fc4, Fc1.

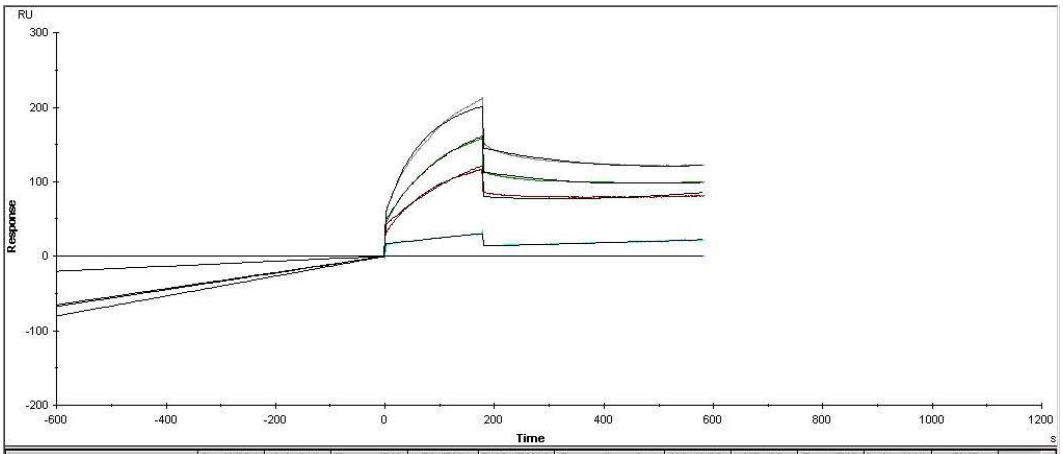

	ka (1/Ms)	kd (1/s)	Rmax (RU)	RI (RU)	Drift (RU/s)	Conc of analyte	KA (1/M)	KD (M)	Req (RU)	kobs (1/s)	Chi2
	1.55e4	2.49e-3	148				6.25e6	1.6e-7			3.01
ht40 hsp70 kinetics tr Fc=4 - 1				-8.54e-142	1.03e-143	0n			0	2.49e-3	
ht40 hsp70 kinetics tr Fc=4 - 2				16.3	0.0336	25n			20	2.88e-3	
ht40 hsp70 kinetics tr Fc=4 - 3				41.7	0.109	250n			90.1	6.37e-3	
ht40 hsp70 kinetics tr Fc=4 - 4				47.6	0.112	500n			112	0.0103	
ht40 hsp70 kinetics tr Fc=4 - 5				55.7	0.134	1000n			127	0.018	

Figure A.11 2N4R tau and Hsp70 kinetic analysis. Despite having issues with tau binding in the reference channel we proceeded to determine if we could get any numbers for binding that correlate to previous data for tau and Hsc70 (*186*). Tau (ligand at 0.5 µM) was captured by immobilized Tau12 antibody in Fc4, and Hsp70 (analyte at 0-1000 nM) was flowed over with regeneration by 10 mM glycine at pH 1.5. Data for 0 nM Hsp70 was subtracted from (25 nM-1000 nM) and fit to a drifting baseline model. The data had a Chi^2 fit of 3.01, which is within the range of good fit, and a K_D of 1.6 µM which is consistent with previous results for Hsc70 and 2N4R tau (*186*).

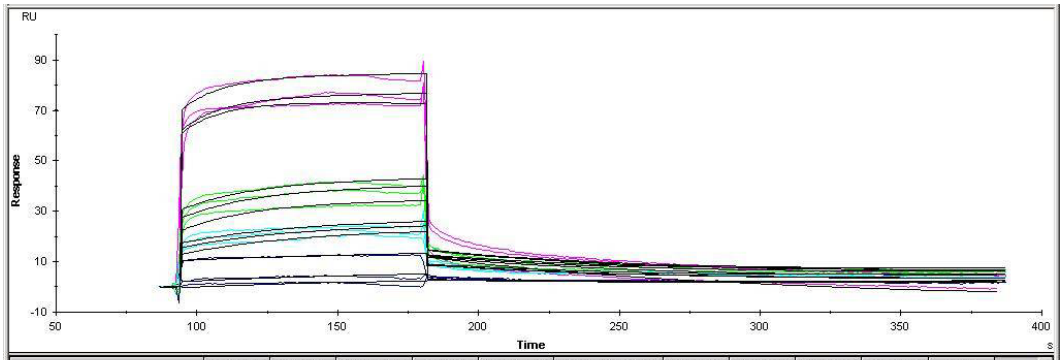

	ka (1/Ms)	kd (1/s)	Rmax (RU)	RI (RU)	Drift (RU/s)	Conc of analyte	KA (1/M)	KD (M)	Req (RU)	kobs (1/s)	Chi2
	5.84e4	0.0106	15.3				5.5e6	1.82e-7			0.757
1-4-11 ht39 kinetics F Fc=2 - 1				70.2	0.018	1000n			12.9	0.0691	
1-4-11 ht39 kinetics F Fc=2 - 2				27.2	0.0216	500n			11.2	0.0399	
1-4-11 ht39 kinetics F Fc=2 - 3				12.9	0.0137	250n			8.84	0.0252	
1-4-11 ht39 kinetics F Fc=2 - 4				-0.357	5.85e-3	50n			3.29	0.0136	
1-4-11 ht39 kinetics F Fc=2 - 1				62	0.0207	1000n			12.9	0.0691	
1-4-11 ht39 kinetics F Fc=2 - 2				30.5	0.0173	500n			11.2	0.0399	
1-4-11 ht39 kinetics F Fc=2 - 3				15.5	8.32e-3	250n			8.84	0.0252	
1-4-11 ht39 kinetics F Fc=2 - 4				2.09	7.82e-3	50n			3.29	0.0136	
12-22-10 ht39 kinetics Fc=2 - 1				60.9	-0.0122	1000n			12.9	0.0691	
12-22-10 ht39 kinetics Fc=2 - 2				22.3	0.0115	500n			11.2	0.0399	
12-22-10 ht39 kinetics Fc=2 - 3				17.3	9.09e-3	250n			8.84	0.0252	
12-22-10 ht39 kinetics Fc=2 - 4				10.4	7.41e-3	50n			3.29	0.0136	

Figure A.12 SPR of 3R tau. We proceeded to test whether 3R tau (2N3R) had a similar affinity for Hsp70 as 2N4R tau. Shown is the compiled data of 2N3R flowed directly over Fc2 to examine direct binding to Hsp70. Binding of 2N4R tau to Fc2 was similar to Fig A.11 and was not repeated. Shown in Fig A.12 is the aggregation of three separate trials of 2N3R tau (at 50, 250, 500 and 1000 nM (with 0 nM subtracted)) fit to a drifting baseline model. The Chi^2 value is 0.757, and the K_D is 0.182 µM. This K_D is the same as 2N4R tau; however, in examining the maximum response, 2N4R tau was at 148 RU while 2N3R was at 15.3 RU, indicating that even though Hsp70 and tau interact at similar affinities, there are almost 10x less binding of Hsp70 to 3R tau than 4R tau.

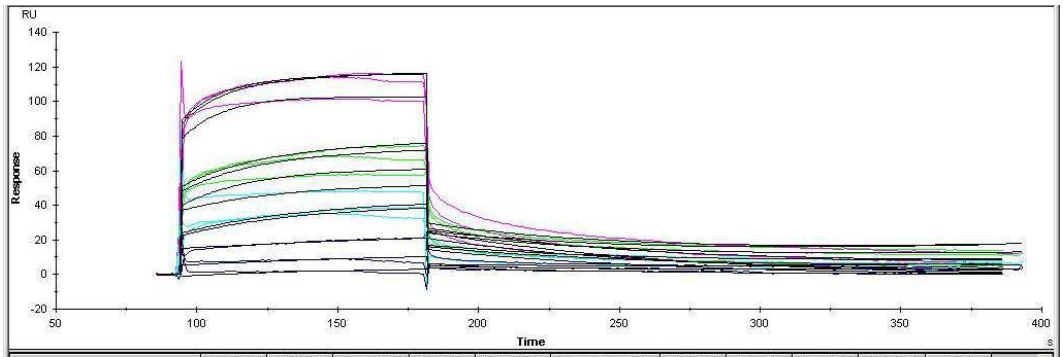

	ka (1/Ms)	kd (1/s)	Rmax (RU)	RI (RU)	Drift (RU/s)	Conc of analyte	KA (1/M)	KD (M)	Req (RU)	kobs (1/s)	Chi2
	5.55e4	0.0118	30.5				4.7e6	2.13e-7			2.65
1-4-11 double delta ht Fc=2 - 1				78.1	-4.13e-3	1000n			25.2	0.0673	
1-4-11 double delta ht Fc=2 - 2				39.9	2.26e-3	500n			21.4	0.0396	
1-4-11 double delta ht Fc=2 - 3				36.9	-3.14e-3	250n			16.5	0.0257	
1-4-11 double delta ht Fc=2 - 4				-1.06	-9.26e-4	50n			5.81	0.0146	
12-22-10 double delta Fc=2 - 1				89	0.0217	1000n			25.2	0.0673	
12-22-10 double delta Fc=2 - 2				50.6	0.0535	500n			21.4	0.0396	
12-22-10 double delta Fc=2 - 3				23.7	0.0264	250n			16.5	0.0257	
12-22-10 double delta Fc=2 - 4				14.9	0.0201	50n			5.81	0.0146	
1-4-11 double delta ht Fc=2 - 1				87	0.0531	1000n			25.2	0.0673	
1-4-11 double delta ht Fc=2 - 2				47.9	0.038	500n			21.4	0.0396	
1-4-11 double delta ht Fc=2 - 3				22.3	0.0151	250n			16.5	0.0257	
1-4-11 double delta ht Fc=2 - 4				5.19	9.59e-3	50n			5.81	0.0146	

Figure A.13 A deletion mutant of 4R tau for the predicted Hsp70 binding sites shows reduced affinity and overall binding. A deletion mutant of residues I277, I278, I308, and V309 on 2N4R tau was analyzed by SPR for binding to Hsp70. The aggregation of three trials is shown, similar to Fig A.12. The Chi^2 value is 2.65, the K_D is 0.213 μM and the maximum response is 30.5 RU. Compared to wild-type 2N4R tau, there is a slightly reduced affinity, and a dramatically reduced (5x) amount of binding of Hsp70 and tau. This indicates that the two hexapeptide regions flanking microtubule binding repeat 2 play a role in Hsp70 binding to tau.

WT 2N4R

	k_a (1/Ms)	k_d (1/s)	K_D (M)	Chi^2
11/22/2010	7.24E+03	1.26E-03	1.73E-07	3.29
12/6/2010	6.84E+04	9.43E-03	1.38E-07	3.78
12/15/2010	1.55E+04	2.49E-03	1.60E-07	3.01
12/22/2010	3.54E+04	3.89E-03	1.10E-07	1.01
average	3.16E+04	4.27E-03	1.45E-07	2.77
stdev	2.72E+04	3.61E-03	2.76E-08	1.22
% SD of avg	86.02	84.49	18.99	43.91

WT 2N3R

	k_a (1/Ms)	k_d (1/s)	K_D (M)	Chi^2
Trial 1 (12-22-10)	1.23E+05	1.17E-02	9.51E-08	0.10
Trial 2 (1-4-11)	3.20E+04	1.09E-02	3.40E-07	0.43
Trial 3 (1-4-11)	6.53E+04	1.05E-02	1.61E-07	0.35
average	7.34E+04	1.10E-02	1.99E-07	0.29
stdev	4.60E+04	6.11E-04	1.27E-07	0.17
% SD of avg	62.70	5.54	63.78	59.34
all at once	5.84E+04	1.06E-02	1.82E-07	0.76

Δ 278,279,308,309 2N4R

	k_a (1/Ms)	k_d (1/s)	K_D (M)	Chi^2
Trial 1 (12-22-10)	5.84E+04	1.22E-02	2.08E-07	0.43
Trial 2 (1-4-11)	5.03E+04	1.21E-02	2.40E-07	2.11
Trial 3 (1-4-11)	5.26E+04	9.20E-03	1.75E-07	0.61
average	5.38E+04	1.12E-02	2.08E-07	1.05
stdev	4.17E+03	1.70E-03	3.25E-08	0.92
% SD of avg	7.76	15.26	15.65	88.16
all at once	5.55E+04	1.18E-02	2.13E-07	2.65

Table A.1 Analysis of binding of Hsp70 to various tau constructs. Data from individual fits (black outline) was averaged together for wild-type 2N4R, wild-type 2N3R, and Δ277, 278,308,309 2N4R. Also, wild-type 2N3R, and Δ277, 278,308,309 2N4R had all three trials fit at once, with similar outputs to individual fits. The data shows the affinity of Hsp70 to the various tau constructs is similar, however as is shown in Fig A.11-13, the overall binding of Hsp70 and tau is less with 3R and deletion of hydrophobic residues in the hexapeptide regions.

Works Cited

1. Weingarten, M. D., Lockwood, A. H., Hwo, S. Y., and Kirschner, M. W. (1975) A protein factor essential for microtubule assembly, *Proc Natl Acad Sci U S A 72*, 1858-1862.
2. Neve, R. L., Harris, P., Kosik, K. S., Kurnit, D. M., and Donlon, T. A. (1986) Identification of cDNA clones for the human microtubule-associated protein tau and chromosomal localization of the genes for tau and microtubule-associated protein 2, *Brain Res 387*, 271-280.
3. Andreadis, A., Brown, W. M., and Kosik, K. S. (1992) Structure and novel exons of the human tau gene, *Biochemistry 31*, 10626-10633.
4. Andreadis, A., Broderick, J. A., and Kosik, K. S. (1995) Relative exon affinities and suboptimal splice site signals lead to non-equivalence of two cassette exons, *Nucleic Acids Res 23*, 3585-3593.
5. Himmler, A. (1989) Structure of the bovine tau gene: alternatively spliced transcripts generate a protein family, *Mol Cell Biol 9*, 1389-1396.
6. Nelson, P. T., Stefansson, K., Gulcher, J., and Saper, C. B. (1996) Molecular evolution of tau protein: implications for Alzheimer's disease, *J Neurochem 67*, 1622-1632.
7. Goedert, M., Spillantini, M. G., Jakes, R., Rutherford, D., and Crowther, R. A. (1989) Multiple isoforms of human microtubule-associated protein tau: sequences and localization in neurofibrillary tangles of Alzheimer's disease, *Neuron 3*, 519-526.
8. Goedert, M., Spillantini, M. G., Potier, M. C., Ulrich, J., and Crowther, R. A. (1989) Cloning and sequencing of the cDNA encoding an isoform of microtubule-associated protein tau containing four tandem repeats: differential expression of tau protein mRNAs in human brain, *Embo J 8*, 393-399.
9. Kosik, K. S., Orecchio, L. D., Bakalis, S., and Neve, R. L. (1989) Developmentally regulated expression of specific tau sequences, *Neuron 2*, 1389-1397.
10. Goedert, M., and Spillantini, M. G. (1990) Molecular neuropathology of Alzheimer's disease: in situ hybridization studies, *Cell Mol Neurobiol 10*, 159-174.
11. Hong, M., Zhukareva, V., Vogelsberg-Ragaglia, V., Wszolek, Z., Reed, L., Miller, B. I., Geschwind, D. H., Bird, T. D., McKeel, D., Goate, A., Morris, J. C., Wilhelmsen, K. C., Schellenberg, G. D., Trojanowski, J. Q., and Lee, V. M. (1998) Mutation-specific functional impairments in distinct tau isoforms of hereditary FTDP-17, *Science 282*, 1914-1917.
12. Hirokawa, N., Shiomura, Y., and Okabe, S. (1988) Tau proteins: the molecular structure and mode of binding on microtubules, *J Cell Biol 107*, 1449-1459.
13. Brandt, R., Leger, J., and Lee, G. (1995) Interaction of tau with the neural plasma membrane mediated by tau's amino-terminal projection domain, *J Cell Biol 131*, 1327-1340.

14. Chen, J., Kanai, Y., Cowan, N. J., and Hirokawa, N. (1992) Projection domains of MAP2 and tau determine spacings between microtubules in dendrites and axons, *Nature 360*, 674-677.
15. Lee, G., Cowan, N., and Kirschner, M. (1988) The primary structure and heterogeneity of tau protein from mouse brain, *Science 239*, 285-288.
16. Lee, G., Neve, R. L., and Kosik, K. S. (1989) The microtubule binding domain of tau protein, *Neuron 2*, 1615-1624.
17. Ennulat, D. J., Liem, R. K., Hashim, G. A., and Shelanski, M. L. (1989) Two separate 18-amino acid domains of tau promote the polymerization of tubulin, *J Biol Chem 264*, 5327-5330.
18. Butner, K. A., and Kirschner, M. W. (1991) Tau protein binds to microtubules through a flexible array of distributed weak sites, *J Cell Biol 115*, 717-730.
19. Goode, B. L., and Feinstein, S. C. (1994) Identification of a novel microtubule binding and assembly domain in the developmentally regulated inter-repeat region of tau, *J Cell Biol 124*, 769-782.
20. Panda, D., Goode, B. L., Feinstein, S. C., and Wilson, L. (1995) Kinetic stabilization of microtubule dynamics at steady state by tau and microtubule-binding domains of tau, *Biochemistry 34*, 11117-11127.
21. Ackmann, M., Wiech, H., and Mandelkow, E. (2000) Nonsaturable binding indicates clustering of tau on the microtubule surface in a paired helical filament-like conformation, *J Biol Chem 275*, 30335-30343.
22. Serrano, L., Montejo de Garcini, E., Hernandez, M. A., and Avila, J. (1985) Localization of the tubulin binding site for tau protein, *Eur J Biochem 153*, 595-600.
23. Serrano, L., Avila, J., and Maccioni, R. B. (1984) Controlled proteolysis of tubulin by subtilisin: localization of the site for MAP2 interaction, *Biochemistry 23*, 4675-4681.
24. Goode, B. L., Denis, P. E., Panda, D., Radeke, M. J., Miller, H. P., Wilson, L., and Feinstein, S. C. (1997) Functional interactions between the proline-rich and repeat regions of tau enhance microtubule binding and assembly, *Mol Biol Cell 8*, 353-365.
25. Mukrasch, M. D., Bibow, S., Korukottu, J., Jeganathan, S., Biernat, J., Griesinger, C., Mandelkow, E., and Zweckstetter, M. (2009) Structural polymorphism of 441-residue tau at single residue resolution, *PLoS Biol 7*, e34.
26. Goode, B. L., Chau, M., Denis, P. E., and Feinstein, S. C. (2000) Structural and functional differences between 3-repeat and 4-repeat tau isoforms. Implications for normal tau function and the onset of neurodegenerative disease, *J Biol Chem 275*, 38182-38189.
27. Mercken, M., Fischer, I., Kosik, K. S., and Nixon, R. A. (1995) Three distinct axonal transport rates for tau, tubulin, and other microtubule-associated proteins: evidence for dynamic interactions of tau with microtubules in vivo, *J Neurosci 15*, 8259-8267.

28. Konzack, S., Thies, E., Marx, A., Mandelkow, E. M., and Mandelkow, E. (2007) Swimming against the tide: mobility of the microtubule-associated protein tau in neurons, *J Neurosci 27*, 9916-9927.
29. Utton, M. A., Noble, W. J., Hill, J. E., Anderton, B. H., and Hanger, D. P. (2005) Molecular motors implicated in the axonal transport of tau and alpha-synuclein, *J Cell Sci 118*, 4645-4654.
30. Lee, V. M., Goedert, M., and Trojanowski, J. Q. (2001) Neurodegenerative tauopathies, *Annu Rev Neurosci 24*, 1121-1159.
31. Mandelkow, E. M., Thies, E., Trinczek, B., Biernat, J., and Mandelkow, E. (2004) MARK/PAR1 kinase is a regulator of microtubule-dependent transport in axons, *J Cell Biol 167*, 99-110.
32. Kopke, E., Tung, Y. C., Shaikh, S., Alonso, A. C., Iqbal, K., and Grundke-Iqbal, I. (1993) Microtubule-associated protein tau. Abnormal phosphorylation of a non-paired helical filament pool in Alzheimer disease, *J Biol Chem 268*, 24374-24384.
33. Bramblett, G. T., Goedert, M., Jakes, R., Merrick, S. E., Trojanowski, J. Q., and Lee, V. M. (1993) Abnormal tau phosphorylation at Ser396 in Alzheimer's disease recapitulates development and contributes to reduced microtubule binding, *Neuron 10*, 1089-1099.
34. Cleveland, D. W., Hwo, S. Y., and Kirschner, M. W. (1977) Physical and chemical properties of purified tau factor and the role of tau in microtubule assembly, *J Mol Biol 116*, 227-247.
35. Cleveland, D. W., Hwo, S. Y., and Kirschner, M. W. (1977) Purification of tau, a microtubule-associated protein that induces assembly of microtubules from purified tubulin, *J Mol Biol 116*, 207-225.
36. Drubin, D. G., and Kirschner, M. W. (1986) Tau protein function in living cells, *J Cell Biol 103*, 2739-2746.
37. Lindwall, G., and Cole, R. D. (1984) Phosphorylation affects the ability of tau protein to promote microtubule assembly, *J Biol Chem 259*, 5301-5305.
38. Yamamoto, H., Saitoh, Y., Fukunaga, K., Nishimura, H., and Miyamoto, E. (1988) Dephosphorylation of microtubule proteins by brain protein phosphatases 1 and 2A, and its effect on microtubule assembly, *J Neurochem 50*, 1614-1623.
39. Biernat, J., Gustke, N., Drewes, G., Mandelkow, E. M., and Mandelkow, E. (1993) Phosphorylation of Ser262 strongly reduces binding of tau to microtubules: distinction between PHF-like immunoreactivity and microtubule binding, *Neuron 11*, 153-163.
40. Seubert, P., Mawal-Dewan, M., Barbour, R., Jakes, R., Goedert, M., Johnson, G. V., Litersky, J. M., Schenk, D., Lieberburg, I., Trojanowski, J. Q., and et al. (1995) Detection of phosphorylated Ser262 in fetal tau, adult tau, and paired helical filament tau, *J Biol Chem 270*, 18917-18922.
41. Mawal-Dewan, M., Henley, J., Van de Voorde, A., Trojanowski, J. Q., and Lee, V. M. (1994) The phosphorylation state of tau in the developing rat brain is regulated by phosphoprotein phosphatases, *J Biol Chem 269*, 30981-30987.

42. Rosner, H., Rebhan, M., Vacun, G., and Vanmechelen, E. (1995) Developmental expression of tau proteins in the chicken and rat brain: rapid down-regulation of a paired helical filament epitope in the rat cerebral cortex coincides with the transition from immature to adult tau isoforms, *Int J Dev Neurosci 13*, 607-617.
43. Goldschmidt, L., Teng, P. K., Riek, R., and Eisenberg, D. (2010) Identifying the amylome, proteins capable of forming amyloid-like fibrils, *Proc Natl Acad Sci U S A 107*, 3487-3492.
44. Ghiso, J., and Frangione, B. (2002) Amyloidosis and Alzheimer's disease, *Adv Drug Deliv Rev 54*, 1539-1551.
45. Divry, P., and Florkin, M. (1927) Présentée par J. Firket. Sur les properties optiques de l`amyloide, *C R Soc Biol (Paris) 97*, 1808-1810.
46. Geddes, A. J., Parker, K. D., Atkins, E. D., and Beighton, E. (1968) "Cross-beta" conformation in proteins, *J Mol Biol 32*, 343-358.
47. Makin, O. S., and Serpell, L. C. (2005) Structures for amyloid fibrils, *FEBS J 272*, 5950-5961.
48. Makin, O. S., and Serpell, L. C. (2005) X-ray diffraction studies of amyloid structure, *Methods Mol Biol 299*, 67-80.
49. Makin, O. S., Atkins, E., Sikorski, P., Johansson, J., and Serpell, L. C. (2005) Molecular basis for amyloid fibril formation and stability, *Proc Natl Acad Sci U S A 102*, 315-320.
50. Wood, S. J., Wypych, J., Steavenson, S., Louis, J. C., Citron, M., and Biere, A. L. (1999) alpha-synuclein fibrillogenesis is nucleation-dependent. Implications for the pathogenesis of Parkinson's disease, *J Biol Chem 274*, 19509-19512.
51. Carlson, S. W., Branden, M., Voss, K., Sun, Q., Rankin, C. A., and Gamblin, T. C. (2007) A complex mechanism for inducer mediated tau polymerization, *Biochemistry 46*, 8838-8849.
52. Friedhoff, P., von Bergen, M., Mandelkow, E. M., Davies, P., and Mandelkow, E. (1998) A nucleated assembly mechanism of Alzheimer paired helical filaments, *Proc Natl Acad Sci U S A 95*, 15712-15717.
53. Canet, D., Last, A. M., Tito, P., Sunde, M., Spencer, A., Archer, D. B., Redfield, C., Robinson, C. V., and Dobson, C. M. (2002) Local cooperativity in the unfolding of an amyloidogenic variant of human lysozyme, *Nat Struct Biol 9*, 308-315.
54. Chiti, F., Stefani, M., Taddei, N., Ramponi, G., and Dobson, C. M. (2003) Rationalization of the effects of mutations on peptide and protein aggregation rates, *Nature 424*, 805-808.
55. Villegas, V., Zurdo, J., Filimonov, V. V., Aviles, F. X., Dobson, C. M., and Serrano, L. (2000) Protein engineering as a strategy to avoid formation of amyloid fibrils, *Protein Sci 9*, 1700-1708.
56. Colon, W., and Kelly, J. W. (1992) Partial denaturation of transthyretin is sufficient for amyloid fibril formation in vitro, *Biochemistry 31*, 8654-8660.

57. Swietnicki, W., Petersen, R., Gambetti, P., and Surewicz, W. K. (1997) pH-dependent stability and conformation of the recombinant human prion protein PrP(90-231), *J Biol Chem 272*, 27517-27520.
58. Wood, S. J., Maleeff, B., Hart, T., and Wetzel, R. (1996) Physical, morphological and functional differences between ph 5.8 and 7.4 aggregates of the Alzheimer's amyloid peptide Abeta, *J Mol Biol 256*, 870-877.
59. Furukawa, Y., and O'Halloran, T. V. (2006) Posttranslational modifications in Cu,Zn-superoxide dismutase and mutations associated with amyotrophic lateral sclerosis, *Antioxid Redox Signal 8*, 847-867.
60. Sergeant, N., Bretteville, A., Hamdane, M., Caillet-Boudin, M. L., Grognet, P., Bombois, S., Blum, D., Delacourte, A., Pasquier, F., Vanmechelen, E., Schraen-Maschke, S., and Buee, L. (2008) Biochemistry of Tau in Alzheimer's disease and related neurological disorders, *Expert Rev Proteomics 5*, 207-224.
61. Valentine, J. S. (2002) Do oxidatively modified proteins cause ALS?, *Free Radic Biol Med 33*, 1314-1320.
62. Brash, A. R. (2001) Arachidonic acid as a bioactive molecule, *J Clin Invest 107*, 1339-1345.
63. Goedert, M., Jakes, R., Spillantini, M. G., Hasegawa, M., Smith, M. J., and Crowther, R. A. (1996) Assembly of microtubule-associated protein tau into Alzheimer-like filaments induced by sulphated glycosaminoglycans, *Nature 383*, 550-553.
64. Betancourt, M. R., and Thirumalai, D. (1999) Exploring the kinetic requirements for enhancement of protein folding rates in the GroEL cavity, *J Mol Biol 287*, 627-644.
65. Uversky, V. N. (2008) Amyloidogenesis of natively unfolded proteins, *Curr Alzheimer Res 5*, 260-287.
66. Wischik, C. M., Novak, M., Edwards, P. C., Klug, A., Tichelaar, W., and Crowther, R. A. (1988) Structural characterization of the core of the paired helical filament of Alzheimer disease, *Proc Natl Acad Sci U S A 85*, 4884-4888.
67. Wischik, C. M., Novak, M., Thogersen, H. C., Edwards, P. C., Runswick, M. J., Jakes, R., Walker, J. E., Milstein, C., Roth, M., and Klug, A. (1988) Isolation of a fragment of tau derived from the core of the paired helical filament of Alzheimer disease, *Proc Natl Acad Sci U S A 85*, 4506-4510.
68. Barre, P., and Eliezer, D. (2006) Folding of the repeat domain of tau upon binding to lipid surfaces, *J Mol Biol 362*, 312-326.
69. Khlistunova, I., Biernat, J., Wang, Y., Pickhardt, M., von Bergen, M., Gazova, Z., Mandelkow, E., and Mandelkow, E. M. (2006) Inducible expression of Tau repeat domain in cell models of tauopathy: aggregation is toxic to cells but can be reversed by inhibitor drugs, *J Biol Chem 281*, 1205-1214.
70. (2011) Alzheimer's Disease Facts and Figures, In *Alzheimer's and Dementia*, Alzheimer's Association.

71. Alzheimer, A. (1907) Uber eine eigenartige Erkrankung der Hirnrinde, *Allgemeine Zeitschrift fur Psychiatrie und Psychisch-gerichtliche Medizin. 64*, 146-148.
72. West, M. J., Coleman, P. D., Flood, D. G., and Troncoso, J. C. (1994) Differences in the pattern of hippocampal neuronal loss in normal ageing and Alzheimer's disease, *Lancet 344*, 769-772.
73. Jobst, K. A., Smith, A. D., Szatmari, M., Esiri, M. M., Jaskowski, A., Hindley, N., McDonald, B., and Molyneux, A. J. (1994) Rapidly progressing atrophy of medial temporal lobe in Alzheimer's disease, *Lancet 343*, 829-830.
74. Mirra, S. S., Heyman, A., McKeel, D., Sumi, S. M., Crain, B. J., Brownlee, L. M., Vogel, F. S., Hughes, J. P., van Belle, G., and Berg, L. (1991) The Consortium to Establish a Registry for Alzheimer's Disease (CERAD). Part II. Standardization of the neuropathologic assessment of Alzheimer's disease, *Neurology 41*, 479-486.
75. Selkoe, D. J., Bell, D. S., Podlisny, M. B., Price, D. L., and Cork, L. C. (1987) Conservation of brain amyloid proteins in aged mammals and humans with Alzheimer's disease, *Science 235*, 873-877.
76. Delacourte, A., and Defossez, A. (1986) Alzheimer's disease: Tau proteins, the promoting factors of microtubule assembly, are major components of paired helical filaments, *J Neurol Sci 76*, 173-186.
77. Grundke-Iqbal, I., Iqbal, K., Tung, Y. C., Quinlan, M., Wisniewski, H. M., and Binder, L. I. (1986) Abnormal phosphorylation of the microtubule-associated protein tau (tau) in Alzheimer cytoskeletal pathology, *Proc Natl Acad Sci U S A 83*, 4913-4917.
78. Wood, J. G., Mirra, S. S., Pollock, N. J., and Binder, L. I. (1986) Neurofibrillary tangles of Alzheimer disease share antigenic determinants with the axonal microtubule-associated protein tau (tau) [published erratum appears in Proc Natl Acad Sci U S A 1986 Dec;83(24):9773], *Proc Natl Acad Sci U S A 83*, 4040-4043.
79. Kosik, K. S., Joachim, C. L., and Selkoe, D. J. (1986) Microtubule-associated protein tau (tau) is a major antigenic component of paired helical filaments in Alzheimer disease, *Proc Natl Acad Sci U S A 83*, 4044-4048.
80. Kidd, M. (1963) Paired helical filaments in electron microscopy of Alzheimer's disease, *Nature 197*, 192-193.
81. Perry, G., Mulvihill, P., Manetto, V., Autilio-Gambetti, L., and Gambetti, P. (1987) Immunocytochemical properties of Alzheimer straight filaments, *J Neurosci 7*, 3736-3738.
82. Ihara, Y., Nukina, N., Miura, R., and Ogawara, M. (1986) Phosphorylated tau protein is integrated into paired helical filaments in Alzheimer's disease, *J Biochem (Tokyo) 99*, 1807-1810.
83. Grundke-Iqbal, I., Iqbal, K., Quinlan, M., Tung, Y. C., Zaidi, M. S., and Wisniewski, H. M. (1986) Microtubule-associated protein tau. A component of Alzheimer paired helical filaments, *J Biol Chem 261*, 6084-6089.

84. Iqbal, K., Grundke-Iqbal, I., Zaidi, T., Merz, P. A., Wen, G. Y., Shaikh, S. S., Wisniewski, H. M., Alafuzoff, I., and Winblad, B. (1986) Defective brain microtubule assembly in Alzheimer's disease, *Lancet 2*, 421-426.
85. Mayer, R. J., Landon, M., and Lowe, J. (1998) *Ubiquitin and the molecular pathology of human disease*, Plenum Press, New York.
86. Braak, H., and Braak, E. (1995) Staging of Alzheimer's disease-related neurofibrillary changes, *Neurobiol Aging 16*, 271-278; discussion 278-284.
87. Arriagada, P. V., Growdon, J. H., Hedley-Whyte, E. T., and Hyman, B. T. (1992) Neurofibrillary tangles but not senile plaques parallel duration and severity of Alzheimer's disease, *Neurology 42*, 631-639.
88. Hof, P. R., Bierer, L. M., Purohit, D. P., Carlin, L., Schmeidler, J., Davis, K. L., and Perl, D. P. (1995) Neocortical neurofibrillary tangles correlate with dementia severity in Alzheimer's disease, *Arch Neurol 52*, 81-88.
89. Finckh, U. (2003) The future of genetic association studies in Alzheimer disease, *J Neural Transm 110*, 253-266.
90. McKhann, G. M., Albert, M. S., Grossman, M., Miller, B., Dickson, D., and Trojanowski, J. Q. (2001) Clinical and pathological diagnosis of frontotemporal dementia: report of the Work Group on Frontotemporal Dementia and Pick's Disease, *Arch Neurol 58*, 1803-1809.
91. Zhukareva, V., Mann, D., Pickering-Brown, S., Uryu, K., Shuck, T., Shah, K., Grossman, M., Miller, B. L., Hulette, C. M., Feinstein, S. C., Trojanowski, J. Q., and Lee, V. M. (2002) Sporadic Pick's disease: a tauopathy characterized by a spectrum of pathological tau isoforms in gray and white matter, *Ann Neurol 51*, 730-739.
92. Williams, A., Jahreiss, L., Sarkar, S., Saiki, S., Menzies, F. M., Ravikumar, B., and Rubinsztein, D. C. (2006) Aggregate-prone proteins are cleared from the cytosol by autophagy: therapeutic implications, *Curr Top Dev Biol 76*, 89-101.
93. Yamada, T., McGeer, P. L., and McGeer, E. G. (1992) Appearance of paired nucleated, Tau-positive glia in patients with progressive supranuclear palsy brain tissue, *Neurosci Lett 135*, 99-102.
94. Komori, T. (1999) Tau-positive glial inclusions in progressive supranuclear palsy, corticobasal degeneration and Pick's disease, *Brain Pathol 9*, 663-679.
95. Hauw, J. J., Verny, M., Delaere, P., Cervera, P., He, Y., and Duyckaerts, C. (1990) Constant neurofibrillary changes in the neocortex in progressive supranuclear palsy. Basic differences with Alzheimer's disease and aging, *Neurosci Lett 119*, 182-186.
96. Tellez-Nagel, I., and Wisniewski, H. M. (1973) Ultrastructure of neurofibrillary tangles in Steele-Richardson-Olszewski syndrome, *Arch Neurol 29*, 324-327.
97. Roy, S., Datta, C. K., Hirano, A., Ghatak, N. R., and Zimmerman, H. M. (1974) Electron microscopic study of neurofibrillary tangles in Steele-Richardson-Olszewski syndrome, *Acta Neuropathol 29*, 175-179.
98. Spillantini, M. G., Goedert, M., Crowther, R. A., Murrell, J. R., Farlow, M. R., and Ghetti, B. (1997) Familial multiple system tauopathy with presenile

dementia: a disease with abundant neuronal and glial tau filaments, *Proc Natl Acad Sci U S A 94*, 4113-4118.
99. Sergeant, N., Wattez, A., and Delacourte, A. (1999) Neurofibrillary degeneration in progressive supranuclear palsy and corticobasal degeneration: tau pathologies with exclusively "exon 10" isoforms, *J Neurochem 72*, 1243-1249.
100. Feany, M. B., and Dickson, D. W. (1995) Widespread cytoskeletal pathology characterizes corticobasal degeneration, *Am J Pathol 146*, 1388-1396.
101. Feany, M. B., Ksiezak-Reding, H., Liu, W. K., Vincent, I., Yen, S. H., and Dickson, D. W. (1995) Epitope expression and hyperphosphorylation of tau protein in corticobasal degeneration: differentiation from progressive supranuclear palsy, *Acta Neuropathol 90*, 37-43.
102. Feany, M. B., and Dickson, D. W. (1996) Neurodegenerative disorders with extensive tau pathology: a comparative study and review, *Ann Neurol 40*, 139-148.
103. Feany, M. B., Mattiace, L. A., and Dickson, D. W. (1996) Neuropathologic overlap of progressive supranuclear palsy, Pick's disease and corticobasal degeneration, *J Neuropathol Exp Neurol 55*, 53-67.
104. Ksiezak-Reding, H., Morgan, K., Mattiace, L. A., Davies, P., Liu, W. K., Yen, S. H., Weidenheim, K., and Dickson, D. W. (1994) Ultrastructure and biochemical composition of paired helical filaments in corticobasal degeneration, *Am J Pathol 145*, 1496-1508.
105. Goedert, M., and Jakes, R. (2005) Mutations causing neurodegenerative tauopathies, *Biochim Biophys Acta 1739*, 240-250.
106. Hutton, M., Lendon, C. L., Rizzu, P., Baker, M., Froelich, S., Houlden, H., Pickering-Brown, S., Chakraverty, S., Isaacs, A., Grover, A., Hackett, J., Adamson, J., Lincoln, S., Dickson, D., Davies, P., Petersen, R. C., Stevens, M., de Graaff, E., Wauters, E., van Baren, J., Hillebrand, M., Joosse, M., Kwon, J. M., Nowotny, P., Che, L. K., Norton, J., Morris, J. C., Reed, L. A., Trojanowski, J., Basun, H., Lannfelt, L., Neystat, M., Fahn, S., Dark, F., Tannenberg, T., Dodd, P. R., Hayward, N., Kwok, J. B., Schofield, P. R., Andreadis, A., Snowden, J., Craufurd, D., Neary, D., Owen, F., Oostra, B. A., Hardy, J., Goate, A., van Swieten, J., Mann, D., Lynch, T., and Heutink, P. (1998) Association of missense and 5'-splice-site mutations in tau with the inherited dementia FTDP-17, *Nature 393*, 702-705.
107. Spillantini, M. G., Murrell, J. R., Goedert, M., Farlow, M. R., Klug, A., and Ghetti, B. (1998) Mutation in the tau gene in familial multiple system tauopathy with presenile dementia, *Proc Natl Acad Sci U S A 95*, 7737-7741.
108. D'Souza, I., Poorkaj, P., Hong, M., Nochlin, D., Lee, V. M., Bird, T. D., and Schellenberg, G. D. (1999) Missense and silent tau gene mutations cause frontotemporal dementia with parkinsonism-chromosome 17 type, by affecting multiple alternative RNA splicing regulatory elements, *Proc Natl Acad Sci U S A 96*, 5598-5603.

109. Yoshida, H., Crowther, R. A., and Goedert, M. (2002) Functional effects of tau gene mutations deltaN296 and N296H, *J Neurochem 80*, 548-551.
110. Grover, A., DeTure, M., Yen, S. H., and Hutton, M. (2002) Effects on splicing and protein function of three mutations in codon N296 of tau in vitro, *Neurosci Lett 323*, 33-36.
111. Hasegawa, M., Smith, M. J., Iijima, M., Tabira, T., and Goedert, M. (1999) FTDP-17 mutations N279K and S305N in tau produce increased splicing of exon 10, *FEBS Lett 443*, 93-96.
112. Iseki, E., Matsumura, T., Marui, W., Hino, H., Odawara, T., Sugiyama, N., Suzuki, K., Sawada, H., Arai, T., and Kosaka, K. (2001) Familial frontotemporal dementia and parkinsonism with a novel N296H mutation in exon 10 of the tau gene and a widespread tau accumulation in the glial cells, *Acta Neuropathol 102*, 285-292.
113. Spillantini, M. G., Yoshida, H., Rizzini, C., Lantos, P. L., Khan, N., Rossor, M. N., Goedert, M., and Brown, J. (2000) A novel tau mutation (N296N) in familial dementia with swollen achromatic neurons and corticobasal inclusion bodies, *Ann Neurol 48*, 939-943.
114. Miyamoto, K., Kowalska, A., Hasegawa, M., Tabira, T., Takahashi, K., Araki, W., Akiguchi, I., and Ikemoto, A. (2001) Familial frontotemporal dementia and parkinsonism with a novel mutation at an intron 10+11-splice site in the tau gene, *Ann Neurol 50*, 117-120.
115. Goedert, M., Spillantini, M. G., Crowther, R. A., Chen, S. G., Parchi, P., Tabaton, M., Lanska, D. J., Markesbery, W. R., Wilhelmsen, K. C., Dickson, D. W., Petersen, R. B., and Gambetti, P. (1999) Tau gene mutation in familial progressive subcortical gliosis, *Nat Med 5*, 454-457.
116. Hasegawa, M., Smith, M. J., and Goedert, M. (1998) Tau proteins with FTDP-17 mutations have a reduced ability to promote microtubule assembly, *FEBS Lett 437*, 207-210.
117. Pickering-Brown, S. M., Baker, M., Nonaka, T., Ikeda, K., Sharma, S., Mackenzie, J., Simpson, S. A., Moore, J. W., Snowden, J. S., de Silva, R., Revesz, T., Hasegawa, M., Hutton, M., and Mann, D. M. (2004) Frontotemporal dementia with Pick-type histology associated with Q336R mutation in the tau gene, *Brain 127*, 1415-1426.
118. Nacharaju, P., Lewis, J., Easson, C., Yen, S., Hackett, J., Hutton, M., and Yen, S. H. (1999) Accelerated filament formation from tau protein with specific FTDP-17 missense mutations, *FEBS Lett 447*, 195-199.
119. Goedert, M., Jakes, R., and Crowther, R. A. (1999) Effects of frontotemporal dementia FTDP-17 mutations on heparin-induced assembly of tau filaments, *FEBS Lett 450*, 306-311.
120. Gamblin, T. C., King, M. E., Dawson, H., Vitek, M. P., Kuret, J., Berry, R. W., and Binder, L. I. (2000) In vitro polymerization of tau protein monitored by laser light scattering: method and application to the study of FTDP-17 mutants, *Biochemistry 39*, 6136-6144.

121. von Bergen, M., Barghorn, S., Li, L., Marx, A., Biernat, J., Mandelkow, E. M., and Mandelkow, E. (2001) Mutations of tau protein in frontotemporal dementia promote aggregation of paired helical filaments by enhancing local beta-structure, *J Biol Chem 276*, 48165-48174.
122. Barghorn, S., Zheng-Fischhofer, Q., Ackmann, M., Biernat, J., von Bergen, M., Mandelkow, E. M., and Mandelkow, E. (2000) Structure, microtubule interactions, and paired helical filament aggregation by tau mutants of frontotemporal dementias, *Biochemistry 39*, 11714-11721.
123. Grover, A., England, E., Baker, M., Sahara, N., Adamson, J., Granger, B., Houlden, H., Passant, U., Yen, S. H., DeTure, M., and Hutton, M. (2003) A novel tau mutation in exon 9 (1260V) causes a four-repeat tauopathy, *Exp Neurol 184*, 131-140.
124. Avila, J., Lucas, J. J., Perez, M., and Hernandez, F. (2004) Role of tau protein in both physiological and pathological conditions, *Physiol Rev 84*, 361-384.
125. Buee, L., Bussiere, T., Buee-Scherrer, V., Delacourte, A., and Hof, P. R. (2000) Tau protein isoforms, phosphorylation and role in neurodegenerative disorders, *Brain Res Brain Res Rev 33*, 95-130.
126. Baumann, K., Mandelkow, E. M., Biernat, J., Piwnica-Worms, H., and Mandelkow, E. (1993) Abnormal Alzheimer-like phosphorylation of tau-protein by cyclin-dependent kinases cdk2 and cdk5, *FEBS Lett 336*, 417-424.
127. Holzer, M., Gartner, U., Klinz, F. J., Narz, F., Heumann, R., and Arendt, T. (2001) Activation of mitogen-activated protein kinase cascade and phosphorylation of cytoskeletal proteins after neurone-specific activation of p21ras. I. Mitogen-activated protein kinase cascade, *Neuroscience 105*, 1031-1040.
128. Hanger, D. P., Hughes, K., Woodgett, J. R., Brion, J. P., and Anderton, B. H. (1992) Glycogen synthase kinase-3 induces Alzheimer's disease-like phosphorylation of tau: generation of paired helical filament epitopes and neuronal localisation of the kinase, *Neurosci Lett 147*, 58-62.
129. Imahori, K., and Uchida, T. (1997) Physiology and pathology of tau protein kinases in relation to Alzheimer's disease, *J Biochem (Tokyo) 121*, 179-188.
130. Cuenda, A., Cohen, P., Buee-Scherrer, V., and Goedert, M. (1997) Activation of stress-activated protein kinase-3 (SAPK3) by cytokines and cellular stresses is mediated via SAPKK3 (MKK6); comparison of the specificities of SAPK3 and SAPK2 (RK/p38), *EMBO J 16*, 295-305.
131. Correas, I., Diaz-Nido, J., and Avila, J. (1992) Microtubule-associated protein tau is phosphorylated by protein kinase C on its tubulin binding domain, *J Biol Chem 267*, 15721-15728.
132. Drewes, G., Lichtenberg-Kraag, B., Doring, F., Mandelkow, E. M., Biernat, J., Goris, J., Doree, M., and Mandelkow, E. (1992) Mitogen activated protein (MAP) kinase transforms tau protein into an Alzheimer-like state, *EMBO J 11*, 2131-2138.

133. Baudier, J., and Cole, R. D. (1987) Phosphorylation of tau proteins to a state like that in Alzheimer's brain is catalyzed by a calcium/calmodulin-dependent kinase and modulated by phospholipids, *J Biol Chem 262*, 17577-17583.
134. Scott, C. W., Fieles, A., Sygowski, L. A., and Caputo, C. B. (1993) Aggregation of tau protein by aluminum, *Brain Res 628*, 77-84.
135. Lucas, J. J., Hernandez, F., Gomez-Ramos, P., Moran, M. A., Hen, R., and Avila, J. (2001) Decreased nuclear beta-catenin, tau hyperphosphorylation and neurodegeneration in GSK-3beta conditional transgenic mice, *EMBO J 20*, 27-39.
136. Lee, G., Thangavel, R., Sharma, V. M., Litersky, J. M., Bhaskar, K., Fang, S. M., Do, L. H., Andreadis, A., Van Hoesen, G., and Ksiezak-Reding, H. (2004) Phosphorylation of tau by fyn: implications for Alzheimer's disease, *J Neurosci 24*, 2304-2312.
137. Derkinderen, P., Scales, T. M., Hanger, D. P., Leung, K. Y., Byers, H. L., Ward, M. A., Lenz, C., Price, C., Bird, I. N., Perera, T., Kellie, S., Williamson, R., Noble, W., Van Etten, R. A., Leroy, K., Brion, J. P., Reynolds, C. H., and Anderton, B. H. (2005) Tyrosine 394 is phosphorylated in Alzheimer's paired helical filament tau and in fetal tau with c-Abl as the candidate tyrosine kinase, *J Neurosci 25*, 6584-6593.
138. Geddes, J. F., Hughes, A. J., Lees, A. J., and Daniel, S. E. (1993) Pathological overlap in cases of parkinsonism associated with neurofibrillary tangles. A study of recent cases of postencephalitic parkinsonism and comparison with progressive supranuclear palsy and Guamanian parkinsonism-dementia complex, *Brain 116 (Pt 1)*, 281-302.
139. Goedert, M., Cohen, E. S., Jakes, R., and Cohen, P. (1992) p42 MAP kinase phosphorylation sites in microtubule-associated protein tau are dephosphorylated by protein phosphatase 2A1. Implications for Alzheimer's disease [corrected], *FEBS Lett 312*, 95-99.
140. Szucs, K., Ledesma, M. D., Dombradi, V., Gergely, P., Avila, J., and Friedrich, P. (1994) Dephosphorylation of tau protein from Alzheimer's disease patients, *Neurosci Lett 165*, 175-178.
141. Yamamoto, H., Hasegawa, M., Ono, T., Tashima, K., Ihara, Y., and Miyamoto, E. (1995) Dephosphorylation of fetal-tau and paired helical filaments-tau by protein phosphatases 1 and 2A and calcineurin, *J Biochem 118*, 1224-1231.
142. Gong, C. X., Grundke-Iqbal, I., and Iqbal, K. (1994) Dephosphorylation of Alzheimer's disease abnormally phosphorylated tau by protein phosphatase-2A, *Neuroscience 61*, 765-772.
143. Gong, C. X., Singh, T. J., Grundke-Iqbal, I., and Iqbal, K. (1994) Alzheimer's disease abnormally phosphorylated tau is dephosphorylated by protein phosphatase-2B (calcineurin), *J Neurochem 62*, 803-806.
144. Goedert, M., Jakes, R., Qi, Z., Wang, J. H., and Cohen, P. (1995) Protein phosphatase 2A is the major enzyme in brain that dephosphorylates tau

protein phosphorylated by proline-directed protein kinases or cyclic AMP-dependent protein kinase, *J Neurochem 65*, 2804-2807.
145. Gong, C. X., Lidsky, T., Wegiel, J., Zuck, L., Grundke-Iqbal, I., and Iqbal, K. (2000) Phosphorylation of microtubule-associated protein tau is regulated by protein phosphatase 2A in mammalian brain. Implications for neurofibrillary degeneration in Alzheimer's disease, *J Biol Chem 275*, 5535-5544.
146. Goedert, M., Satumtira, S., Jakes, R., Smith, M. J., Kamibayashi, C., White, C. L., 3rd, and Sontag, E. (2000) Reduced binding of protein phosphatase 2A to tau protein with frontotemporal dementia and parkinsonism linked to chromosome 17 mutations, *J Neurochem 75*, 2155-2162.
147. Butterfield, D. A., Abdul, H. M., Opii, W., Newman, S. F., Joshi, G., Ansari, M. A., and Sultana, R. (2006) Pin1 in Alzheimer's disease, *J Neurochem 98*, 1697-1706.
148. Lu, Q., and Wood, J. G. (1993) Characterization of fluorescently derivatized bovine tau protein and its localization and functions in cultured Chinese hamster ovary cells, *Cell Motil Cytoskeleton 25*, 190-200.
149. Lovestone, S., Hartley, C. L., Pearce, J., and Anderton, B. H. (1996) Phosphorylation of tau by glycogen synthase kinase-3 beta in intact mammalian cells: the effects on the organization and stability of microtubules, *Neuroscience 73*, 1145-1157.
150. Voss, K., and Gamblin, T. C. (2009) GSK-3β phosphorylation of functionally distinct tau isoforms has differential, but mild effects, *Mol Neurodegener 4*, 1-12.
151. Lucas, J. J., Hernandez, F., and Avila, J. (1999) Nuclear localization of beta-catenin in adult mouse thalamus correlates with low levels of GSK-3beta, *Neuroreport 10*, 2699-2703.
152. Engel, T., Hernandez, F., Avila, J., and Lucas, J. J. (2006) Full reversal of Alzheimer's disease-like phenotype in a mouse model with conditional overexpression of glycogen synthase kinase-3, *J Neurosci 26*, 5083-5090.
153. Liu, F., Li, B., Tung, E. J., Grundke-Iqbal, I., Iqbal, K., and Gong, C. X. (2007) Site-specific effects of tau phosphorylation on its microtubule assembly activity and self-aggregation, *Eur J Neurosci 26*, 3429-3436.
154. Evans, D. B., Rank, K. B., Bhattacharya, K., Thomsen, D. R., Gurney, M. E., and Sharma, S. K. (2000) Tau phosphorylation at serine 396 and serine 404 by human recombinant tau protein kinase II inhibits Tau's ability to promote microtubule assembly, *J Biol Chem 275*, 24977-24983.
155. Mandelkow, E. M., Schweers, O., Drewes, G., Biernat, J., Gustke, N., Trinczek, B., and Mandelkow, E. (1996) Structure, microtubule interactions, and phosphorylation of tau protein, *Ann N Y Acad Sci 777*, 96-106.
156. Amniai, L., Barbier, P., Sillen, A., Wieruszeski, J. M., Peyrot, V., Lippens, G., and Landrieu, I. (2008) Alzheimer disease specific phosphoepitopes of Tau interfere with assembly of tubulin but not binding to microtubules, *Faseb J.*

157. Zhou, X. W., Gustafsson, J. A., Tanila, H., Bjorkdahl, C., Liu, R., Winblad, B., and Pei, J. J. (2008) Tau hyperphosphorylation correlates with reduced methylation of protein phosphatase 2A, *Neurobiol Dis 31*, 386-394.
158. Liu, R., Zhou, X. W., Tanila, H., Bjorkdahl, C., Wang, J. Z., Guan, Z. Z., Cao, Y., Gustafsson, J. A., Winblad, B., and Pei, J. J. (2008) Phosphorylated PP2A (tyrosine 307) is associated with Alzheimer neurofibrillary pathology, *J Cell Mol Med 12*, 241-257.
159. Bukau, B., and Horwich, A. L. (1998) The Hsp70 and Hsp60 chaperone machines, *Cell 92*, 351-366.
160. Hartl, F. U., and Hayer-Hartl, M. (2002) Molecular chaperones in the cytosol: from nascent chain to folded protein, *Science 295*, 1852-1858.
161. Hartl, F. U. (1996) Molecular chaperones in cellular protein folding, *Nature 381*, 571-579.
162. Ritossa, F. (1962) A new puffing pattern induced by temperature shock and DNP in Drosophila, *Experimentia 18*, 571-573.
163. Berendes, H. D. (1968) Factors involved in the expression of gene activity in polytene chromosomes, *Chromosoma 24*, 418-437.
164. Ashburner, M. (1970) Patterns of puffing activity in the salivary gland chromosomes of Drosophila. V. Responses to environmental treatments, *Chromosoma 31*, 356-376.
165. Leenders, H. J., and Berendes, H. D. (1972) The effect of changes in the respiratory metabolism upon genome activity in Drosophila. I. The induction of gene activity, *Chromosoma 37*, 433-444.
166. Tissieres, A., Mitchell, H. K., and Tracy, U. M. (1974) Protein synthesis in salivary glands of Drosophila melanogaster: relation to chromosome puffs, *J Mol Biol 84*, 389-398.
167. Lindquist, S., and Craig, E. A. (1988) The heat-shock proteins, *Annu Rev Genet 22*, 631-677.
168. Gupta, R. S., and Singh, B. (1994) Phylogenetic analysis of 70 kD heat shock protein sequences suggests a chimeric origin for the eukaryotic cell nucleus, *Curr Biol 4*, 1104-1114.
169. Hunt, C., and Morimoto, R. I. (1985) Conserved features of eukaryotic hsp70 genes revealed by comparison with the nucleotide sequence of human hsp70, *Proc Natl Acad Sci U S A 82*, 6455-6459.
170. Tavaria, M., Gabriele, T., Kola, I., and Anderson, R. L. (1996) A hitchhiker's guide to the human Hsp70 family, *Cell Stress Chaperones 1*, 23-28.
171. Daugaard, M., Rohde, M., and Jaattela, M. (2007) The heat shock protein 70 family: Highly homologous proteins with overlapping and distinct functions, *FEBS Lett 581*, 3702-3710.
172. Bukau, B., Weissman, J., and Horwich, A. (2006) Molecular chaperones and protein quality control, *Cell 125*, 443-451.
173. Wu, B., Hunt, C., and Morimoto, R. (1985) Structure and expression of the human gene encoding major heat shock protein HSP70, *Mol Cell Biol 5*, 330-341.

174. Milarski, K. L., and Morimoto, R. I. (1986) Expression of human HSP70 during the synthetic phase of the cell cycle, *Proc Natl Acad Sci U S A 83*, 9517-9521.
175. Taira, T., Narita, T., Iguchi-Ariga, S. M., and Ariga, H. (1997) A novel G1-specific enhancer identified in the human heat shock protein 70 gene, *Nucleic Acids Res 25*, 1975-1983.
176. Kwon, S. B., Young, C., Kim, D. S., Choi, H. O., Kim, K. H., Chung, J. H., Eun, H. C., Park, K. C., Oh, C. K., and Seo, J. S. (2002) Impaired repair ability of hsp70.1 KO mouse after UVB irradiation, *J Dermatol Sci 28*, 144-151.
177. Lee, S. H., Kim, M., Yoon, B. W., Kim, Y. J., Ma, S. J., Roh, J. K., Lee, J. S., and Seo, J. S. (2001) Targeted hsp70.1 disruption increases infarction volume after focal cerebral ischemia in mice, *Stroke 32*, 2905-2912.
178. Lee, S. J., Choi, S. A., Lee, K. H., Chung, H. Y., Kim, T. H., Cho, C. K., and Lee, Y. S. (2001) Role of inducible heat shock protein 70 in radiation-induced cell death, *Cell Stress Chaperones 6*, 273-281.
179. Flaherty, K. M., DeLuca-Flaherty, C., and McKay, D. B. (1990) Three-dimensional structure of the ATPase fragment of a 70K heat-shock cognate protein, *Nature 346*, 623-628.
180. Zhu, X., Zhao, X., Burkholder, W. F., Gragerov, A., Ogata, C. M., Gottesman, M. E., and Hendrickson, W. A. (1996) Structural analysis of substrate binding by the molecular chaperone DnaK, *Science 272*, 1606-1614.
181. Salbaum, J. M., Weidemann, A., Lemaire, H. G., Masters, C. L., and Beyreuther, K. (1988) The promoter of Alzheimer's disease amyloid A4 precursor gene, *EMBO J 7*, 2807-2813.
182. Hamos, J. E., Oblas, B., Pulaski-Salo, D., Welch, W. J., Bole, D. G., and Drachman, D. A. (1991) Expression of heat shock proteins in Alzheimer's disease, *Neurology 41*, 345-350.
183. Dou, F., Netzer, W. J., Tanemura, K., Li, F., Hartl, F. U., Takashima, A., Gouras, G. K., Greengard, P., and Xu, H. (2003) Chaperones increase association of tau protein with microtubules, *Proc Natl Acad Sci U S A 100*, 721-726.
184. Shimura, H., Schwartz, D., Gygi, S. P., and Kosik, K. S. (2004) CHIP-Hsc70 complex ubiquitinates phosphorylated tau and enhances cell survival, *J Biol Chem 279*, 4869-4876.
185. Petrucelli, L., Dickson, D., Kehoe, K., Taylor, J., Snyder, H., Grover, A., De Lucia, M., McGowan, E., Lewis, J., Prihar, G., Kim, J., Dillmann, W. H., Browne, S. E., Hall, A., Voellmy, R., Tsuboi, Y., Dawson, T. M., Wolozin, B., Hardy, J., and Hutton, M. (2004) CHIP and Hsp70 regulate tau ubiquitination, degradation and aggregation, *Hum Mol Genet 13*, 703-714.
186. Sarkar, M., Kuret, J., and Lee, G. (2008) Two motifs within the tau microtubule-binding domain mediate its association with the hsc70 molecular chaperone, *J Neurosci Res 86*, 2763-2773.

187. Sahara, N., Maeda, S., Yoshiike, Y., Mizoroki, T., Yamashita, S., Murayama, M., Park, J. M., Saito, Y., Murayama, S., and Takashima, A. (2007) Molecular chaperone-mediated tau protein metabolism counteracts the formation of granular tau oligomers in human brain, *J Neurosci Res 85*, 3098-3108.
188. King, M. E., Gamblin, T. C., Kuret, J., and Binder, L. I. (2000) Differential assembly of human tau isoforms in the presence of arachidonic acid, *J Neurochem 74*, 1749-1757.
189. Rankin, C. A., Sun, Q., and Gamblin, T. C. (2005) Pseudo-phosphorylation of tau at Ser202 and Thr205 affects tau filament formation, *Brain Res Mol Brain Res 138*, 84-93.
190. Tobacman, L. S., and Korn, E. D. (1983) The kinetics of actin nucleation and polymerization, *J Biol Chem 258*, 3207-3214.
191. Rankin, C. A., Sun, Q., and Gamblin, T. C. (2007) Tau phosphorylation by GSK-3beta promotes tangle-like filament morphology, *Mol Neurodegener 2*, 12.
192. Sun, Q., and Gamblin, T. C. (2009) Pseudohyperphosphorylation causing AD-like changes in tau has significant effects on its polymerization, *Biochemistry 48*, 6002-6011.
193. Rankin, C. A., Sun, Q., and Gamblin, T. C. (2008) Pre-assembled tau filaments phosphorylated by GSK-3b form large tangle-like structures, *Neurobiol Dis 31*, 368-377.
194. Sarthy, J., and Gamblin, T. C. (2006) A light scattering assay for arachidonic acid-induced tau fibrillization without interfering micellization, *Anal Biochem 353*, 150-152.
195. Bandyopadhyay, B., Li, G., Yin, H., and Kuret, J. (2007) Tau aggregation and toxicity in a cell culture model of tauopathy, *J Biol Chem 282*, 16454-16464.
196. Morris, A. M., Watzky, M. A., Agar, J. N., and Finke, R. G. (2008) Fitting neurological protein aggregation kinetic data via a 2-step, minimal/"Ockham's razor" model: the Finke-Watzky mechanism of nucleation followed by autocatalytic surface growth, *Biochemistry 47*, 2413-2427.
197. Winsor, C. P. (1932) The Gompertz Curve as a Growth Curve, *Proc Natl Acad Sci U S A 18*, 1-8.
198. Wille, H., Drewes, G., Biernat, J., Mandelkow, E. M., and Mandelkow, E. (1992) Alzheimer-like paired helical filaments and antiparallel dimers formed from microtubule-associated protein tau in vitro, *J Cell Biol 118*, 573-584.
199. Auer, S., Dobson, C. M., and Vendruscolo, M. (2007) Characterization of the nucleation barriers for protein aggregation and amyloid formation, *HFSP J 1*, 137-146.
200. Berriman, J., Serpell, L. C., Oberg, K. A., Fink, A. L., Goedert, M., and Crowther, R. A. (2003) Tau filaments from human brain and from in vitro assembly of recombinant protein show cross-beta structure, *Proc Natl Acad Sci U S A 100*, 9034-9038.

201. King, M. E., Ahuja, V., Binder, L. I., and Kuret, J. (1999) Ligand-dependent tau filament formation: implications for Alzheimer's disease progression, *Biochemistry 38*, 14851-14859.
202. King, M. E., Ghoshal, N., Wall, J. S., Binder, L. I., and Ksiezak-Reding, H. (2001) Structural analysis of Pick's disease-derived and In vitro assembled tau filaments, *Am J Pathol 158*, 1481-1490.
203. Gamblin, T. C., Berry, R. W., and Binder, L. I. (2003) Modeling tau polymerization in vitro: a review and synthesis, *Biochemistry 42*, 15009-15017.
204. Hernandez, F., and Avila, J. (2007) Tauopathies, *Cell Mol Life Sci 64*, 2219-2233.
205. Andreadis, A. (2005) Tau gene alternative splicing: expression patterns, regulation and modulation of function in normal brain and neurodegenerative diseases, *Biochim Biophys Acta 1739*, 91-103.
206. Iqbal, K., Alonso Adel, C., Chen, S., Chohan, M. O., El-Akkad, E., Gong, C. X., Khatoon, S., Li, B., Liu, F., Rahman, A., Tanimukai, H., and Grundke-Iqbal, I. (2005) Tau pathology in Alzheimer disease and other tauopathies, *Biochim Biophys Acta 1739*, 198-210.
207. Stoothoff, W. H., and Johnson, G. V. (2005) Tau phosphorylation: physiological and pathological consequences, *Biochim Biophys Acta 1739*, 280-297.
208. Sergeant, N., Delacourte, A., and Buee, L. (2005) Tau protein as a differential biomarker of tauopathies, *Biochim Biophys Acta 1739*, 179-197.
209. Connell, J. W., Gibb, G. M., Betts, J. C., Blackstock, W. P., Gallo, J., Lovestone, S., Hutton, M., and Anderton, B. H. (2001) Effects of FTDP-17 mutations on the in vitro phosphorylation of tau by glycogen synthase kinase 3beta identified by mass spectrometry demonstrate certain mutations exert long-range conformational changes, *FEBS Lett 493*, 40-44.
210. Reynolds, C. H., Betts, J. C., Blackstock, W. P., Nebreda, A. R., and Anderton, B. H. (2000) Phosphorylation sites on tau identified by nanoelectrospray mass spectrometry: differences in vitro between the mitogen-activated protein kinases ERK2, c-Jun N-terminal kinase and P38, and glycogen synthase kinase-3beta, *J Neurochem 74*, 1587-1595.
211. Engel, T., Goni-Oliver, P., Lucas, J. J., Avila, J., and Hernandez, F. (2006) Chronic lithium administration to FTDP-17 tau and GSK-3beta overexpressing mice prevents tau hyperphosphorylation and neurofibrillary tangle formation, but pre-formed neurofibrillary tangles do not revert, *J Neurochem 99*, 1445-1455.
212. Noble, W., Planel, E., Zehr, C., Olm, V., Meyerson, J., Suleman, F., Gaynor, K., Wang, L., LaFrancois, J., Feinstein, B., Burns, M., Krishnamurthy, P., Wen, Y., Bhat, R., Lewis, J., Dickson, D., and Duff, K. (2005) Inhibition of glycogen synthase kinase-3 by lithium correlates with reduced tauopathy and degeneration in vivo, *Proc Natl Acad Sci U S A 102*, 6990-6995.

213. Spittaels, K., Van den Haute, C., Van Dorpe, J., Geerts, H., Mercken, M., Bruynseels, K., Lasrado, R., Vandezande, K., Laenen, I., Boon, T., Van Lint, J., Vandenheede, J., Moechars, D., Loos, R., and Van Leuven, F. (2000) Glycogen synthase kinase-3beta phosphorylates protein tau and rescues the axonopathy in the central nervous system of human four-repeat tau transgenic mice, *J Biol Chem 275*, 41340-41349.
214. Mandelkow, E. M., Drewes, G., Biernat, J., Gustke, N., Van Lint, J., Vandenheede, J. R., and Mandelkow, E. (1992) Glycogen synthase kinase-3 and the Alzheimer-like state of microtubule-associated protein tau, *FEBS Lett 314*, 315-321.
215. Barghorn, S., and Mandelkow, E. (2002) Toward a unified scheme for the aggregation of tau into Alzheimer paired helical filaments, *Biochemistry 41*, 14885-14896.
216. DeTure, M., Granger, B., Grover, A., Hutton, M., and Yen, S. H. (2006) Evidence for independent mechanisms and a multiple-hit model of tau assembly, *Biochem Biophys Res Commun 339*, 858-864.
217. Sibille, N., Sillen, A., Leroy, A., Wieruszeski, J. M., Mulloy, B., Landrieu, I., and Lippens, G. (2006) Structural impact of heparin binding to full-length Tau as studied by NMR spectroscopy, *Biochemistry 45*, 12560-12572.
218. Drewes, G., Trinczek, B., Illenberger, S., Biernat, J., Schmitt-Ulms, G., Meyer, H. E., Mandelkow, E. M., and Mandelkow, E. (1995) Microtubule-associated protein/microtubule affinity-regulating kinase (p110mark). A novel protein kinase that regulates tau-microtubule interactions and dynamic instability by phosphorylation at the Alzheimer-specific site serine 262, *J Biol Chem 270*, 7679-7688.
219. Necula, M., and Kuret, J. (2004) A static laser light scattering assay for surfactant-induced tau fibrillization, *Anal Biochem 333*, 205-215.
220. Berne, B. J. (1974) Interpretation of the light scattering from long rods, *J Mol Biol 89*, 755-758.
221. Chirita, C. N., and Kuret, J. (2004) Evidence for an intermediate in tau filament formation, *Biochemistry 43*, 1704-1714.
222. Friedhoff, P., Schneider, A., Mandelkow, E. M., and Mandelkow, E. (1998) Rapid assembly of Alzheimer-like paired helical filaments from microtubule-associated protein tau monitored by fluorescence in solution, *Biochemistry 37*, 10223-10230.
223. Panda, D., Samuel, J. C., Massie, M., Feinstein, S. C., and Wilson, L. (2003) Differential regulation of microtubule dynamics by three- and four-repeat tau: implications for the onset of neurodegenerative disease, *Proc Natl Acad Sci U S A 100*, 9548-9553.
224. Liou, Y. C., Sun, A., Ryo, A., Zhou, X. Z., Yu, Z. X., Huang, H. K., Uchida, T., Bronson, R., Bing, G., Li, X., Hunter, T., and Lu, K. P. (2003) Role of the prolyl isomerase Pin1 in protecting against age-dependent neurodegeneration, *Nature 424*, 556-561.

225. Lu, P. J., Wulf, G., Zhou, X. Z., Davies, P., and Lu, K. P. (1999) The prolyl isomerase Pin1 restores the function of Alzheimer-associated phosphorylated tau protein, *Nature 399*, 784-788.
226. Floege, J., and Ehlerding, G. (1996) Beta-2-microglobulin-associated amyloidosis, *Nephron 72*, 9-26.
227. Sinha, S. (2002) The role of beta-amyloid in Alzheimer's disease, *Med Clin North Am 86*, 629-639.
228. Phinney, A. L., Drisaldi, B., Schmidt, S. D., Lugowski, S., Coronado, V., Liang, Y., Horne, P., Yang, J., Sekoulidis, J., Coomaraswamy, J., Chishti, M. A., Cox, D. W., Mathews, P. M., Nixon, R. A., Carlson, G. A., St George-Hyslop, P., and Westaway, D. (2003) In vivo reduction of amyloid-beta by a mutant copper transporter, *Proc Natl Acad Sci U S A 100*, 14193-14198.
229. Brown, I. R. (2007) Heat shock proteins and protection of the nervous system, *Ann N Y Acad Sci 1113*, 147-158.
230. Young, J. C. (2010) Mechanisms of the Hsp70 chaperone system, *Biochem Cell Biol 88*, 291-300.
231. Jinwal, U. K., Miyata, Y., Koren, J., 3rd, Jones, J. R., Trotter, J. H., Chang, L., O'Leary, J., Morgan, D., Lee, D. C., Shults, C. L., Rousaki, A., Weeber, E. J., Zuiderweg, E. R., Gestwicki, J. E., and Dickey, C. A. (2009) Chemical manipulation of hsp70 ATPase activity regulates tau stability, *J Neurosci 29*, 12079-12088.
232. Akiyama, H., Barger, S., Barnum, S., Bradt, B., Bauer, J., Cole, G. M., Cooper, N. R., Eikelenboom, P., Emmerling, M., Fiebich, B. L., Finch, C. E., Frautschy, S., Griffin, W. S., Hampel, H., Hull, M., Landreth, G., Lue, L., Mrak, R., Mackenzie, I. R., McGeer, P. L., O'Banion, M. K., Pachter, J., Pasinetti, G., Plata-Salaman, C., Rogers, J., Rydel, R., Shen, Y., Streit, W., Strohmeyer, R., Tooyoma, I., Van Muiswinkel, F. L., Veerhuis, R., Walker, D., Webster, S., Wegrzyniak, B., Wenk, G., and Wyss-Coray, T. (2000) Inflammation and Alzheimer's disease, *Neurobiol Aging 21*, 383-421.
233. Markesbery, W. R., and Carney, J. M. (1999) Oxidative alterations in Alzheimer's disease, *Brain Pathol 9*, 133-146.
234. McGeer, E. G., and McGeer, P. L. (1998) The importance of inflammatory mechanisms in Alzheimer disease, *Exp Gerontol 33*, 371-378.
235. Ray, W. J., Ashall, F., and Goate, A. M. (1998) Molecular pathogenesis of sporadic and familial forms of Alzheimer's disease, *Mol Med Today 4*, 151-157.
236. Aksenov, M. Y., Aksenova, M. V., Butterfield, D. A., Geddes, J. W., and Markesbery, W. R. (2001) Protein oxidation in the brain in Alzheimer's disease, *Neuroscience 103*, 373-383.
237. Swain, J. F., Schulz, E. G., and Gierasch, L. M. (2006) Direct comparison of a stable isolated Hsp70 substrate-binding domain in the empty and substrate-bound states, *J Biol Chem 281*, 1605-1611.

238. Jeganathan, S., von Bergen, M., Brutlach, H., Steinhoff, H. J., and Mandelkow, E. (2006) Global hairpin folding of tau in solution, *Biochemistry 45*, 2283-2293.
239. von Bergen, M., Friedhoff, P., Biernat, J., Heberle, J., and Mandelkow, E. (2000) Assembly of tau protein into Alzheimer paired helical filaments depends on a local sequence motif (306VQIVYK311) forming beta structure, *Proc Natl Acad Sci U S A 97*, 5129-5134.
240. Goux, W. J., Kopplin, L., Nguyen, A. D., Leak, K., Rutkofsky, M., Shanmuganandam, V. D., Sharma, D., Inouye, H., and Kirschner, D. A. (2004) The formation of straight and twisted filaments from short tau peptides, *J Biol Chem 279*, 26868-26875.
241. Ishizawa, T., Sahara, N., Ishiguro, K., Kersh, J., McGowan, E., Lewis, J., Hutton, M., Dickson, D. W., and Yen, S. H. (2003) Co-localization of glycogen synthase kinase-3 with neurofibrillary tangles and granulovacuolar degeneration in transgenic mice, *Am J Pathol 163*, 1057-1067.
242. Hernandez, F., Lucas, J. J., Cuadros, R., and Avila, J. (2003) GSK-3 dependent phosphoepitopes recognized by PHF-1 and AT-8 antibodies are present in different tau isoforms, *Neurobiol Aging 24*, 1087-1094.
243. Gamblin, T. C., Berry, R. W., and Binder, L. I. (2003) Tau polymerization: role of the amino terminus, *Biochemistry 42*, 2252-2257.
244. Lapointe, N. E., Horowitz, P. M., Guillozet-Bongaarts, A. L., Silva, A., Andreadis, A., and Binder, L. I. (2009) Tau 6D and 6P isoforms inhibit polymerization of full-length tau in vitro, *Biochemistry 48*, 12290-12297.
245. Horowitz, P. M., LaPointe, N., Guillozet-Bongaarts, A. L., Berry, R. W., and Binder, L. I. (2006) N-terminal fragments of tau inhibit full-length tau polymerization in vitro, *Biochemistry 45*, 12859-12866.
246. Kyte, J., and Doolittle, R. F. (1982) A simple method for displaying the hydropathic character of a protein, *J Mol Biol 157*, 105-132.
247. Liebscher, M., and Roujeinikova, A. (2009) Allosteric coupling between the lid and interdomain linker in DnaK revealed by inhibitor binding studies, *J Bacteriol 191*, 1456-1462.